Investigation of MgH_2 composite electrodes for all-solid-state Li-ion batteries working at room temperature

(室温で動作する全固体リチウムイオン電池用 MgH_2 複合電極の研究)

Graduate School of Engineering

Hiroshima University

学位取得年月 2021 年 5 月

Cano-Banda Fernando

ABSTRACT

Energy storage plays a vital role in the development of many applications from portable electronics to transportation furthermore generation of electricity. Portable electronics such as smartphones and personal computers are part of our daily life. In our modern world, this kind of devices has become important tools for many activities. From the alarm that waking us up in the morning, managing our agenda, our communications, working instruments and entertainment are in our smartphones, tablets and laptops. The development of these technologies has been strongly supported by the growth of batteries technology. After the commercialization of the first rechargeable Li-ion battery in 1992 by Japanese compony Sony, the market of portable electronics has grown year after year. In fact, in year 1993, they sold 3 million units. Supporting the introduction and development of modern innovative devices for health applications, digital cameras, drones, etc. On the same road, the progress of electric vehicles also depends on energy storage systems capable to offer autonomy compared to gasoline. On the other side, power generation using intermittent energy sources (solar energy, wind energy, etc.) requires high-capacity storage systems to take full advantage of these kinds of energy sources. For example, solar energy can provide a huge amount of energy during the daylight period, some part of this energy could be store and then use during the night when the energy source is not available. In this way, solar energy could be a reliable energy source.

From past to present, various class of batteries including Nickel cadmium batteries, lead acid batteries, lead metal batteries have been focused. Among them Li ion batteries are considered best among the rest due to their higher cycle life, higher energy density, better cyclability, and cost effective. However, achieving all these characteristics is not a simple task, it requires an exhaustive investigation of many aspects, electrode materials, electrolyte materials, optimization of fabrication processes, etc. In this scenery, metal hydrides appear as potential candidates for electrode materials possessing remarkable theoretical capacities. MgH_2 owns a high specific capacity (2036 mAh g^{-1}) which is higher than the commercially available graphite-based electrodes and suitable reaction potential as anode material. All-solid-state batteries have been considered as a possible next-generation battery because it solves some safety issues associated with liquid electrolytes. The liquid combustible electrolyte of Li-ion batteries is replaced by a solid electrolyte. Also, the use of solid electrolytes can avoid problems

such as dendrite formations, which is one of the main concerns about the use of Li-metal electrodes.

In this study several solid electrolytes with suitable properties were selected to study their compatibility with MgH_2, focusing on room temperature operation. Metal hydrides electrodes have been reported operating with solid electrolytes mainly at high temperatures because of limitations of conductivity of solid electrolytes at room temperatures. An earlier study about MgH_2-$LiBH_4$ (electrode-electrolyte) was reported by our research group with remarkable results operating at 120 °C. The high-temperature phase of $LiBH_4$ shows a good conductivity (>10^{-3} S cm^{-1}), However, this phase change from a hexagonal to the orthorhombic structure below 117 °C. The low-temperature phase of $LiBH_4$ has a lower conductivity (<10^{-5} S cm^{-1}) than its high-temperature phase. This drastic difference in conductivity forbids the operation of the battery at room temperatures.

Here, all-solid-state Li-metal batteries were fabricated using different electrolytes, electrolytes with high conductivity at room temperatures. The electrolytes were prepared based on $LiBH_4$ mixed electrolytes: $75LiBH_4$+$25LiI$, $90LiBH_4$+$10P_2S_5$, $33LiBH_4$+$67(80Li_2S$+$20P_2S_5)$ and $80Li_2S$+$20P_2S_5$. The batteries were analyzed using electrochemical and XRD characterization techniques.

First section of the study was focused on the halide-stabilized $LiBH_4$. Operation of batteries using $LiBH_4$ at room temperature is strongly limited by the low ionic conductivity of $LiBH_4$. LiI, LiBr and other halides can be used to improve the conductivity of $LiBH_4$ at room temperatures. The electrolyte $75LiBH_4$+$25LiI$ keeps a high ionic conductivity at room temperature. This improvement in conductivity allows the operation of the MgH_2 electrode at room temperatures. Half-cell batteries shown a good performance during initial cycle (discharge: 1300 mAh/g, reversibility: ~800 mAh/g), but some stability issues produce a low cyclability. An alternative configuration using an $80Li_2S$+$20P_2S_5$ layer enhance the performance of composite electrode MgH_2/$75LiBH_4$+$25LiI$/carbon.

Second section was focused on the electrolyte $Li_6PS_5(BH_4)$. This electrolyte was prepared by two methods: $90LiBH_4$+$10P_2S_5$ and $33LiBH_4$+$67(80Li_2S$+$20P_2S_5)$. In both cases, the obtained ionic conductivity was similar and higher than $LiBH_4$ and $80Li_2S$+$20P_2S_5$ (LPS). The electrodes prepared with this electrolyte can operate at room temperature with a limited capacity. The composite electrode with $90LiBH_4$+$10P_2S_5$

shown a remarkable capacity and more important with a good stability during cycling. After a comparison keeping the same electrolyte layer (LPS), it was concluded that $90LiBH_4+10P_2S_5$ worked better as ionic conductor in composite electrode. The $90LiBH_4+10P_2S_5$ electrolyte enhanced the reversibility of the conversion reaction. This improvement was attributed to the higher content of $LiBH_4$. Previous reports have shown an effect of hydrogen exchange between $LiBH_4$ and MgH_2, this could be the reason for the improvement of the reversibility of the reaction. For the conversion reaction of MgH_2, the mobility of hydrogen is as necessary as the mobility of Li-ions.

Among all the combinations, the preparation of MgH_2 composite electrode using only $LiBH_4$ was identified as the best option for the preparation of the electrode. However, as was mentioned before battery using only $LiBH_4$ as an electrolyte are not able to operate at room temperature. The use of MgH_2-$LiBH_4$ composite electrode was achievable with the use of an electrolyte layer in the cell. This electrolyte layer consisted of a layer of mixed electrolytes. Among them, the best battery configuration was founded for an electrode of MgH_2-$LiBH_4$-AB carbon and an electrolyte layer of $90LiBH_4+P_2S_5$ (initial capacity ~1000 mAh g^{-1}, 645.7 mAh g^{-1} after 10 cycles).

The thesis work was compiled in 6 chapters. Chapter 1, in this introductory chapter the importance of batteries was discussed. Focus on the importance of the development of next generation batteries and the benefits for the development of electronics applications, transportation, etc. the second part of this chapter present fundamentals related to the understanding of batteries operation. Then, metal hydrides as battery materials were reviewed. The objectives are described in Chapter 2. In Chapter 3, Materials and experimental methods for the preparation and characterization of battery composite materials used in this work are explained. Chapter 4 contains all the results. This chapter is divided in two sections. First section discussed the results when high temperature phase of $LiBH_4$ was stabilized with LiI at room temperature. Additionally, some battery configurations with $80Li_2S$-$20P_2S_5$ were analyzed. Same materials can be used mixed to prepare a different phase with a similar ionic conductivity. $LiBH_4$ with Li_2S and P_2S_5 was used to prepare $Li_6PS_5(BH_4)$. This alternative was discussed in the second section of Chapter 5. Finally, Chapter 6 compiles all the relevant references consulted during preparation of this work.

Contents

1 Introduction

Today, batteries are one of the most important energy storage systems widely used for a huge variety of applications such as portable electronics. Portable electronic devices are a common part of our daily life, such as portable computers, wearable gadgets, digital cameras, working tools, mobile phones, etc. These devices are used for many applications from working to entertaining in order to facilitate current activities. Batteries are divided into three general classes: first, primary batteries that are discharged once and discarded; second, secondary rechargeable batteries that can be discharged and then restored to their original condition by reversing the current flow through the cell; and third, specialty batteries that are designed to fulfil a specific purpose. The latter are mainly military and medical batteries that do not find a wide commercial use for various reasons of cost, environmental issues, and limited market application. The advantages of battery systems are listed in Table 1.1. For transportation, fossil fuels still represent the energy source with a higher energy density (autonomy, longer range), However, research community put their enormous efforts in the development of future battery technology to overcome the limitations of current batteries [1]–[3].

The development of electronics is strongly related to the development of energy storage devices. Table 1.2 shows the evolution and development of mobile phones with the available energy storage technology. A similar development can also be observed for other portable electronics [4]. Since the commercialization of Li-ion battery (LIB) by

SONY in 1991, Li-ion batteries have been widely known as the owner of an outstanding capacity to store energy with high energy density attributes and practical qualities, suitable for mentioned applications. Besides, stationary electricity storage systems combined with solar cells and wind turbines are a necessary due to exploit the potential of intermittent energy sources[5]. It requires large and high-performance energy storage systems, i. e., high energy density, long cycle life, high efficiency, lower cost, and so on. Any conventional secondary batteries, such as lead-acid, NiCd, NiMH batteries, cannot accomplish the requirements. The importance of the development of LIB technology and its impact in modern society was recognized with the 2019 Nobel Prize in Chemistry. This prize was awarded to John B. Goodenough, M. Stanley Whittingham, and Akira Yoshino, in 2019 for their contributions to the development of the rechargeable lithium-ion battery. However, the demand for energy storage devices is growing based on trends such as population increase and cities growth, the shift in energy production. For example, smartphones and personal computers are one of the biggest markets for batteries among all portable electronic devices. Figure 1.1 shows the market growth of batteries for mobile phones and personal computers from 2000 to 2018 [6]. The development of high-density energy storage systems for a near and far future require the continues improvement of energy storage technology[1].

Table 1.1. Battery as an energy storage system.

Advantages	Disadvantages
Operate over a wide temperature range	Low energy content compared to gasoline and other fuels
Choice of chemical system and voltage	Expensive compared to coal and gasoline
Variable in size	
The commonality of cell sizes, worldwide	
Can deliver high current pulses	
Can choose the best battery for a specific purpose (mobile, portable, and stationary applications)	

Table 1.2. Development of mobile phones and their batteries[4].

Period	Historical stages	Representative product	Actual photo	Launch time	Battery type	Voltage (V)	Capacity (mAh)
1983-1993	Era of cellular phone	Motorola DynaTac 8000X (the world's first mobile phone)		1983	Ni-Cd battery	7.5	500
1993-1995	Miniaturization and intelligence	IBM Simon (the world's first smart phone)		1993	Ni-Cd battery	7.5	
		Motorola 8900 (the world's first flip mobile phone)		1995	Ni-Cd battery	6	950
1995-1997	Era of Ni-MH battery	Motorola 166C		1997	Ni-MH battery	6	1300
1998-2007	Era of popularization of mobile phone	Motorola GC87C		1998	Liquefied Li-ion battery	7.2	1200
2007-present	Era of new smart mobile phone	iPhone		2007	Li-ion polymer battery	3.7	1500
		Galaxy SIII		2012	Soft-pouch liquefied Li-ion battery	3.8	2100
		iPhone 6		2014	Li-ion polymer battery	3.8	1810
		Huawei mate 20p		2018	Li-ion polymer battery	3.82	4200

1.1 Li-ion battery

The lithium-ion battery is a rechargeable battery (also known as secondary batteries), which is capable of either generating electrical energy from chemical reactions or using electrical energy to cause chemical reactions. Li-ion battery shows the highest energy density and efficiency among practical secondary batteries (Figure 1.2 and Figure 1.3).

1.1.1 Working principle of Li-ion batteries

The essential components for a battery are the positive electrode (cathode), the negative electrode (anode) and electrolyte. The electrodes store the lithium, then, during charging or discharging the ionic current flow from one electrode to the opposite one. The electrolyte provides the conductivity to lithium ions to transfer the charge between the electrodes. Both electrodes are electrically separated by a separator, it is a physical barrier permeable to ionic flow to prevent electrical shorting. The separator typically is a porous membrane for liquid electrolyte batteries, but in the case of all-solid-state batteries, the solid electrolyte can play the role of electrolyte and separator. The important part is to disconnect the electrodes because the electrical connection must be made using an external circuit. Using the external circuit, the electrical current can be utilized to power some electric device. Figure 1.4a shows a representation of the discharge process. Once the external electric circuit is closed, the oxidation reaction at anode releases the electrons

and Li-ions from the anode. The Li-ions flow in the electrolyte whereas the electrons are transported by the electric circuit. At the cathode, the Li-ions are reduced within the hosting material. From all this process electrical energy is obtained from the electrochemical reactions. During charge the opposite process takes place, this is possible due to the reversibility of the lithium storage mechanisms. Electrical energy is provided to the cell producing the opposite electrochemical reactions in the electrodes, producing the flow of electrons and Li-ions from cathode to anode. Figure 1.4b shows a representation of the charging process.

1.2 Thermodynamics

The energy storage properties of electrochemical energy conversion systems follow the thermodynamic formulations for the chemical reactions. The basic thermodynamic equation for a reversible process is given as:

$$\Delta G = \Delta H - T\Delta S \tag{1-1}$$

where ΔG is the Gibbs free energy, ΔH is the enthalpy, ΔS is the entropy, and T is the absolute temperature. Gibbs free energy represents the net energy available for useful work. In electrical terms, the net energy available from a given reaction is given by

$$\Delta G = -nFE \tag{1-2}$$

$$\Delta G^{\circ} = -nFE^{\circ} \tag{1-3}$$

where n is the number of electrons transferred per mole of reactants, F is the Faraday constant (the electrical charge of 1 mol of electrons), and E is the cell voltage, the electromotive force of the cell reaction. The voltage of the cell is unique for each reaction. The amount of electricity produced is determined by the total amount of reactants. $\Delta G°$ and $\Delta E°$ are the functions evaluated at standard conditions (25 °C).

For spontaneous processes, free energy is negative with a positive voltage. The van´t Hoff isotherm relate the free energy with the bulk chemical reactions as

$$\Delta G = \Delta G° + RTln(A_P/A_R) \quad (1\text{-}4)$$

where R is the gas constant, T the absolute temperature, A_P the activity product of the products and A_R the activity product of the reactants. Combining equations (1-3) and (1-4), with the van´t Hoff isotherm, The Nernst equation for electrochemical reactions is given below:

$$E = E° + \frac{RT}{nF} ln(A_P/A_R) \quad (1\text{-}4)$$

The total amount of reaction and the current flow is given by the Faraday´s laws

$$m = \frac{I\ t\ MW}{nF} \quad (1\text{-}5)$$

where *m* is the mass of material transformed (grams), *I* is the current (amps), *t* is the time of the current flow (seconds, hours), *MW* is the molecular or atomic weight of the material

being transformed. *nF* represents the amount of electricity produced (n, the number of electrons in the reaction).

1.4 Kinetics

Thermodynamics describes the reactions at equilibrium and the maximum energy release for a given reaction. However, during real processes, the equilibrium voltage or open-circuit voltage (E_{OC}) drops off when current is flowing during operation because of the kinetics limitations of reactions and other processes. The kinetics of electrochemical reactions follow the same general considerations as those for bulk chemical reactions, but electrode kinetics differs from chemical kinetics in two important aspects: (1) the influence of the potential drop in the electrical double layer at an electrode interface as it directly affects the activated couples and (2) the fact that reactions at electrode interfaces are two-dimensional, not three-dimensional. The detailed mechanism of battery electrode reactions often involves a series of physical, chemical, and electrochemical steps, including charge-transfer and charge transport reactions. The rates of these individual steps determine the kinetics of the electrode and, thus, of the cell/battery. Three different kinetics effects for polarization must be considered:

(1) activation polarization is related to the kinetics of the electrochemical redox (or charge-transfer) reactions taking place at the electrode/electrolyte interfaces of anode and cathode;

(2) ohmic polarization is interconnected to the resistance of individual cell components and the resistance due to contact problems between the cell components;

(3) concentration polarization is due to mass transport limitations during cell operation.

The polarization, denoted as η, is given by

$$\eta = E_{OC} - E_T \tag{1-6}$$

where E_{OC} is the voltage of the cell at open circuit and E_T is the terminal cell voltage with current, I, flowing.

Activation polarization arises from kinetics barriers of the charge-transfer reaction taking place at the electrode/electrolyte interface. The rate, current flow, i ($i=I/A$, where A is the electrode surface area), of a charge-transfer-controlled battery reaction can be given by the Butler-Volmer equation as

$$i = i_0[\exp(\alpha F\eta/RT) - \exp((1-\alpha)F\eta/RT)] \tag{1-7}$$

where the exchange current density, $i_0 = k_0FA$ is the exchange of current density (k_0 is the reaction rate constant for the electrode reaction, A is the activity product of the reactants), η is the polarization, and α is the transfer coefficient, which is best considered as the fraction of the change of overpotential that leads to a change in the rate constant for the charge-transfer reaction. The exchange current density is directly related to the reaction rate constant, to the activities of reactants and products, and the potential drop

across the double layer. Reactions with larger i_0 are more reversible and have lower polarization for a given current flow.

The activation polarization follows the Tafel equation derived from (1-7)

$$\eta = a - b\log(I/I_0) \tag{1-7}$$

Ohmic polarization is the straightforward resistance to the flow of electrons through the material of the electrodes and the various interconnections, as well as the resistance to the flow of ions through the electrolyte. This voltage drop is essentially linearly proportional to the current density, and so is called ohmic losses, or sometimes as resistive losses. For the effect of ohmic resistance, R, Ohm´s Law gives a relationship between I and η.

$$\eta = IR \tag{1-8}$$

As the redox reactions proceed, the availability of the active species at the electrode/electrolyte interface changes. Concentration polarization arises from limited mass transport capabilities, for example, limited diffusion of active species to and from the electrode surface to replace the reacted material to sustain the reaction. The concentration polarization can be expressed as

$$\eta = (RT/n)\ln(C/C_0) \tag{1-8}$$

where C is the concentration at the electrode surface and C_0 is the concentration in the bulk of the solution.

The direct measurement of the instantaneous current-voltage characteristics on the discharge curve shown in Figure 1.5. This curve can be used to determine the cell capacity, the effect of the discharge-charge rate, and temperature and information on the state of health of the battery.

1.4 Electrode materials

Both anode and cathode are materials into which, and from which, lithium can migrate. Lithium can be "stored" at electrodes in metal phase, inserted in layered structures or found in a specific phase with a host material. The maximum energy storage capacity of electrodes (C_{max}, in units of mAh/g) is determined by the number of electrons inserted or removed during cycling, and the molecular weight of the insertion material. The maximum capacity is given by

$$C_{max} = \frac{nF}{3.6\ MW} \tag{1-9}$$

The mechanism to store the lithium in the electrodes depends on the host material. Three of the known mechanism are intercalation reaction, alloying reaction, and conversion reaction, which are described in the next sections.

1.4.1 Intercalation reaction electrodes

In these electrodes, Li-ions are inserted into crystalline materials, for example, graphite or $Li_4Ti_5O_{12}$, without big changes in the crystal structure of the hosts, Figure 1.6.

[7]. During insertion/intercalation lithium moves into the electrode, while during extraction/deintercalation lithium moves back out. This reaction has showed high reversibility due to the simple reaction, However, the disadvantage of this kind of materials is a low capacity. Some examples of these materials are listed in Table 1.3. Graphite is widely used as anode material due to the low potential of the reaction with lithium. The reaction can be simply expressed as:

$$C + xLi \rightleftarrows LixC \tag{1-10}$$

The ionic intercalation phenomena into graphite are not completely understood, but it is widely accepted that the Li intercalation into graphite mainly follows the Daumas-Hérold model[8], Figure 1.7. The intercalation/deintercalation process is a multi-stage process with the successive formation of LiC_{72}, LiC_{36}, LiC_{12}, and LiC_6. The maximum theoretical capacity for graphite is 372 mAh/g with the formation of LiC_6.

Three categories of intercalation materials have been widely used: layered, spinel, and olivine, Figure 1.8. In olivine family, for example, $LiFePO_4$, the lattice allows diffusion of Li-ion in octahedral sites in a 1D channel along a curved trajectory. In transition-metal oxides (these include lithiated transition metal oxides of the form $LiMO_2$), the material alternates between transition-metal and Li (or vacancies) in the octahedral sites (O), allowing 2D Li diffusion. Spinels are structurally related to the layered oxides. For example, in $Li_xMn_2O_4$, the unit cell is composed of a cubic close-packed array of oxygen atoms and edge-sharing MnO_6 octahedra. However, whereas the layered oxides

have all-metal octahedra in the same plane, each plane in the spinel has half of the possible octahedral sites occupied by Mn atoms (Figure 1.8c). This forms a 3D diffusion network for the inserted ions, with octahedral interstitial sites connected by vacant tetrahedral sites [9].

Table 1.3. Intercalation electrode materials.

	Material	Structure	Average voltage (V vs Li)	Practical capacity (mAh/g)	Date first reported	Reference
Cathodes	$LiCoO_2$	Layered	3.9	140	1980	[10]
	$LiMn_2O_4$	Spinel	4.1	120	1983	[11]
	LiFePO	Olivine	3.45	160	1997	[12]
	$LiNi_{1/3}Mn_{1/3}Co_{1/3}O_2$	Layered	3.8	200	2001	[13]
	$LiNi_{0.8}Co_{0.15}Al_{0.05}O_2$	Layered	3.8	200	2003	[14]
Anodes	Graphite (LiC_6)	Layered	0.1	360	1983	[15]
	$Li_4Ti_5O_{12}$	Spinel	1.5	175	1994	[16]

1.4.2 Alloying reaction electrodes

Alloy anodes are well known for their high specific capacity, compared to graphite or $Li_4Ti_5O_{12}$. The alloying reaction of elements such as Sn and Si with lithium follows the reaction:

$$A + xLi \rightleftarrows Li_xA \tag{1-11}$$

where A is Sn or Si, x may reach 4.4. This reaction involves a huge volume expansion (>300%). This change produces a mechanical instability of these electrodes upon cycling, which leads to poor cycle stability. Another quality of alloying electrodes is the low

potential reaction, lower than 1 V (vs Li). Different metals can be used as electrode materials, Si, Sn, Sb, Al, Mg, Bi, In, Zn, Pb, Ag, Cd, As, Ga and Ge. However, the research is focused on cost effective, abundant, and environmentally friendly materials. Properties of several materials are listed in Table 1.4.

Some strategies have been reported to overcome the volume expansion induced problems, such as reduction of particle size [17], the introduction of a buffer layer in the metals [18]. Also, it was found that some nanostructures such as Si nanowires, carbon–Si composites, use of specific binders and choice of unique electrolyte solutions may enable the fabrication of highly stable composite silicon electrodes that can demonstrate very high capacities and impressive cycle life [19], [20].

Table 1.*4. Alloying electrode materials* [21].

Materials	Si	Sn	Sb	Al	Mg	Bi
Density ($g\,cm^{-3}$)	2.33	7.29	6.7	2.7	1.3	9.78
Lithiated phase	$Li_{4.4}Si$	$Li_{4.4}Sn$	Li_3Sb	LiAl	Li_3Mg	Li_3Bi
Theoretical specific capacity ($mAh\,g^{-1}$)	4200	994	660	993	3350	385
Theoretical charge density ($mAh\,cm^{-3}$)	9786	7246	4422	2681	4355	3765
Volume change (%)	320	260	200	96	100	215
Potential vs. Li (~V)	0.4	0.6	0.9	0.3	0.1	0.8

1.4.3 Conversion reaction electrodes

The concept of conversion reaction electrodes was introduced for lithium reacting with transition metal oxides [22]. The conversion reaction can be expressed as follows:

$$M_aX_b + (b \cdot n)Li \rightleftarrows aM + bLi_nX \qquad (1\text{-}12)$$

where M=transition metal, X= anion, and n= oxidation state of X. Since then, several studies have reported for different reversible conversion reactions with X= O, N, F, S, P, and H. Conversion reaction electrode experiences a conversion to a different phase. This can produce a higher volume change compared to intercalation electrodes but smaller than alloying reaction electrodes. A representation of this mechanism is depicted in Figure 1.9. In the same concept of conversion reactions, some can be expressed as follows

$$X + aLi \rightleftarrows Li_aX \quad (1\text{-}13)$$

This is the case of some chalcogens such as S, Se, and Te, and halogens such as Br and I. S have been considered as a promising candidate as cathode material for Li rechargeable batteries. Sulfur has a very high capacity of 1672 mAh/g. [23]

Metal oxides have been studied as potential anode materials due to the low potential reaction. The reaction potential of the conversion reaction is strongly dependent on the atomic number of the transition metal and the anionic species, Figure 1.10. The calculated emf for specific anion increases as the atomic number of transition metal increases. Therefore, some transition metal fluorides and oxyfluorides such as FeOF, have been investigated as potential cathode materials.

1.4.3.1 Metal hydrides

Figure 1.11. shows the typical low reaction voltage for metal hydrides compared to other conversion reaction materials. Metal hydrides are suitable materials for negative

electrodes because of the low potential reaction. Metal hydrides as conversion reaction electrode materials were introduced in 2008 by Oumellal [24]. MgH_2 shown a large and reversible capacity during the performance of the first cycle. This demonstration of MgH_2 as conversion electrode was carried out using the liquid electrolyte. Other binary hydrides also have been studied, for example, TiH_2 and AlH_3, as well as ternary metal hydrides based on Mg and Al [25]. From the thermodynamics point of view, the conversion reaction can be expected when:

$$\frac{\Delta G_f(MH_x)}{x} > \Delta G_f(LiH) \tag{1-14}$$

for

$$MH_x + xLi \rightleftarrows M + xLiH \tag{1-15}$$

MgH_2 as an active electrode material, have a high theoretical capacity suitable as the negative electrode. Figure 1.12 shown a comparison of the theoretical capacity of different metal hydrides, where MgH_2 has a higher theoretical capacity (2036 mAh/g) higher than other binary metal hydrides. Based on the applications mentioned before, it is important to have compact and light systems. Capacity can be expressed in terms of size or weight. Specific capacity represents a relation between the available energy in the system and the weight of the system. An energy storage system with high specific energy means a light system and a system with lower specific capacity means a heavier system. It is typically expressed in terms of Ah/kg or mAh/g. On the other hand, volumetric capacity is the ratio between the same available energy but related to the volume occupied

by the system. In this way, a system with a high volumetric capacity is a small system and a system with a lower specific capacity means a bigger system. The units used for volumetric capacity are Ah/m^3 or mAh/l. In transportation, a vehicle with a compact energy storage system represents more space that can be used by the users, it can be used to transport more passenger or load. And a car with a lighter energy storage system can drive a longer range every charge. Also, power of the batteries can be expressed in terms of size or weight, with a similar interpretation as well as capacity but about the power of the system.

Recently, FeTiH system was studied as a collaborative work considering potential conversion electrode material. Following the conversion reaction

$$FeTi + LiH \rightleftarrows FeTiH_2 + 2Li$$

$FeTiH_2$ has a theoretical capacity of 551 $mAhg^{-1}$. Figure 1.13 shows the discharge/charge curves for this system operating at 120 °C. The capacities released during the first discharge was 418 $mAhg^{-1}$ (75.8% of the theoretical capacity). The half-cell shows the characteristic low potential reaction for metal hydrides electrodes, in this case, 0.7~0.6 V. According to the results, the conversion reaction formed FeTiH and the excess of LiH was decomposed through cycling. The clear plateau observed at ~0.7 is similar to the theoretical 0.8 V of LiH decomposition. It explains why the capacity decreased ~40% after just some cycles and then is stabilized around 300 $mAhg^{-1}$, as shown in Figure 1.14. From XRD patterns (Figure 1.13b) significant changes were not observed. Varying the

ratio LiH/FeTi was observed the capacity of the cell increased for electrodes with a higher concentration of LiH, but in all cases, the same effect occurred. An initial reaction potential was observed during the first discharged (0.6-0.7V) corresponding to FeTiH. Then the rest of capacity decreases through cycling, and this capacity could correspond to carbon in the composite electrode.

Not all the metal hydrides can be used as conversion reaction, and ternary hydrides imply in some cases formation of stable hydrides from the initial materials. That is the case of Mg_2FeH_6 reported by Huen et al. [26]. In other cases, some metal hydrides own suitable ionic conductivity properties and can be used as solid electrolytes. Several studied cases of metal hydrides in Li-ion batteries are listed in Table 1.5. $LiBH_4$ is the most representative electrolyte material.

Table 1.5. Metal hydrides in Li-ion batteries [27].

Battery anode ll cathode/operation temperature (K)	Hydride/role	First discharge capacity (mAh/g)	*n*th discharge capacity (mAh/g)	Capacity retention (%)/*n* (number of cycles)
Li-ion batteries				
Li ll $LiCoO_2$/393	$LiBH_4$/solid state electrolyte	89	30th/86	97/*n* = 30
Li ll $LiCoO_2$/353	$LiBH_4$–C_{60} nanocomposite/solid state electrolyte	10.4	5th/~10	~96/*n* = 5
Li ll $LiCoO_2$/323	$Li_2B_{12}H_{12}$/solid state electrolyte	~64	5th/~54	60/*n* = 20
Li ll $Li_4O_5O_{12}$/333	$Li_4(BH_4)_3I$/solid state electrolyte	142	10th/110	77/*n* = 10
Li ll $Li_4O_5O_{12}$–$Li_4(BH_4)_3I$/296	$Li_4(BH_4)_3I$/solid state electrolyte	122	5th/111	91/*n* = 5
Li ll $Li_4O_5O_{12}$–$Li_4(BH_4)_3I$/423	$Li_4(BH_4)_3I$/solid state electrolyte	179	2nd/158	78/*n* = 100
Li ll $LiCoO_2$–$80Li_2S{\cdot}20P_2S_5$/298	$Li_4(BH_4)_3I$/solid state electrolyte	92	20th/82	90/*n* = 20
Li ll $LiNi_{1/3}Mn_{1/3}Co_{1/3}O_2$–$Li_3BO_3$ without an adhesive layer/423	$Li_4(BH_4)_3I$/solid state electrolyte	56	10th/16	29/*n* = 10
Li ll $LiNi_{1/3}Mn_{1/3}Co_{1/3}O_2$–$Li_3BO_3$ with the $LiBH_4$–$LiNH_2$ adhesive layer/423	$Li_4(BH_4)_3I$/solid state electrolyte	114	10th/81	71/*n* = 10
Li ll S–$LiBH_4$/393	$LiBH_4$/solid state electrolyte	1140	45th/730	64/*n* = 45
Li ll S/373	$Li_4(BH_4)_3Cl$/solid state electrolyte	1377	5th/636	46/*n* = 5
Li ll S/328	Nanoconfined $LiBH_4$/solid state electrolyte	>3000	2nd/1570	78/*n* = 70
LiIn ll S–$LiCe(BH_4)_3Cl$/318	$LiCe(BH_4)_3Cl$/solid state electrolyte	1196	9th/510	43/*n* = 9
Li ll TiS_2–$LiBH_4$/393	$Li_2B_{12}H_{12}$/solid state electrolyte	80	2nd/205	98/*n* = 200
Li ll TiS_2–Li ll TiS_2–$LiBH_4$/393	$Li_4(BH_4)_3I$/solid state electrolyte	49	2nd/141	54/*n* = 15
LiIn ll TiS_2/300	$90LiBH_4{\cdot}10P_2S_5$/solid state electrolyte	192	2nd/228	98/*n* = 10
Li ll TiS_2–$Li_4(BH_4)_3I$–$90LiBH_4{\cdot}10P_2S_5$/303	$Li_4(BH_4)_3I$–$90LiBH_4{\cdot}10P_2S_5$/solid state electrolyte	~650	2nd/~400	54/*n* = 3
Li ll TiS_2–$LiBH_4$/353	$Li_2B_{12}H_{12}$/solid state electrolyte	230	10th/~205	83/*n* = 20
Li ll TiS_2–$LiBH_4$/403	$LiCB_{12}H_{12}$/solid state electrolyte	240	5th/180	75/*n* = 5
TiH_2–$LiBH_4$ ll Li/393	$LiBH_4$/solid state electrolyte	1225	2nd/1094 10th/1035	80/*n* = 50
MgH_2–$LiBH_4$ ll Li/393	$LiBH_4$/solid state electrolyte	1488	93rd/270	18/*n* = 93
MgH_2–$LiBH_4$–Nb_2O_5 ll Li/393	$LiBH_4$/solid state electrolyte	1586	100th/700	44/*n* = 100
MgH_2–$LiBH_4$–C-nanofiber ll Li/393	$LiBH_4$/solid state electrolyte	1728	3rd/1889	59/*n* = 50
MgH_2–CoO_2–$LiBH_4$ ll Li/393	$LiBH_4$/solid state electrolyte	~1200	2nd/~950	~58/*n* = 21
MgH_2 ll Li/303	$Li_4(BH_4)_3I$–$90LiBH_4{\cdot}10P_2S_5$/solid state electrolyte	~750	2nd/~625	~89/*n* = 3
Mg_2FeH_6–$LiBH_4$ ll Li/–	$LiBH_4$/solid state electrolyte	1254	2nd/~625	~24/*n* = 10
$0.8MgH_2$–$0.2TiH_2$–$LiBH_4$ ll Li_2S–$LiBH_4$/393	$LiBH_4$/solid state electrolyte	910	25th/780	86/*n* = 25
Al–$LiBH_4$ ll Li/408	$LiBH_4$/solid state electrolyte	895	2nd/~500	~11/*n* = 10
Bi_2Te_3–$LiBH_4$ ll Li/–	$LiBH_4$/solid state electrolyte	550	...	...
Si–C ll Li/353	$LiBH_4$–C_{60} nanocomposite/solid state electrolyte	3480	2nd/~900	~26/*n* = 2
$Mg(BH_4)_2$ ll Li/–	$Mg(BH_4)_2$/active anode material	~520	2nd/~600	...
$NaBH_4$ ll Li/–	$NaBH_4$/active anode material	~212	2nd/~225	...
$LiAlH_4$ ll Li/RT	$LiAlH_4$/active anode material	1180	...	–*n* = 1
Li_3AlH_6 ll Li/RT	Li_3AlH_6/active anode material	900	...	–*n* = 1
$NaAlH_4$ ll Li/RT	$NaAlH_4$/active anode material	~1700	...	...
$NaAlH_4$ ll Li/RT	Nanoconfined $NaAlH_4$/active anode material	~525	2nd/440	71/*n* = 20
$NaAlH_4$ ll Li/RT	Nanoconfined $NaAlH_4$/active anode material	...	...	46/*n* = 20
Na_3AlH_6 ll Li/RT	Na_3AlH_6/active anode material	...	...	...
$LiNa_3AlH_6$ ll Li/RT	$LiNa_3AlH_6$/active anode material	1872	...	...

1.5 Solid electrolytes

Safety of energy storage systems is an important issue to be solved in current technology. Commercial technology uses organic liquid electrolytes for the transportation of Li-ions between electrodes, this flammable component has produced most of the safety problems of this technology. However, this material also allows the battery operations with high efficiency. Solid electrolytes are an alternative for the safety issues associated with liquid electrolytes and can provide systems with higher volumetric capacities (smaller systems) [28]–[30].

1.5.1 $LiBH_4$

$LiBH_4$ exhibits an outstanding ionic conductivity at high temperatures. However, the high conductive phase undergoes through a structural change from hexagonal to orthorhombic when the temperature is below 117 °C. The low-temperature phase (LT) is characterized by low ionic conductivity. The dependence of the ionic conductivity with temperature is shown in Figure 1.15. The change in ionic conductivity affects the viability of using $LiBH_4$ as a solid electrolyte for room temperature batteries drastically. Table 1.5, shown multiple cases where $LiBH_4$ was used as a solid electrolyte for different electrodes. The case of $LiBH_4$ working with MgH_2 was presented by Zeng in 2015 with a notable capacity and cyclability. These results were obtained at 120 °C due to the limitations of $LiBH_4$.

An alternative to keeping the high conductivity phase of $LiBH_4$ at low temperatures is the stabilization of its HT phase using halides. Replacing a fraction of BH_4^- anions by halide anions (I^-, Br^- or Cl^-) stabilizes the hexagonal structure and leads to high conductivity. Figure 1.16 shows more symbolic cases. The case of $3LiBH_4$•LiI shown the best conductivity compared to other halides ($2x10^{-4}$ S cm^{-1} at room temperature) [31].

1.5.2 LPS

Glass-ceramic composite electrolyte $XLi_2S+(1-X)P_2S_5$ known as LPS has been reported with high conductivities at room temperatures, higher than $LiBH_4$ at room temperature. Figure 1.17 shown the temperature dependence of LPS ionic conductivity. The composite $80Li_2S+20P_2S_5$ and $75Li_2S+25P_2S_5$ have been used for different studies.

The case of LPS combined with MgH_2 was reported by Ikeda *et al.* [32]. During initial discharge, the capacity obtained was almost the theoretical capacity of MgH_2, but it showed problems during the reversible process at high and low temperature. The remarkable point from this study was the use of Nb_2O_5 as the catalyst for the conversion reaction. The use of Nb_2O_5 improved the kinetics of the reaction.

An interesting modification is obtained by adding GeS_2, to obtain a LGPS composite electrolyte, which has a higher conductivity [33]. It showed good results combined with a TiS_2 electrode. Some other interesting composite electrolytes based on

$LiBH_4$ and LPS have also been reported. Yamauchi *et al.* reported the $33(LiBH_4)+67(LPS)$ [34] and Unemoto et al. reported the $90LiBH_4$-$10P_2S_5$ [35]. Both are compared in Figure 1.18 with other solid electrolytes. Recently, combinations such as LPS+$LiBH_4$•LiI have shown an improvement in the reversibility of metal hydride electrodes and the possibility of operation at room temperatures [36].

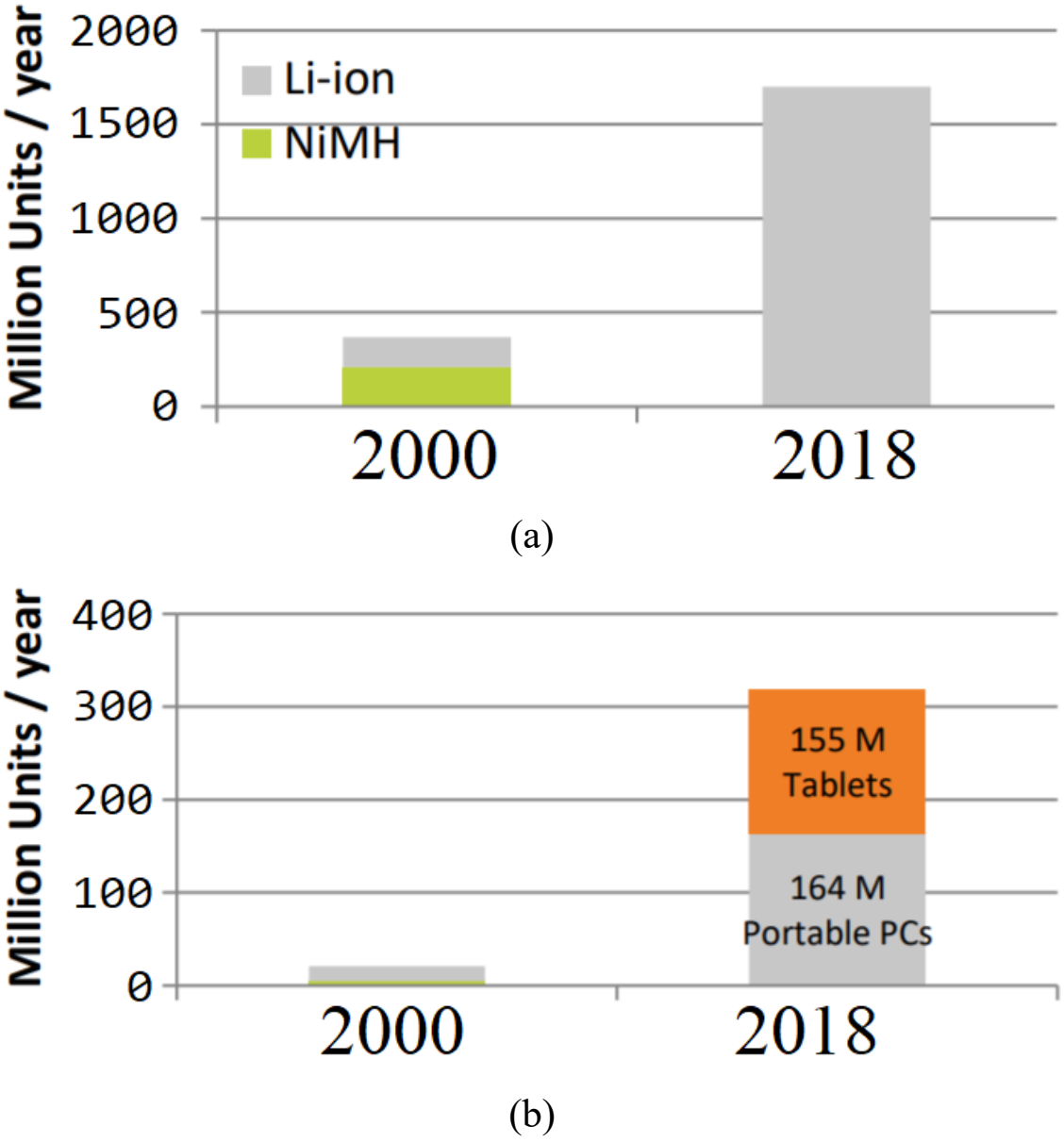

Figure 1.1. (a) Cellular phones sold per year. (b) Portable PC sold per year [6].

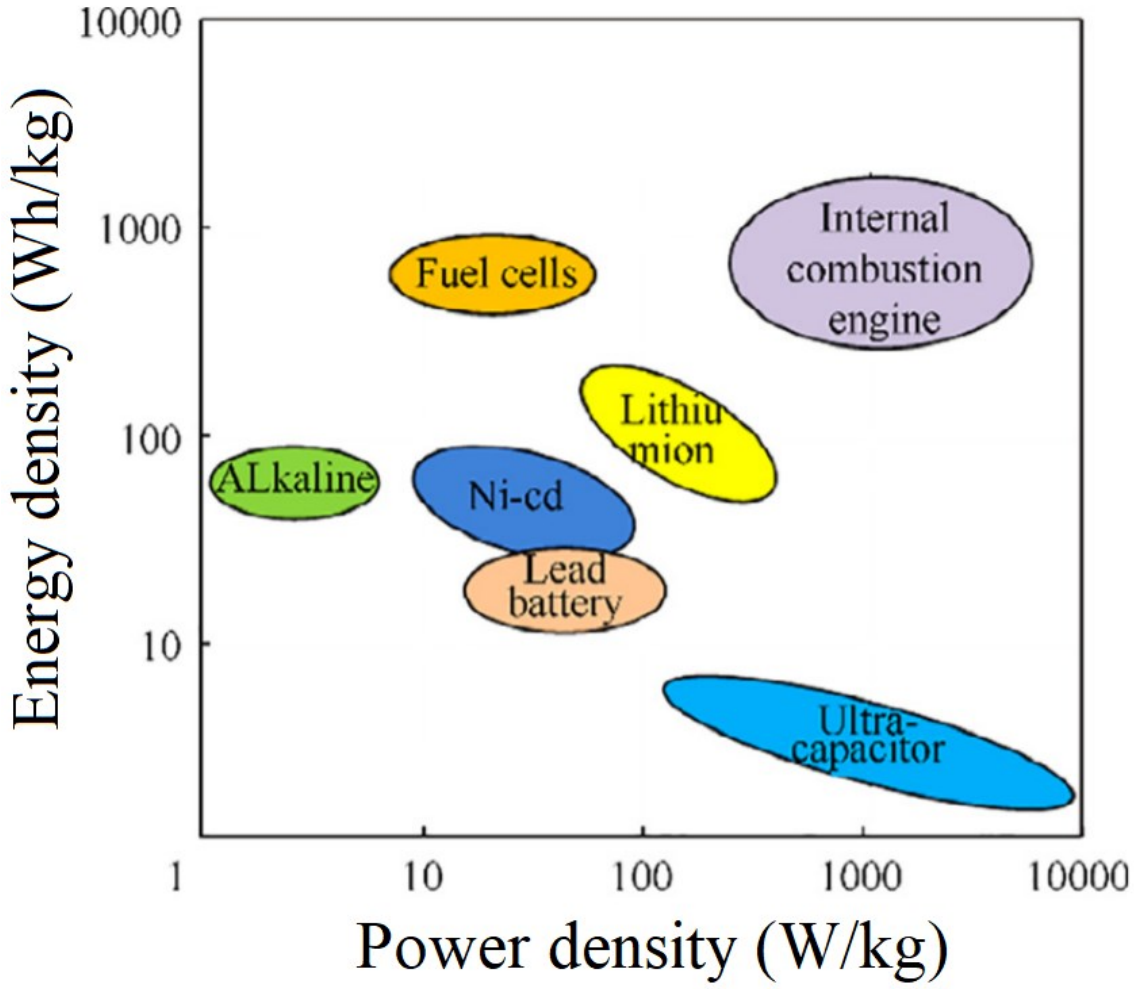

Figure 1.2 A comparison of power and energy density of fuel cell, batteries and UC [37].

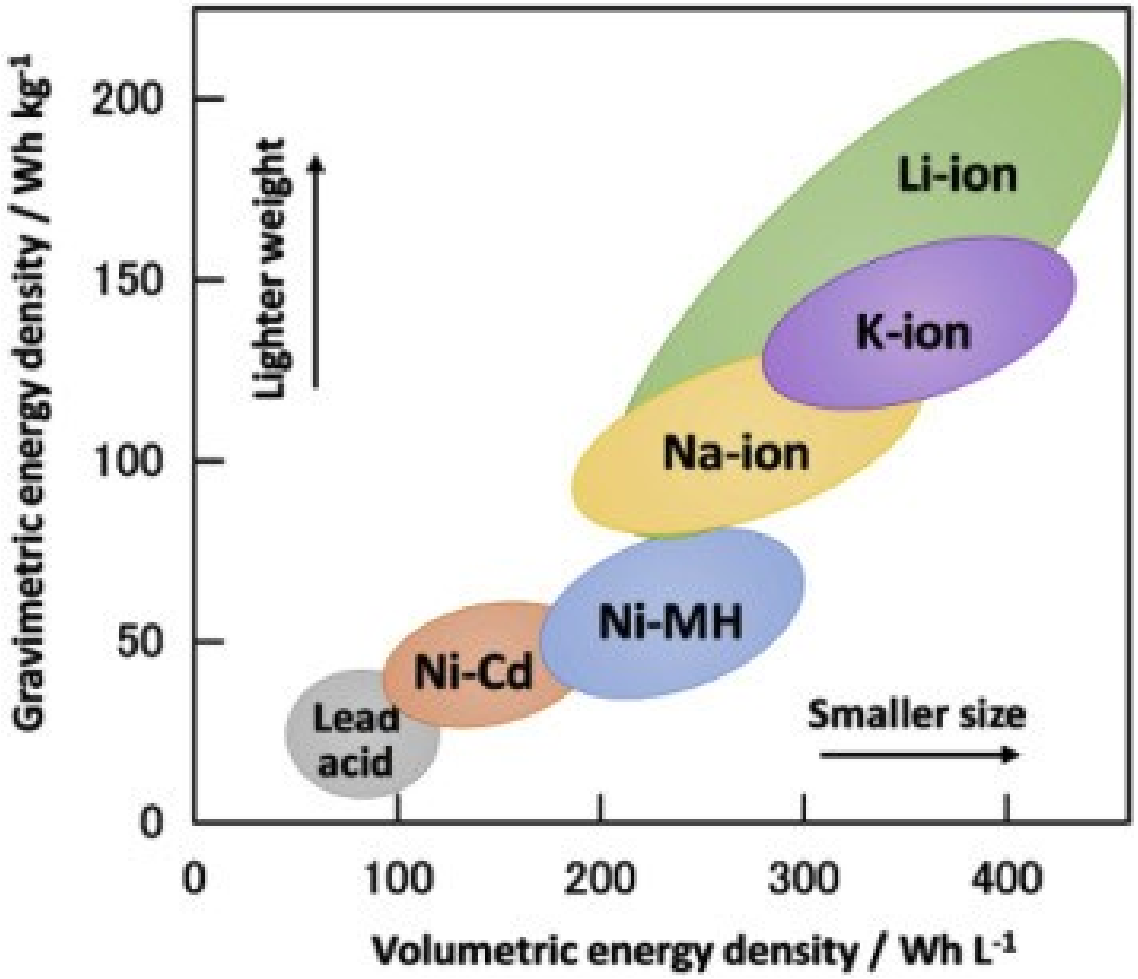

Figure 1.3. The energy density of commercial batteries (Lead-acid, Ni-Cd, Ni-*M*H and Li-ion) as well as novel monovalent technologies (Na-ion and K-ion) [38].

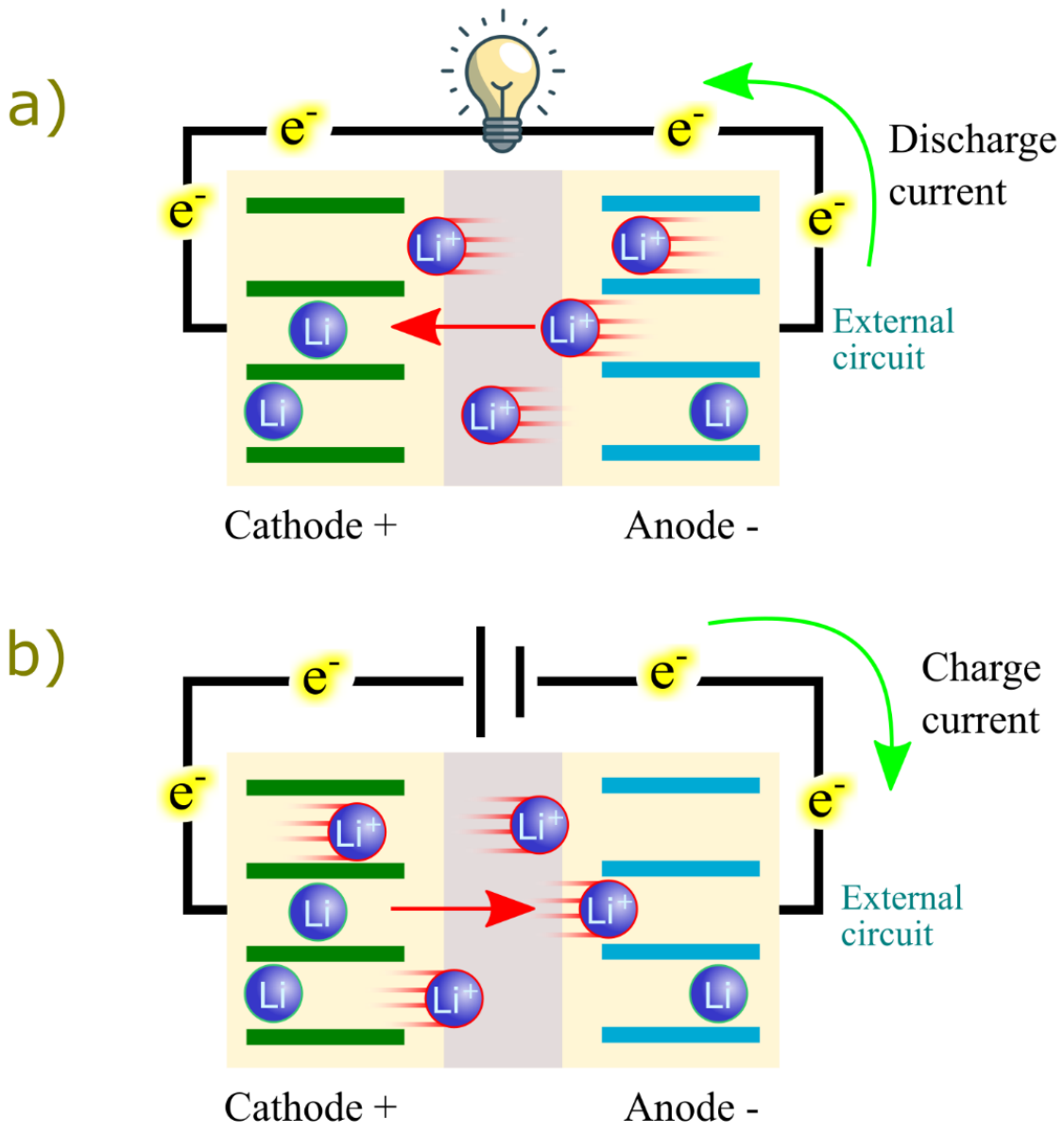

Figure 1.4. Schematic representation of Li-ion battery during operation.

Discharge process (a) and charge process (b).

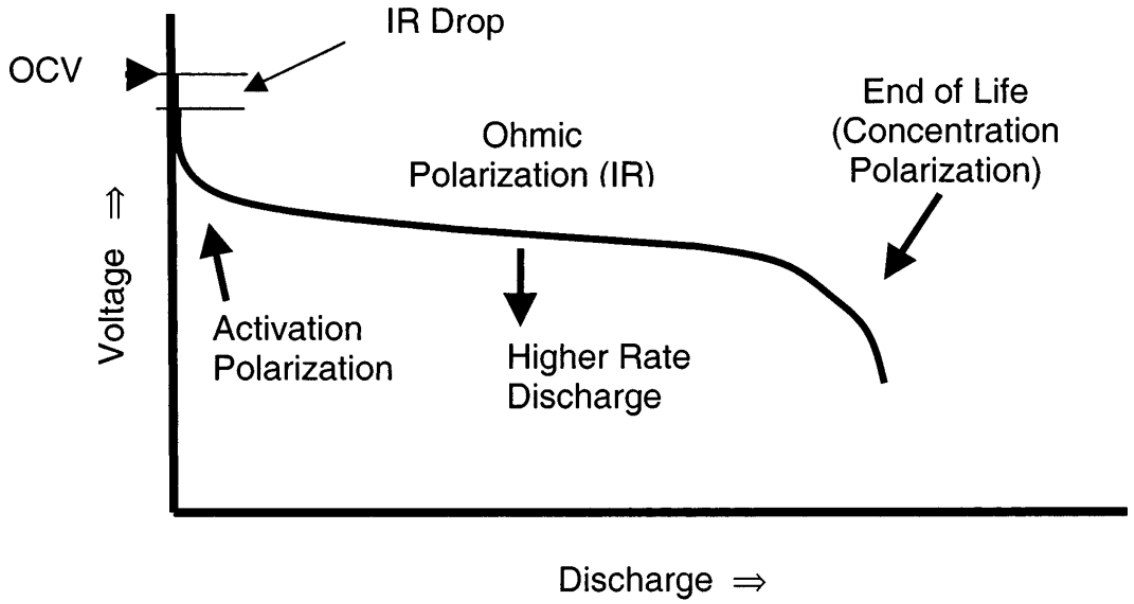

Figure 1.5. Typical discharge of a battery, showing the influence of the various types of polarization [39].

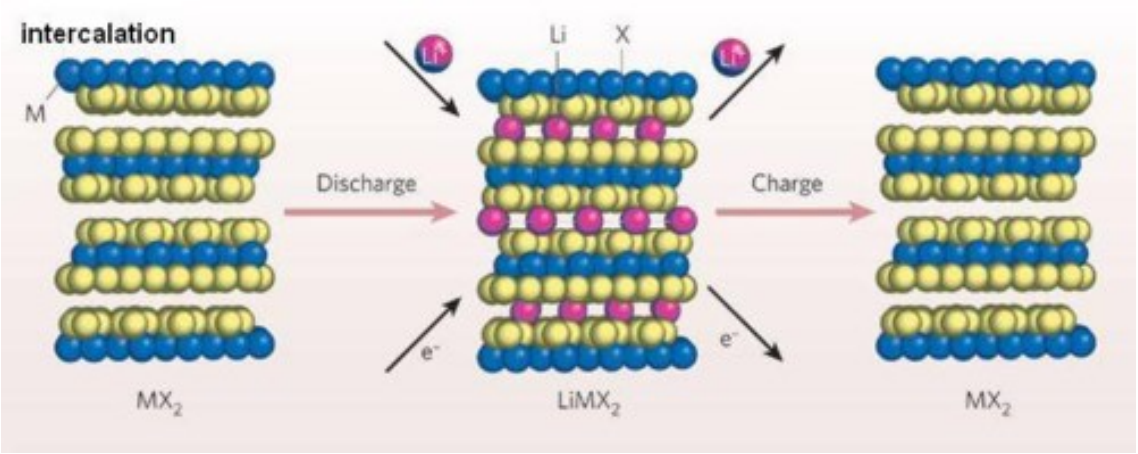

Figure 1.6. Illustration of insertion/de-insertion process in intercalation electrodes[40].

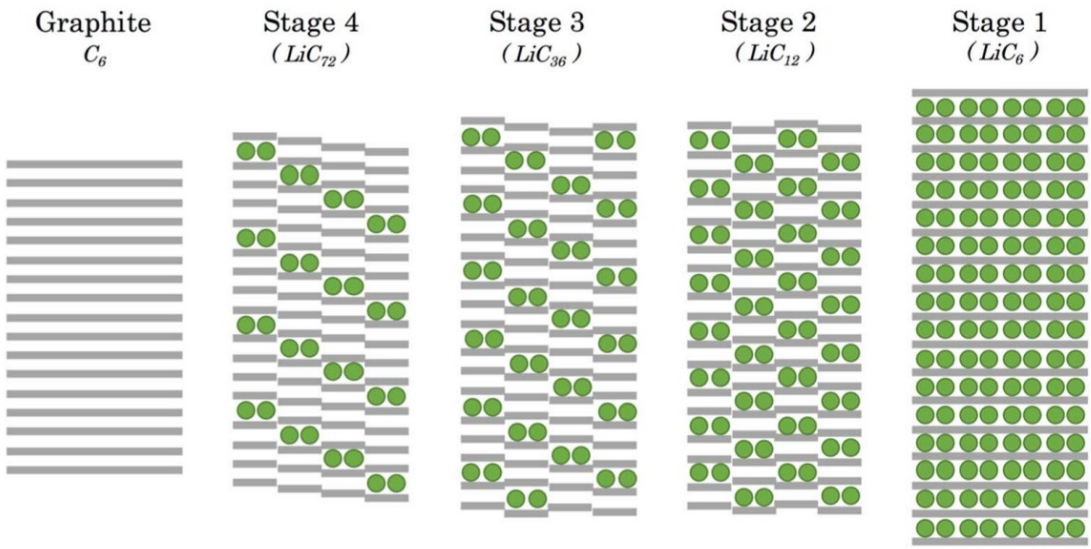

Figure 1.7. Classical representation of Li insertion stages into graphite and based on the Daumas-Hérold model[8].

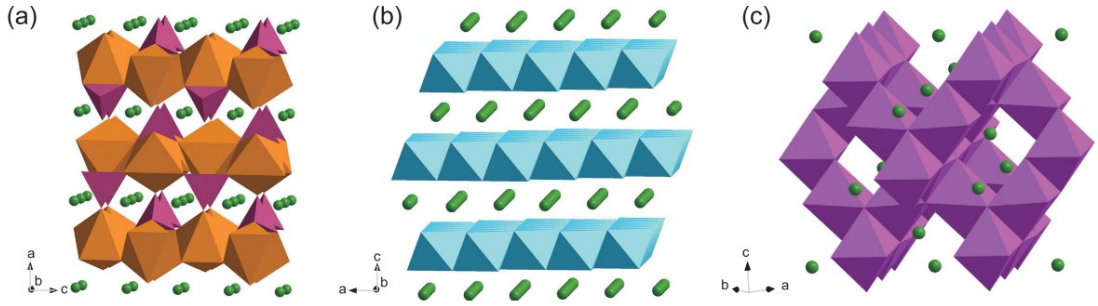

Figure 1.8. Crystal structure for (a) olivineLiFePO4 (Li in green, FeO6 in brown, PO4 in purple), (b) layered LiCoO2 (CoO6 in blue) and (c) spinel LiMn2O4 (MnO6 in magenta), which have 1D, 2D, 3D diffusion channels, respectively [9].

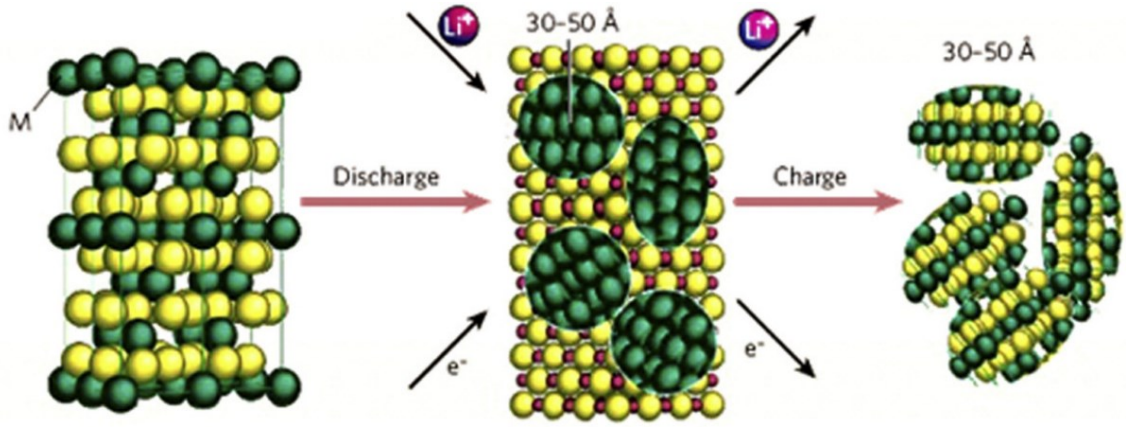

Figure 1.9. Representation of evolution of conversion reaction electrode [40].

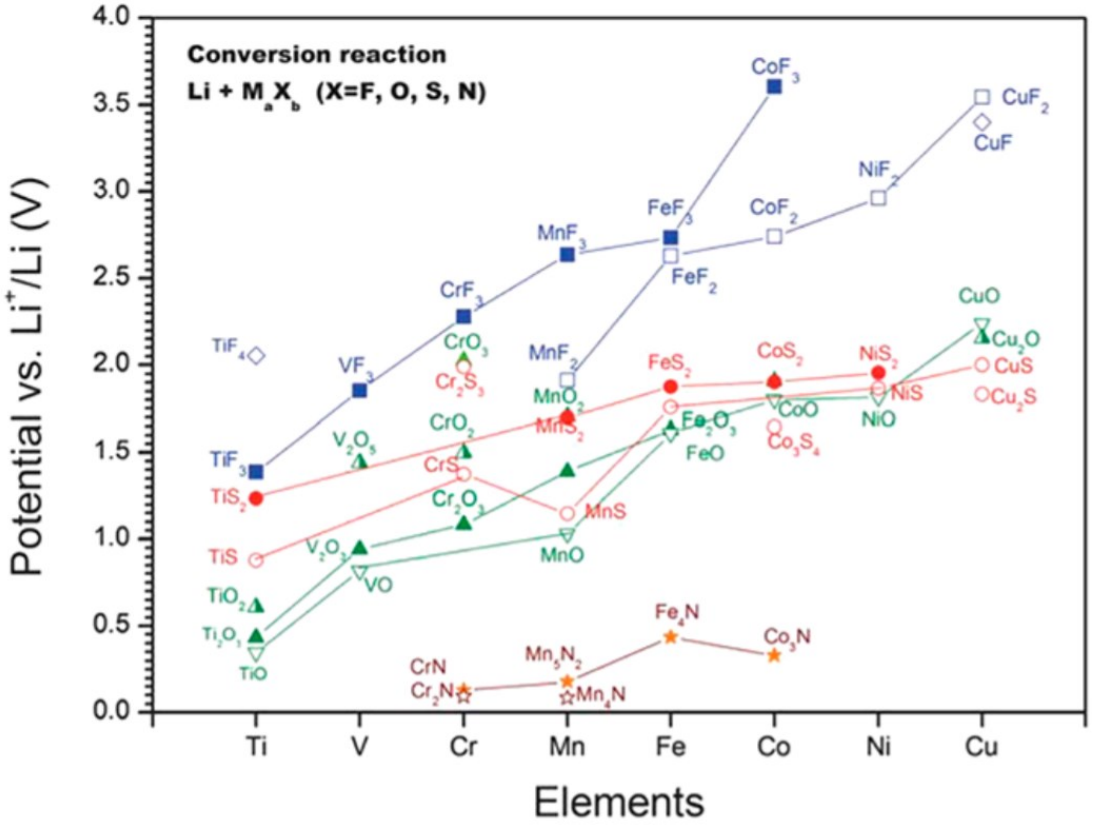

Figure 1.10. Calculated emf of the binary metal compound for conversion reactions [41].

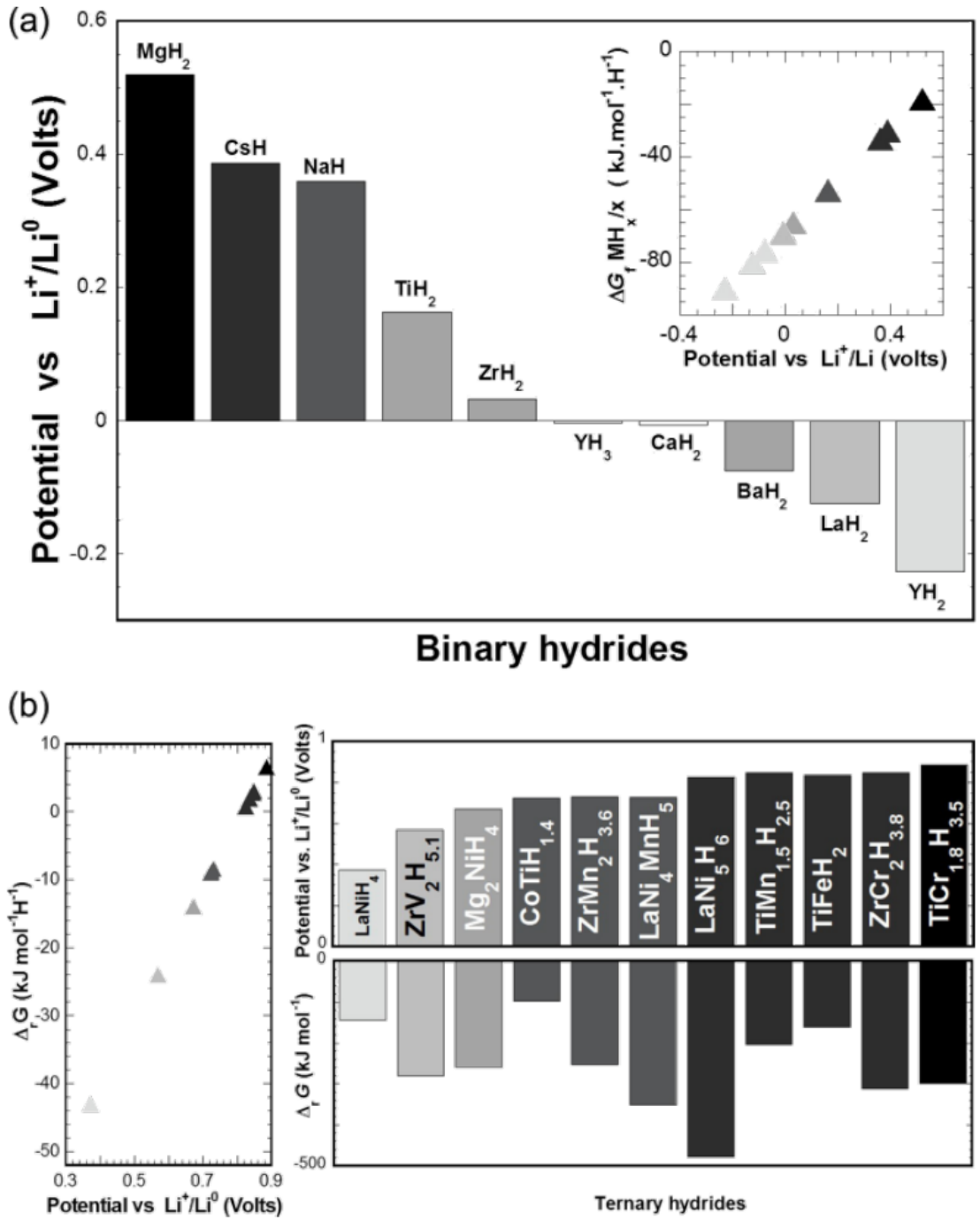

Figure 1.11. Potential and Gibbs free energy of conversion reaction:
(a) binary hydrides, (b) ternary hydrides [42].

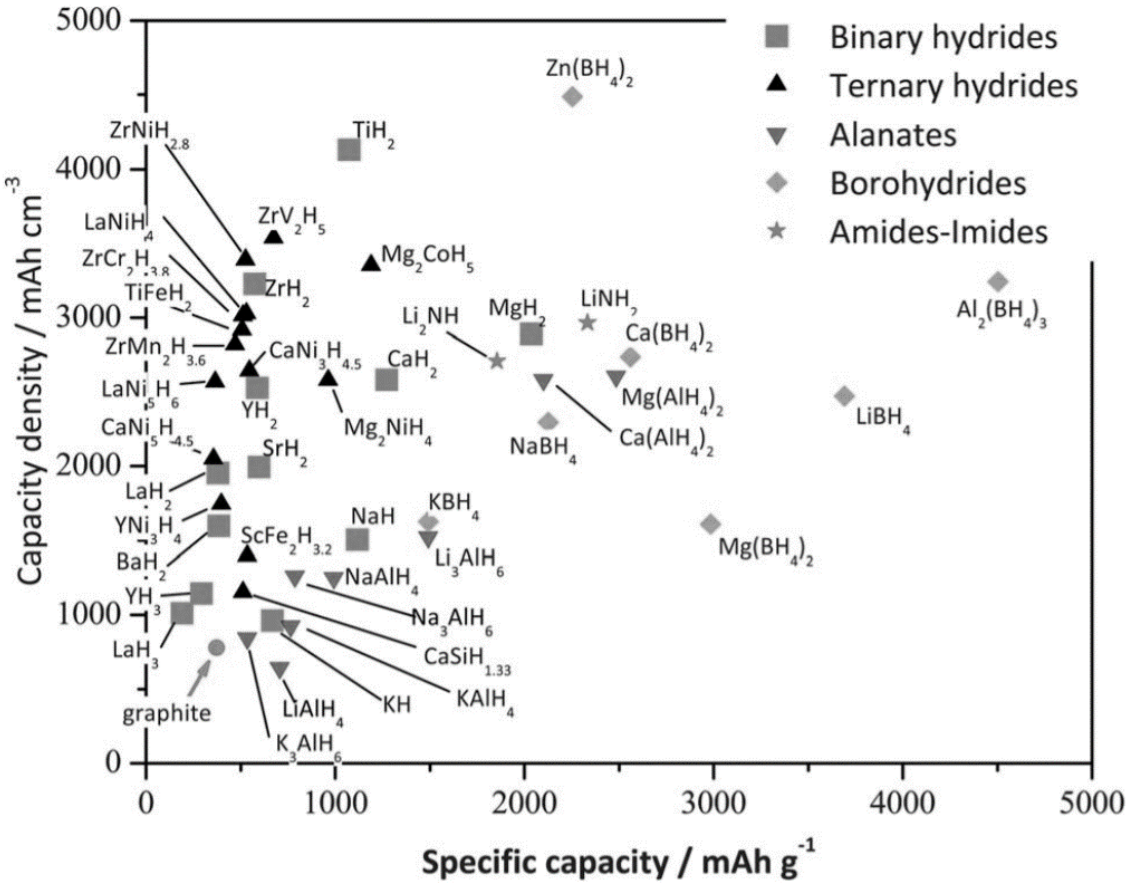

Figure 1.12. The estimated energy storage capacity of metal hydrides [43].

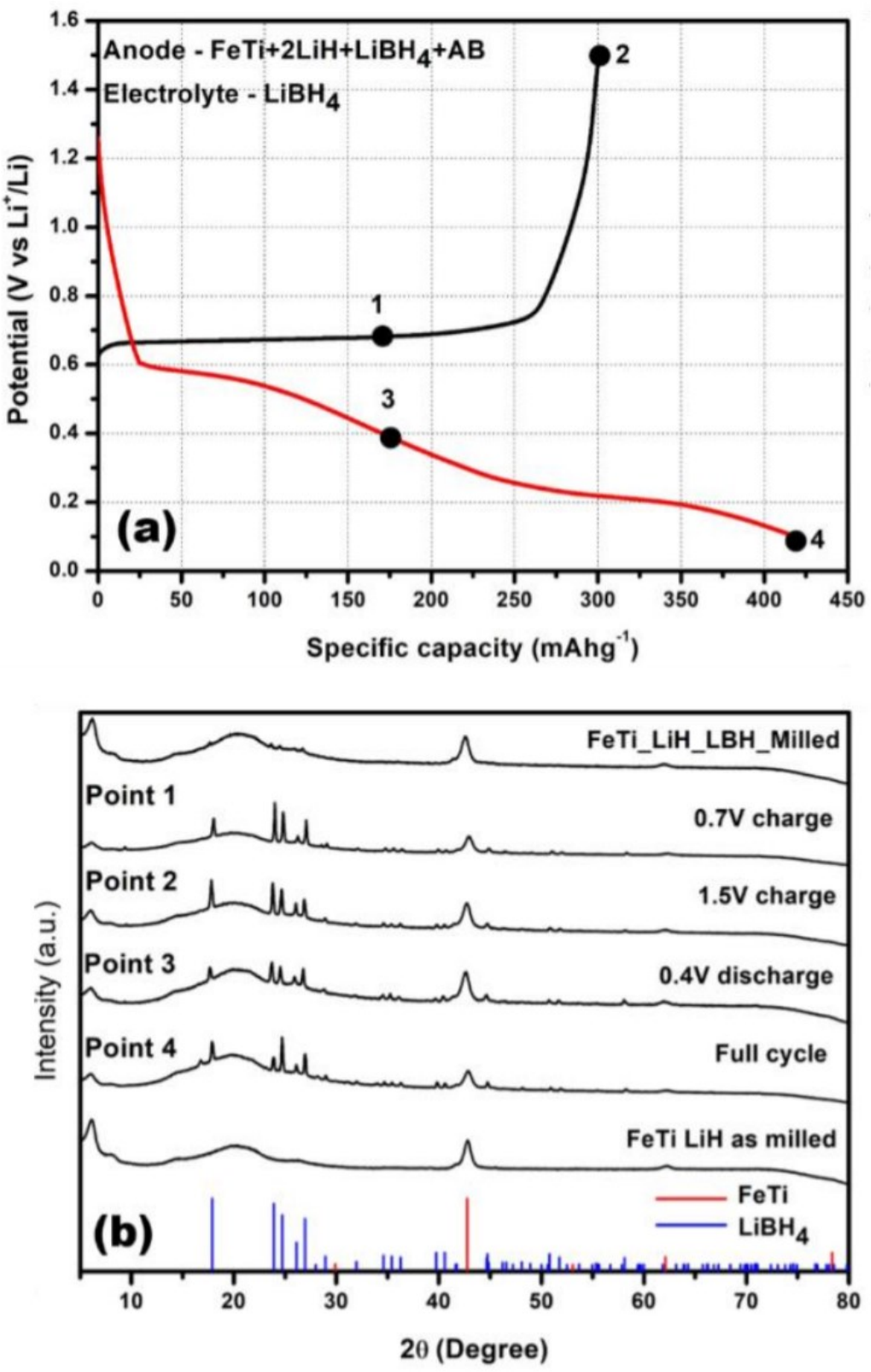

Figure 1.13. (a) The first charge-discharge curves for the FeTi-2LiH-$LiBH_4$_AB composite electrode in potential window 0.01-1.5V; (b) XRD pattern for different stages of electrochemical charging/discharging.

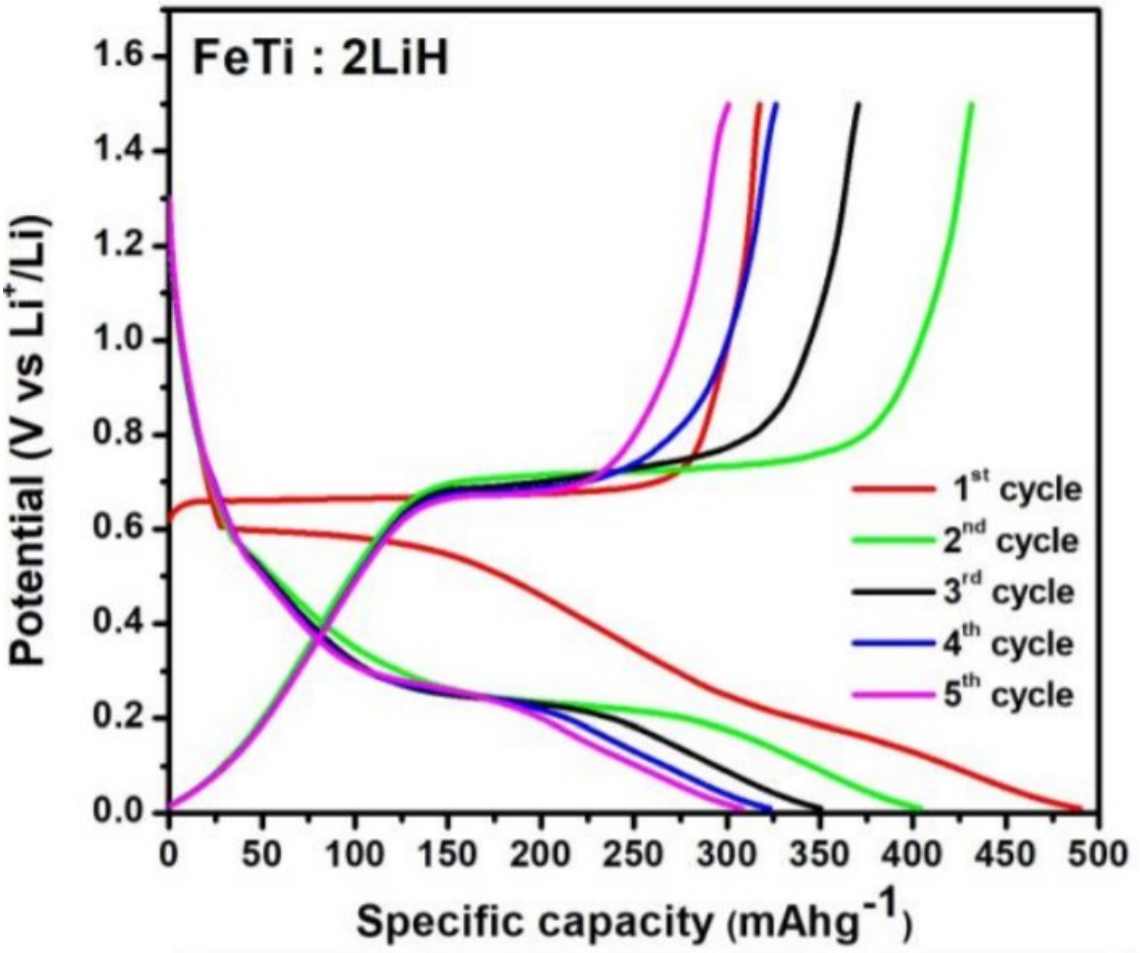

Figure 1.14. Electrochemical cycling up to 5 cycles.

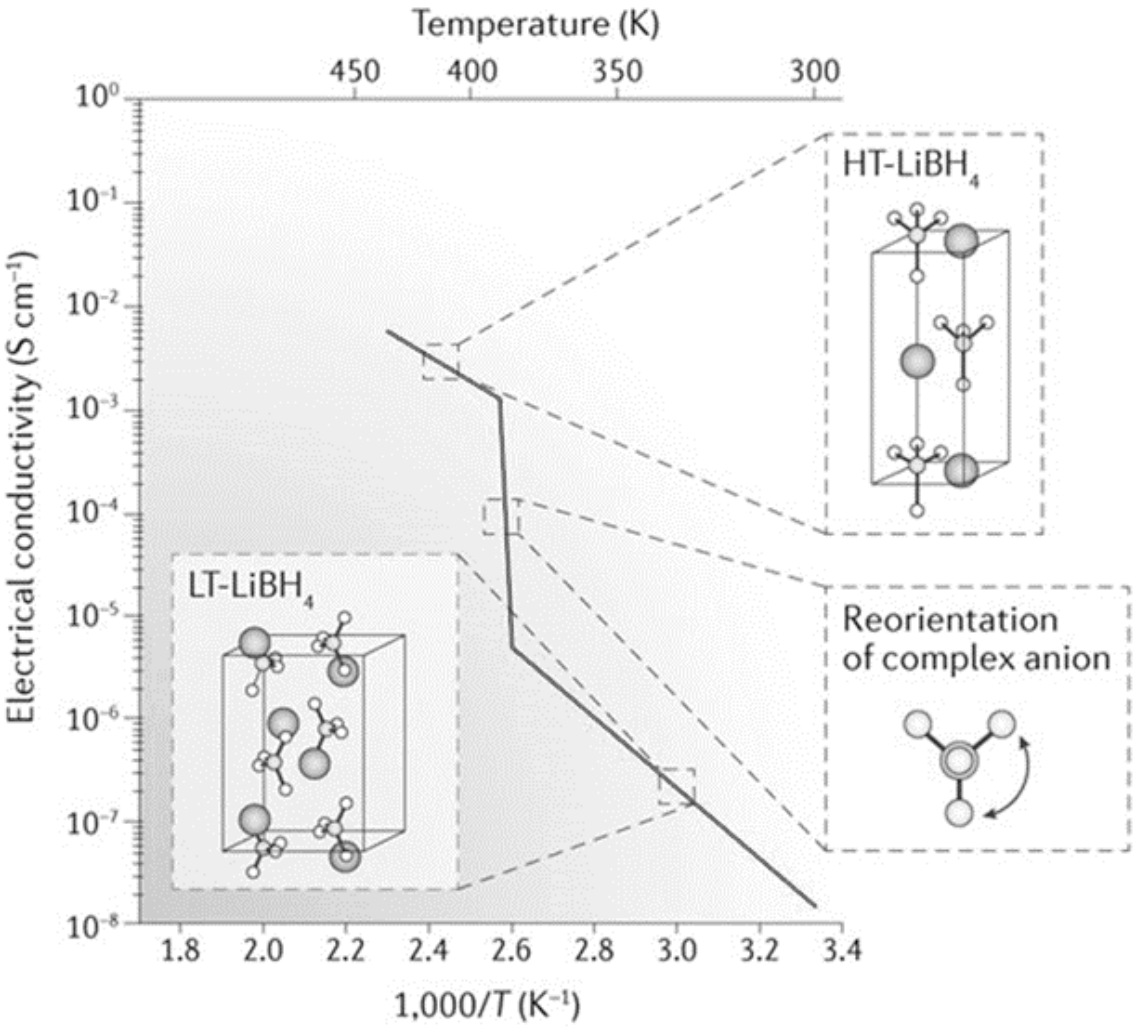

Figure 1.15. The LT-$LiBH_4$ to HT-$LiBH_4$ phase transition triggered by the reorientation of the complex anion with the corresponding Arrhenius plots illustrating changes in ionic conductivity [44].

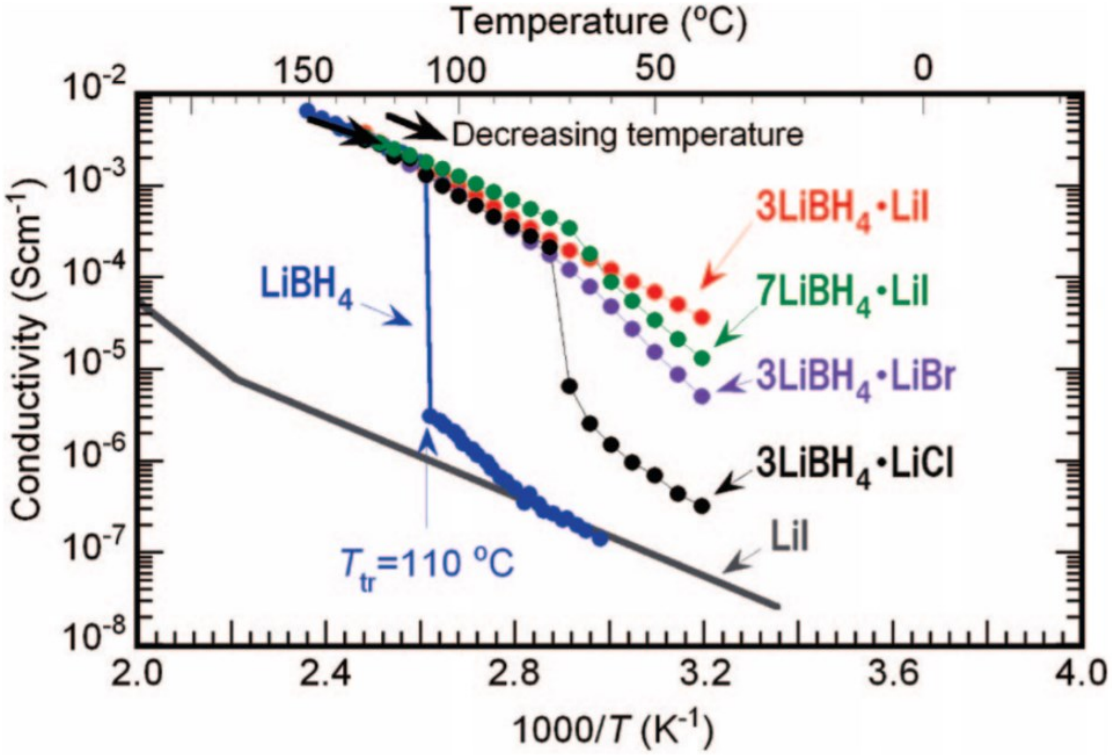

Figure 1.16. Ionic conductivities of $LiBH_4$, LiI, and LiBH4-LiX composites (X = Cl, Br, and I) obtained by ac impedance measurements with 100 mV of applied voltage from their decreasing temperature [45].

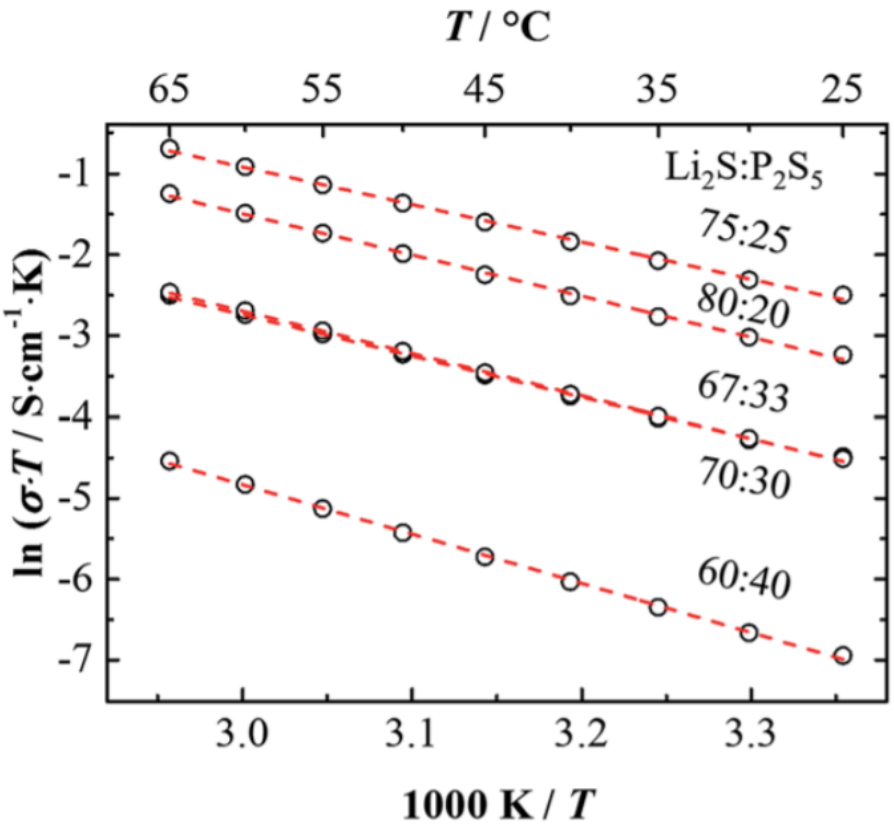

Figure 1.17. Arrhenius plots of the resultant σT of LPS glasses. The activation energy is determined from the slope of the fitted red line [46].

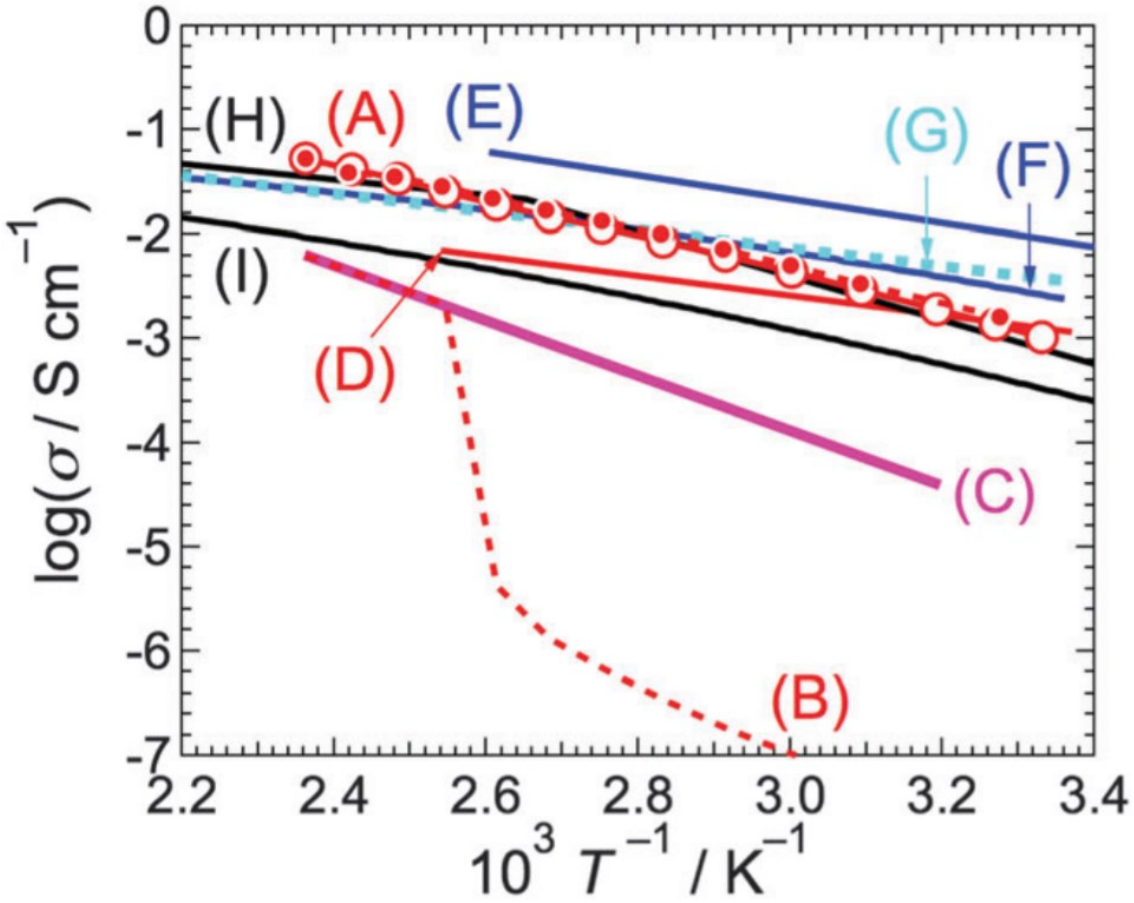

Figure 1.18. Lithium-ionic conductivities of (A) $90LiBH_4{:}10P_2S_5$, where closed and open symbols show the values obtained during heating and cooling runs, respectively [35], (B) $LiBH_4$ [47], (C) $Li_4(BH_4)_3I$ [45], (D) $33LiBH_4$–$67(Li_2S–P_2S_5$ glass) [34], (E) $Li_{10}GeP_2S_{12}$ [48], (F) $Li_7P_3S_{11}$ glass-ceramics [49], (G) $Li_{0.325}Ge_{0.25}P_{0.75}S_4$ (thio-LISICON) [50], (H)$Li_{0.34}La_{0.51}TiO_{2.94}$ [51], and (I) Li7La3Zr2O12 [52].

2 Purpose

Metal hydrides possesses suitable properties which enables their implementation as negative electrode for LIBS. Among metal hydrides, MgH_2 as conversion type of electrode material has a remarkable capacity (2036 mAh/g). This capacity is higher than the maximum capacity of conventional graphite electrodes (372 mAh/g). The present study focusses on MgH_2 as active material for all-solid-state Li-ion battery operating at room temperatures. $LiBH_4$, Li_2S, P_2S_5 and some of their mixtures were used as solid electrolytes. Li-ion batteries operating with MgH_2 as active electrode material have been reported using solid electrolytes mainly at high-temperature conditions (>120 °C). This temperature restriction is due to the limitation of ionic conductivity of solid electrolytes at room temperature. Some cases have been successfully obtained an operation of metal hydrides electrodes at room temperatures but with a poor cyclability. However, the recent progress in solid electrolytes has brought new electrolytes with suitable ionic conductivity at room temperatures. Many of them have been demonstrated for sulfide base electrodes, such as LiS_2 or TiS_2, but the compatibility with MgH_2, one of the most promising metal hydrides conversion electrode materials, has not been explored.

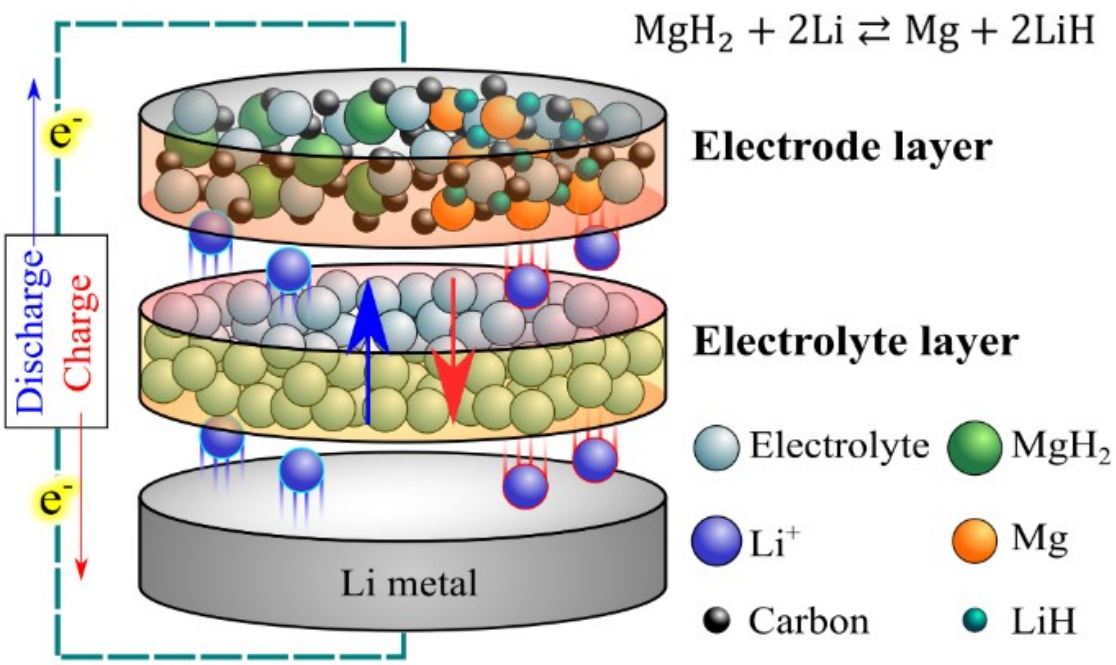

Figure 2.1. ASS-LIB scheme using MgH_2 as electrode active material.

3 Experimental

3.1 Materials

The pristine materials used in this research are listed in Table 3-1. All the samples were handled in glovebox with an argon atmosphere to avoid reactions with air (water and oxygen less than 1 ppm). Different electrolytes and electrodes materials were prepared by ball milling and heat treatments. For the ball-milling process, a planetary ball-mill apparatus, Fritsch P7, was used (Figure 3.1). The samples were milled in an Ar atmosphere in a steel vessel with steel balls (Ø7 mm, 1.4 g per ball).

Acetylene black (AB) carbon was used as an electrical conductor in the composite electrode. It was prepared by heat treatment at 200 °C for 24 h under high dynamic vacuum condition to remove the water and oxygen content.

Table 3.1. Information of the pristine materials.

Material	Purity, state	Company
MgH_2	98%, powder	Alfa Aesar
FeTi	99%, powder	Kojundo Chemical Lab
LiH	99%, powder	Alfa Aesar
Nb_2O_5	99.5, powder	Sigma-Aldrich
$LiBH_4$	95%, powder	Sigma-Aldrich
LiI	99%, powder	Sigma-Aldrich
Li_2S	99.9%, powder	Sigma-Adrich
P_2S_5	99%, powder	Sigma-Aldrich
Lithium	99%, foil	Honjo Metal

3.1.1 Electrolytes

The electrolytes selected for this study were decided based on the ionic conductivity at room temperature as reported in the literature. Although $LiBH_4$ presents the lower ionic conductivity, it is taken as a reference. The other electrolytes have been reported working at room temperature for TiS_2, Li_2S or other electrode materials, only LPS has been reported for metal hydride conversion electrode operating at room temperature [53].

The solid electrolytes were prepared as follows.

$LiBH_4$. Commercial $LiBH_4$ was hand-milled for 15 min and heated at 200 °C for 24 h, to increase its purity. The heat treatment was performed under a dynamic high vacuum condition to remove the solvent from the as-purchased $LiBH_4$. After preparation, it was used for the preparation of electrode composites and directly as an electrolyte in the preparation of the cells.

LPS. LPS was prepared with a ratio $80Li_2S$-$20P_2S_5$, which has been found as the optimal mixture used in previous works [32], [54]. Li_2S and P_2S_5 were milled for 20 h (370 rpm), 1 gram of sample was prepared using 20 steel balls.

$3LiBH_4$•LiI. A stabilized $LiBH_4$ was prepared by anion substitution, I^-. The ratio selected was $3LiBH_4$•LiI, because of the information found in the literature [55]. The electrolyte

was synthesized by milling $LiBH_4$ and LiI for 20h (370 rpm) with 30 min rest between each hour. 1 gram of sample was prepared using 20 steel balls.

LBH+LPS. The electrolyte $LiBH_4+2(80Li_2S+20P_2S_5)$ (named LBH-LPS) was prepared by 5 h ball-milling (1 g of sample, 20 balls) at 350 rpm with 30 min of resting time each hour, followed by heat treatment of 2 h at 150 °C under vacuum. 1 g of sample was prepared using 20 steel balls.

LBH+PS. The electrolyte $90LiBH_4+10P_2S_5$ (named LBH-PS) was prepared by 5 h ball-milling (1 g of sample, 20 balls) at 350 rpm with 30 min of resting time each hour, followed by heat treatment of 2 h at 150 °C under dynamic vacuum. 1 g of sample was prepared using 20 steel balls.

3.1.2 Composite electrodes

c-MgH_2

The active material for the working electrode, MgH_2 (FUJIFILM Wako), was doped using 1 mol% of Nb_2O_5. The Nb_2O_5 improves the kinetics of the hydrogen transfer between Mg and Li for the conversion reaction [32]. The use of this catalyzed MgH_2 (named c-MgH_2) as electrode material has been reported previously with a significant improvement of the capacity [32], [54], [56]. A 300 mg of c-MgH_2 was prepared by 20 hours ball-milling of MgH_2 and Nb_2O_5 with 20 balls and resting time of 30 min / h.

MgH_2 composites

Several MgH_2 composite electrodes were prepared using the different solid electrolytes. They were prepared with a weight ratio of 40:30:30 of c-MgH_2, solid electrolyte and acetylene black carbon, respectively. 200 mg of composite electrode sample was prepared using 10 steel balls by 2h ball-milling at 370 rpm with 30 min of resting time every hour.

3.2 Fabrication of coin cells

The 2032-coin type cells were fabricated for the electrochemical testing. Pellets for coin cells consist of a Li foil, a layer of the solid electrolyte and a layer of the composite electrode, as shown Figure 3.2. Initially, a lithium foil was pressed on a 15 mm diameter stainless steel disc. Then, the electrolyte was spread and pressed on the Li foil. Finally, electrode material was spread over the layered electrolyte pellet and pressed. In the case of $3LiBH_4$•LiI, 140 mg of electrolyte was pressed under 10 MPa pressure, then 2.5 mg of the electrode was pressed under 40 MPa pressure. In the case of $80Li_2S$-$20P_2S_5$, 200 mg electrolyte was pressed under 10 MPa pressure followed by 2.5 mg of electrode layer pressed under 40 MPa pressure. For the electrolytes LBH-LPS and LBH-PS, a 150 mg electrolyte layer was pressed under 10 MPa pressure, followed by 2.5 mg of electrode layer pressed under 40 MPa. After the pellet preparation, the coin cell was assembled with the other components as depicted in Figure 3.3.

3.3 Powder X-ray diffraction (XRD)

X-ray diffraction is a non-destructive technique for the characterization of crystalline materials based on the phenomena of diffraction of X-rays. It provides information about crystalline planes, structures, identification of phases, crystallinity, grain size, and other structural parameters. A specific crystal structure produces a unique peak pattern. XRD peaks are produced when the interaction of X-rays and sample meets the conditions of Bragg´s law. The Bragg´s law is given as follows

$$\lambda = 2dsin\theta \tag{3-1}$$

If the angle of incidence is equal to the angle of the scattering, θ, and the path length difference (d) is equal to an integer number of wavelengths (λ), Figure 3.4a. Figure 3.4b shows the representation of a diffractometer with the incidence angle. The peak intensities are determined by the atomic position within the lattice planes. Consequently, the XRD pattern is the fingerprint of periodic atomic arrangements in each material.

In this work, the XRD characterization technique was utilized mainly to identify changes in phases during battery cycling. XRD measurements were performed using Cu Kα radiation at room temperature (XRD, RINT2000, Rigaku). The samples were protected with a polyimide film to avoid the oxidation and adsorption of water during the measurements. The measurements were performed at room temperature. The peak

patterns observed during measurements were compared with the database to identify the phases presented in the samples.

3.4Electrochemical performance

3.4.1 Galvanostatic discharge/charge

The galvanostatic test provides information directly about the electrode performance. The experiments were conducted using a constant current. The test is known as galvanostatic discharge/charge. In this experimental condition, a wide term is C-rate. The C-rate is the applied current to the cell calculated based on the theoretical capacity of the material. For example, if the capacity of a material is 1000 mAh/g, computed from the equation (1-9).

$$C_{max} = \frac{nF}{3.6\ MW} \tag{1-9}$$

Then, a C-rate of 2 indicates that the battery will release the maximum energy in 0.5 hours, with a discharge current of 2000 mA/g. In this way, a C-rate of 0.2 means a slow discharge rate, interpreted as a discharge current of 200 mA/g, it is a discharge of 5 hours. Total capacity measured, C_m, is given by

$$C_m = \frac{I_g\ t}{m_{AM}} \tag{1-10}$$

where I_g is the imposed constant current, t is the time of the discharge or charge process, and m_{AM} is the mass of the active electrode material.

From the direct measurement of potential vs capacity, it can identify different characteristics of the cell. Figure 3.5 shows three important aspects that must be evaluated in a battery, reversibility, capacity, and life of a battery. Then, it can be interpreted or associated with some effect of a specific component in the observed behavior.

3.4.2 Electrochemical Impedance Spectroscopy (EIS)

On the other hand, electrochemical impedance spectroscopy (EIS) is a technique for obtaining information about the resistivity of the components in a cell. EIS is used to characterize the performance of electrochemical systems for electrical energy storage and conversion, such as batteries, fuel cells, solar panels, or capacitors. The experiment is performed using an imposed time-harmonic oscillating electric potential $\psi_s(t)$ (with an amplitude less than 10mV) around a time-independent direct current potential (DC potential) at the electrode surfaces and measuring the resulting harmonic current density $j_s(t)$. It is expressed as

$$\psi_s(t) = \psi_{dc} + \psi_0 e^{i2\pi ft} \tag{3-2}$$

and

$$j_s(t) = j_{dc} + j_0 e^{i[2\pi ft - \phi(f)]} \tag{3-3}$$

where ψ_{dc} is the time-independent DC potential, ψ_0 is the amplitude of the oscillating potential at frequency *f*, j_{dc} is the time-independent DC current density, and $\phi(f)$ is the

frequency-dependent phase angle between the imposed potential $\psi_s(t)$ and the measured current density $j_s(t)$. The impedance of an electrode or battery is given by

$$Z = \frac{\psi_s(t) - \psi_{dc}}{j_s(t) - j_{dc}} = \frac{\psi_0}{j_0} e^{i\phi} = Z_{re} + iZ_{im} \quad (3\text{-}4)$$

where Z_{re} and Z_{im} (expressed in $\Omega\, m^2$) are the real and imaginary parts of the complex impedance, respectively. The impedance behavior of a cell can reveal a significant amount of information about battery operation characteristics. Figure 3.6 shows a typical plot obtained from a simple electrode measurement. It consists of a semicircle at high frequencies between points A and B, activation processes exhibit a semicircular behavior. Concentration process exhibit a nonvertical line at intermediate frequencies between points B and C, and a nearly vertical line at low frequencies beyond point C. For batteries, R_A indicates the resistance of the electrolyte, R_{AB} is the resistance presented in the electrode, and R_{BC} is the diffuse layer resistance.

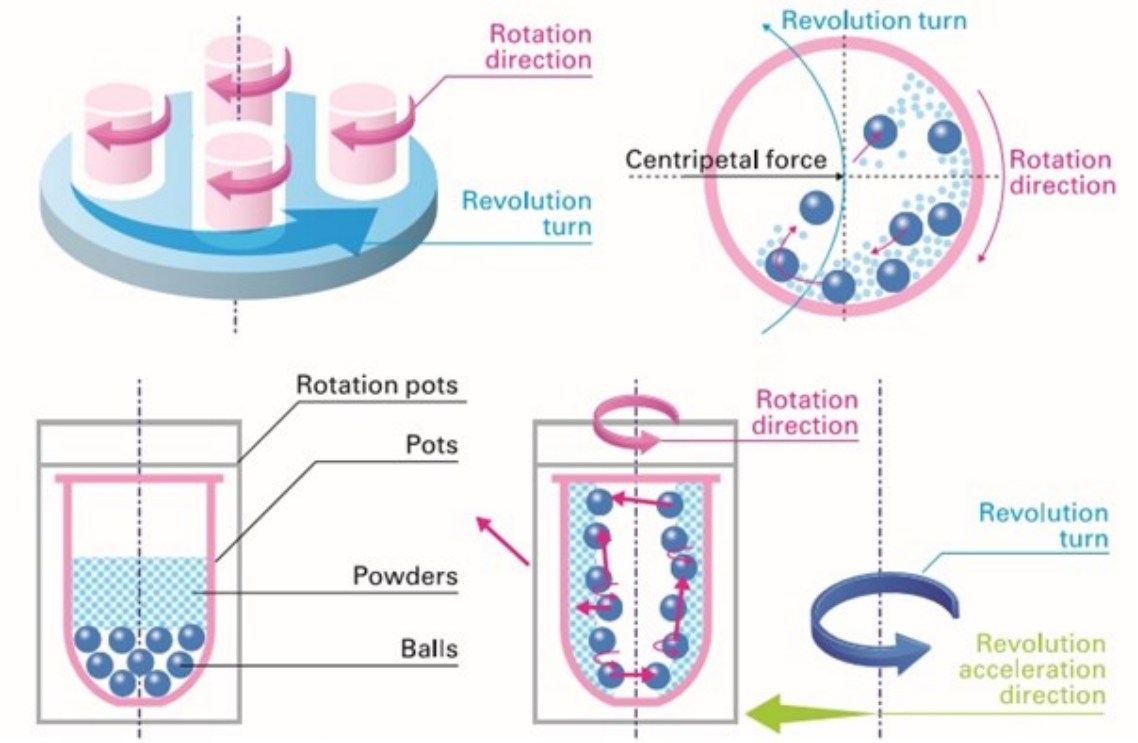

Figure 3.1. Schematic representation of the ball-milling process.

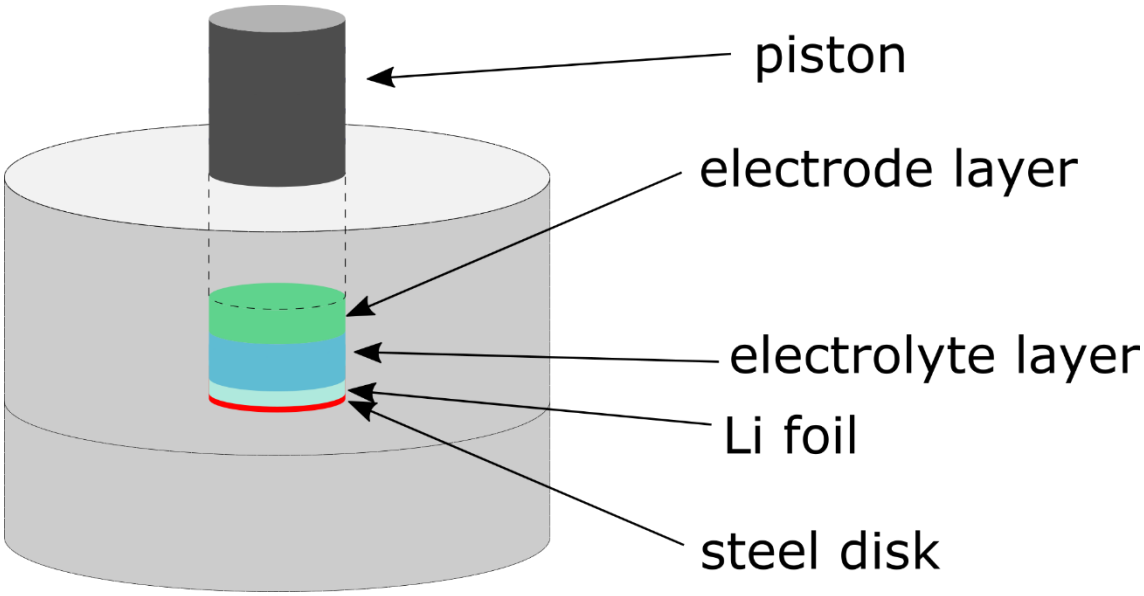

Figure 3.2. Fabrication of the layered pellet for the coin cell battery.

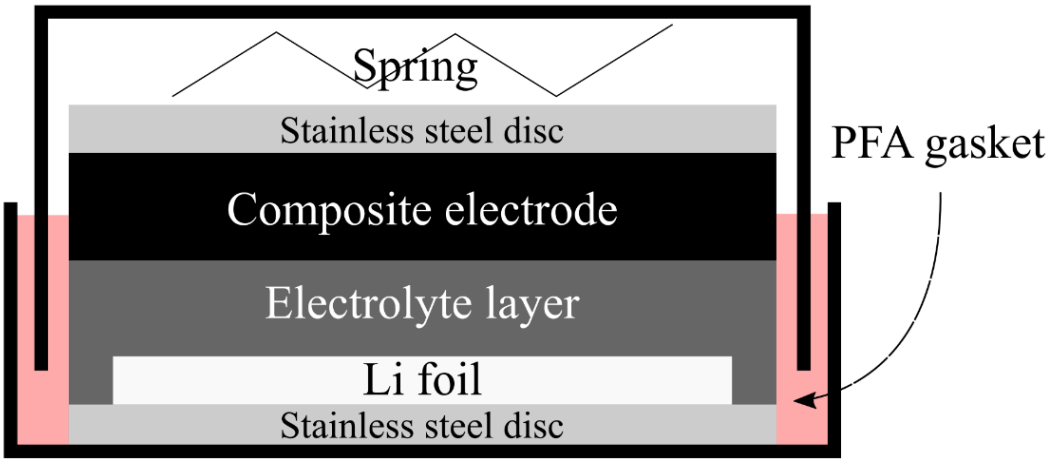

Figure 3.3. Fabrication of 2032 coin cells.

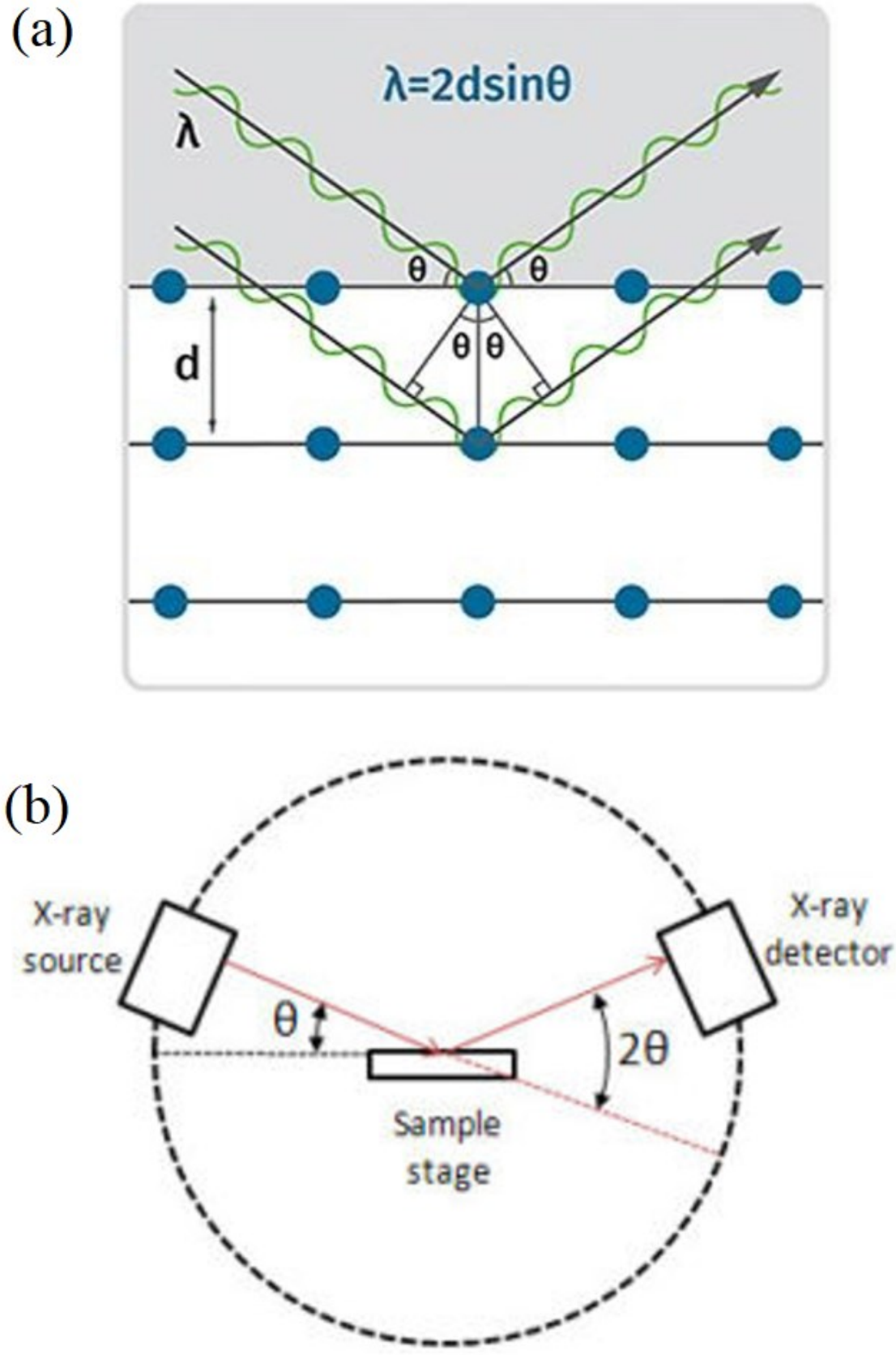

Figure 3.4. (a) Schematic arrangement of XRD diffractometer components.
(b) Diffraction of X-rays, Bragg´s Law.

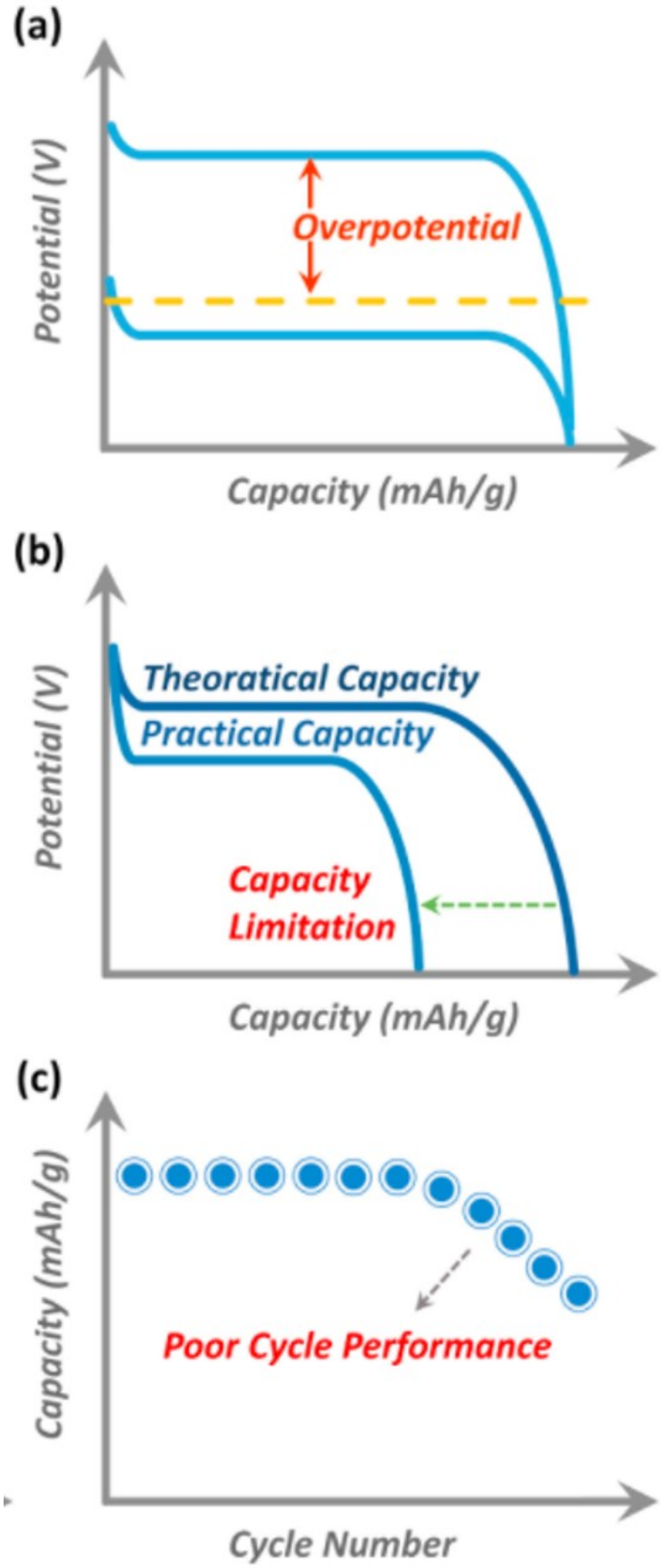

Figure 3.5. Behavior of a battery during galvanostatic experiments: (a) eficiency of the reaction, (b) capacity, (c) health of the battery.

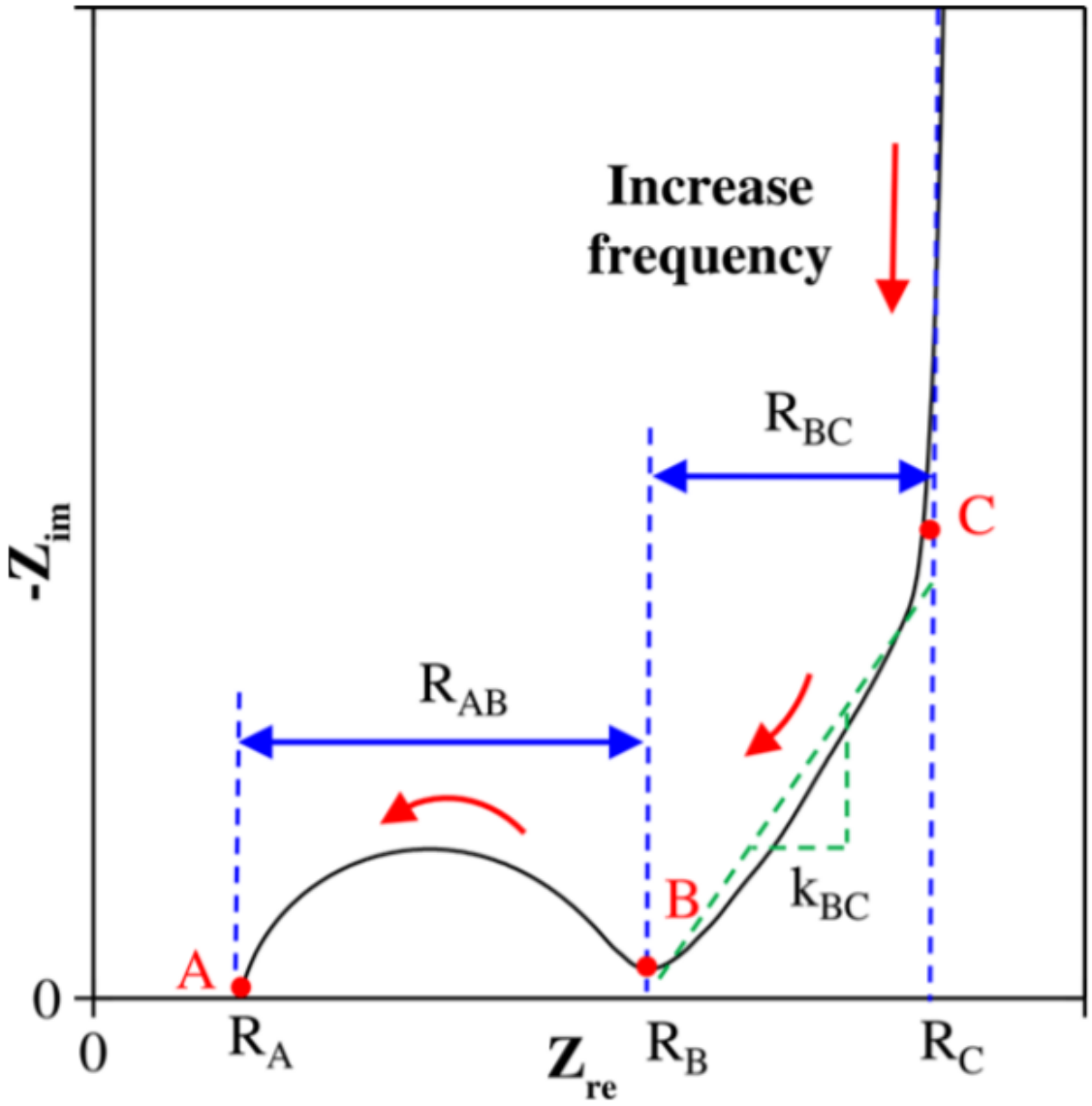

Figure 3.6. Schematic of typical Nyquist plots for EDLC electrodes or devices [57].

4. Results

The results are organized into two sections. The first section is related to the experiments with the electrolyte $3LiBH_4$•LiI. The second section is related to the experiment based on Li_2S-P_2S_5-$LiBH_4$ electrolyte combinations.

4.1 Halide-stabilized $LiBH_4$

After synthesis of $3LiBH_4$•LiI, the stabilized HT phase of $LiBH_4$ was confirmed. Figure 4.1 shows the XRD pattern, $3LiBH_4$•LiI keeps the hexagonal structure of $LiBH_4$ (HT phase) at room temperature, however, a peak shifting was observed for $3LiBH_4$•LiI compared with $LiBH_4$ HT. This must be caused by the expansion of lattice due to the substitution of $(BH_4)^-$ with anion I^- [45]. For the electrode prepared from $LiBH_4$, the observed XRD peak pattern corresponds to the LT phase of $LiBH_4$. In all three composites, MgH_2 could be observed after ball-milling.

The cells reported in this section are listed in Table 4.1.

Table 4.1. Cell configurations.

Cell type	Electrolyte layer	Electrode layer
1	$LiBH_4$	c-MgH_2/$LiBH_4$/AB Carbon
2	$80Li_2S$-$20P_2S_5$	c-MgH_2/$80Li_2S$-$20P_2S_5$/AB Carbon
3	$80Li_2S$-$20P_2S_5$	c-MgH_2/$LiBH_4$/AB Carbon
4	$3LiBH_4$•LiI	c-MgH_2/ $3LiBH_4$•LiI /AB Carbon
5	$80Li_2S$-$20P_2S_5$	c-MgH_2/ $3LiBH_4$•LiI /AB Carbon

4.1.1 Single electrolyte cells

Cell type 1

Li || $LiBH_4$ || c-MgH_2/$LiBH_4$/AB Carbon. This cell was prepared as a reference. The composite electrode was prepared using $LiBH_4$. Some experiments were also conducted at 100 °C but without success. The decrease of conductivity due to the structure change of $LiBH_4$ affect the viability of a battery using this electrolyte at lower temperatures. The results shown in Figure 4.2 were obtained at 120 °C. In these operating conditions, the battery worked well and shown good performance in agreement with the results reported by Zeng *et al.* [56]. A battery using $LiBH_4$ in the electrolyte layer as well as in the composite electrode cannot be compared, but the possibility of using it in combination with other electrolytes is examined in cell type 3.

Cell type 2

Li || 80Li_2S-20P_2S_5 || c-MgH_2/80Li_2S-20P_2S_5/AB Carbon. Figure 4.3 shows the specific discharge capacity of the cell using 80Li_2S-20P_2S_5 glass electrolyte at different temperatures and C-rates, and the discharge/charge profiles of the initial cycles are shown in Figure 4.4. This cell operating at 125 °C was expected to be the best condition and the capacity was reduced below 280 mAh/g after 10 cycles, Figure 4.3a. For higher C-rates, it is expected that the capacity should be reduced due to the kinetics limitation but in this case, the capacity of the cell decreases drastically during cycling for higher C-rates, Fig

4.3b. For a C-rate of 2 C, the capacity was extremely small since the beginning, with an initial capacity of 310 mAh/g. This low capacity of the cell is due to the kinetics limitations of solid-solid reaction. A lower C-rate enhanced the reversibility of the reaction, i.e. for 0.10 C the charge recovery during 1st charging was ~37.5 % (Figure 4.4), while the capacity was ~152 mAh/g after 10 cycles. The capacity of cell type 1 operating at the same temperature and a higher C-rate (0.40 C) remained higher after the same number of cycles (1132 mAh/g at cycle 10, Figure 4.3a). At lower temperatures the capacity of cell type 2 was far below from the theoretical value, however, the conversion reaction could be possible at lower temperatures which were extremely limited for cell type 1. This difference in the discharge-charge process between cell type 1 and 2 can be explained based on the properties of HT $LiBH_4$ as Li-ion conductor and the mobility of H due to the hydrogen exchange effect between MgH_2 and $LiBH_4$[58].

From the results obtained, cells using $80Li_2S$-$20P_2S_5$ in the composite electrode were expected to be the cells with the worst performance. Consequently, the next combinations discarded the use of $80Li_2S$-$20P_2S_5$ as the electrolyte in the composite electrode. On the other hand, at room temperature the ionic conductivity of Li^+ in $80Li_2S$-$20P_2S_5$ is higher than $LiBH_4$, therefore, this property could be used at the electrolyte layer to conduct Li-ions and this idea was explored in the cell type 3.

4.1.2. Combination of electrolytes

Cell type 3

Li || 80Li_2S-20P_2S_5 || c-MgH_2/$LiBH_4$/AB Carbon. Type 3 Cells were fabricated with a composite electrode using $LiBH_4$ and 80Li_2S-20P_2S_5 in the electrolyte layer. After milling $LiBH_4$ in the composite electrode, the defects produced in $LiBH_4$ enhanced the Li^+ conductivity of $LiBH_4$. This effect was reported by Sveinbjörnsson et al.[59], where the creation of defects due to the ball milling increased the conductivity of $LiBH_4$. This effect could enable the composite electrode with $LiBH_4$ to work at lower temperatures, moreover replacing $LiBH_4$ at electrolyte layer with another electrolyte with better conductivity. Figure 4.5a shows the results for this combination operating at 120 °C using a C-rate of 0.4 C. The initial rechargeability corresponded to a coulombic efficiency of 79.5 % and this efficiency was improved through the cycles, as shown in Figure 4.7. The polarization for the lithiation/delithiation process of cell type 3 was ~0.103 V, slightly higher than ~0.088 V observed in cell type 1 (the details are discussed later). Figure 4.5b shows the discharge/charge curves at lower temperatures for a C-rate of 0.05 C. The capacities at 120 °C and 90 °C are very similar and high (~2000mAh/g), but with a coulombic efficiency of 73 % and 66 %, respectively for the 1st cycle. At 30 °C the discharge capacity was reduced to 1033.8 mAh/g and during charging it could reach up to only 47 % of the initial discharge capacity. Comparing with cell type 2, improvement in cycling observed due to the use of $LiBH_4$ instead of LPS in the composite electrode.

And $LiBH_4$ electrode could work at lower temperatures, even with its LT phase. It can be explained by the enhancement of conductivity due to ball milling process.

Cell type 4

Li || $3LiBH_4$•LiI || c-MgH_2/$3LiBH_4$•LiI/AB Carbon. This cell was prepared using $3LiBH_4$•LiI in its electrolyte layer as well as its composite electrode. The discharge/charge curves for a C-rate of 0.4 are shown in Figure 4.6a. The initial specific capacity of the cell working at 120 °C was around 1600 mAh/g with an average polarization of 0.093 V during charge and discharge. Compared to cell type 3, there is an improvement. I t can be attributed to conductivity of $3LiBH_4$•LiI since the conductivity of $3LiBH_4$•LiI is higher than LPS. This cell kept a discharge capacity of 1250 mAh/g after 10 cycles. Cell type 4 was tested at different temperatures for a C-rate of 0.05 C, the results are shown in Figure 4.6b. The performance at 60 °C was quite similar to the performance of the cells working at 90 °C and 120 °C with a remarkable columbic efficiency (~94 %, ~97 % and ~98 %, respectively), the specific capacity decreased but it remained at ~1700 mAh/g. The performance at 30 °C presented a relatively lower specific capacity with a higher polarization (0.203 V) and a coulombic efficiency of 62 % for the initial cycle.

Figure 4.7 shows the specific capacity and coulombic efficiency of cell type 1, 3 and 4 operating at a temperature of 120 °C and a C-rate of 0.4 C. The cells have shown their best performance operating at high temperature. After 10 cycles, cell type 4 retained

79.3 % of the initial capacity in contrast to a 65.6 % of cell type 1. The discharge capacities were 1131.7 mAh/g, 987.5 mAh/g, and 1266.5 mAh/g after 10 cycles for cell type 1, 3 and 4, respectively. Thus, $3LiBH_4$•LiI shows better performance as an electrolyte in the composite electrode, compared to $LiBH_4$. For cell type 3 the use of $LiBH_4$ in the composite benefited the conservation of charge capacity after cycling but the performance was affected by the lower ion conductivity of the Li_2S-P_2S_5 as the electrolyte. From the comparative at high temperature, it could be inferred that the use of $3LiBH_4$•LiI in the composite is the best alternative due to the essential importance of conductivity of lithium ions and promotion of hydrogen mobility during the conversion reaction. Regarding the electrolyte layer between electrodes, $80Li_2S$-$20P_2S_5$ should work better than $3LiBH_4$•LiI at low temperature since the lithium-ion conductivity of $3LiBH_4$•LiI drops below the conductivity of $80Li_2S$-$20P_2S_5$ [60]. Based on this, cell type 5 combining these two electrolytes was proposed and analyzed.

Cell type 5

Li || $80Li_2S$-$20P_2S_5$ || c-MgH_2/$3LiBH_4$•LiI/AB Carbon. Cell type 5 was fabricated combining the best electrolytes for each application at low temperature, i.e. it took advantage of the conductivity of $80Li_2S$-$20P_2S_5$ in the electrolyte layer and using $3LiBH_4$•LiI in the composite electrode to provide the mobility of both Li^+ and hydrogen, during conversion reaction. Figure 8a shows a comparison of the first cycle of cell type 3, 4 and 5 operating at 30 °C and 0.05 C. Cell type 4 and 5 shared the same working

electrode composition and during operation, the polarization was quite comparable. However, the capacity attained by cell type 5 was higher. This makes sense since $80Li_2S$-$20P_2S_5$ can provide a higher conductivity of lithium ions at low temperature, i.e. conductivity of $3LiBH_4$•LiI (~$5x10^{-5}$ S cm^{-1}) is lower than $80Li_2S$-$20P_2S_5$ ($1x10^{-4}$ S cm^{-1}) at 30 °C.[21] This can be the reason for a better performance of cell type 5 than cell type 4, with first cycle reversibility of 60 % and 62 %, respectively. Cell type 2 shown first cycle reversibility of 29 % and 46 % for cell type 3. The effect of temperature in cell type 2, 3 and 4, compared to cell type 5 is summarized in Figure 8b. The performance of cell type 5 at low temperature is superior to the other cells. At lower temperatures, the capacities of different cells decreased due to the decrease in the ionic conductivity. Cell type 3 had a poor capacity recovery during charging. Whereas cell type 4 shown a better recharging efficiency but suffered from a lower capacity at 120 °C. Then, under 60 °C the performance of cell type 4 overcomes the capacity of cell type 3. It can be explained based on the less conductivity of $LiBH_4$ in comparison to $3LiBH_4$•LiI at below this temperature. This can be observed in cell type 3 and 5 (cells sharing the same electrolyte layer), in these cases $3LiBH_4$•LiI composite shown a better performance of $LiBH_4$, for this system $LiBH_4$ is the limiting agent in the performance of the cell. Polarization in cell type 4 and 5 as was quite similar, even if they used different electrolyte layer because polarization depends on the kinetics at electrode interfaces. For cell type 2, polarization and interface resistance values were higher than the results for the other cells, and the

discharge capacity obtained from this configuration was the lowest (324.8 mAh/g). After discharge, the resistances of all cells were decreased, which can be explained by the formation of pathways for Li^+ during discharge, this effect enhanced the conduction of lithium-ions. The lower resistance observed in cell type 5 compared to Cell 4, confirms the advantage of incorporating an $80Li_2S$-$20P_2S_5$ layer at low temperature.

Furthermore, the performance of cell type 5 at different C-rate was tested at low temperature and the results are shown in Figure 9a. Polarization was found to be increased with the increase of C-rate. The polarization showed a smaller value of 0.18 V for a discharge rate of 0.05 C in comparison to 0.36 V for 0.20 C. The increase in the polarization is originated by the slow kinetics for higher C-rate conditions. Initial specific discharge capacity was reduced from 1570 mAh/g at a C-rate of 0.05 C to around 960 mAh/g for a discharge rate of 0.20 C. The capacity during cycling is presented in Figure 9b. On comparing the reduction of initial capacity after 5 cycles, the capacity was reduced to 42 %, 35 % and 27 % for 0.05 C, 0.10 C and 0.20 C, respectively. For a discharge rate of 0.1C, the test was extended to 50 cycles, obtaining that the specific capacity was reduced to 218.4 mAh/g after 20 cycles and 140.9 mAh/g after 50 cycles, which represents a 10.5 % of the initial capacity.

4.2 $Li_2S+P_2S_5+LiBH_4$ composites electrolytes

In this section, the cells were prepared using the electrolytes $33LiBH_4+67(80Li_2S+20P_2S_5)$ and $90LiBH_4+10P_2S_5$. The cells analyzed in this section are listed in Table 4.2.

Table 4.2. Cells configurations for $Li_2S+P_2S_5+LiBH_4$.

Name	Electrolyte layer	Electrode layer
LPS/LPS	$80Li_2S+20P_2S_5$	c-MgH_2+Acetylene Black carbon +($80Li_2S+20P_2S_5$)
LPS/LBH-LPS	$80Li_2S+20P_2S_5$	c-MgH_2+Acetylene Black carbon +[$33LiBH_4+67(80Li_2S+20P_2S_5)$]
LPS/LBH-PS	$80Li_2S+20P_2S_5$	c-MgH_2+Acetylene Black carbon +($90LiBH_4+10P_2S_5$)
LBH-LPS/LBH-LPS	$33LiBH_4+67(80Li_2S+20P_2S_5)$	c-MgH_2+Acetylene Black carbon +[$33LiBH_4+67(80Li_2S+20P_2S_5)$]
LBH-LPS/LBH-PS	$33LiBH_4+67(80Li_2S+20P_2S_5)$	c-MgH_2+Acetylene Black carbon +($90LiBH_4+10P_2S_5$)
LBH-LPS/LBH	$33LiBH_4+67(80Li_2S+20P_2S_5)$	c-MgH_2+Acetylene Black carbon +$LiBH_4$
LBH-PS/LBH-PS	$90LiBH_4+10P_2S_5$	c-MgH_2+Acetylene Black carbon +($90LiBH_4+10P_2S_5$)
LBH-PS/LBH-LPS	$90LiBH_4+10P_2S_5$	c-MgH_2+Acetylene Black carbon +[$33LiBH_4+67(80Li_2S+20P_2S_5)$]
LBH-PS/LBH	$90LiBH_4+10P_2S_5$	c-MgH_2+Acetylene Black carbon +$LiBH_4$

Figure 4.10 shows the XRD pattern for the composites and electrolytes synthesized in this study. In LBH-LPS electrolyte, some of the peaks from the Li_2S phase could be observed, which means that this phase remained in the composite electrolyte. In the case of LBH-PS, a different phase was identified after mechano-chemical preparation. The $Li_6PS_5(BH_4)$ phase was reported by Unemoto et al. [35] and Sakuda et al. [61] using different preparation methods. Sakuda reported $Li_6PS_5(BH_4)$ phase from the starting material as $(100-x)(0.75Li_2S \cdot 0.25P_2S_5) \cdot xLiBH_4$, where the above phase was

observed clearly for $x \geq 0.5$. On the other hand, Unemoto reported the preparation of this phase from the starting material as $xLiBH_4 \cdot (100 - x)P_2S_5$, and the phase could be identified for $x \geq 87.5$. Sakuda identified the crystal structure as $Li_6PS_5(BH_4)$. This phase can be obtained from both compositions. In LBH-LPS, some peaks corresponding to $Li_6PS_5(BH_4)$ were also observed, but with a dominant presence of Li_2S phase. Prepared LBH-PS shown this phase clearly, whereas the remaining $LiBH_4$ and P_2S_5 was not found, probably due to their amorphous state.

LBH-LPS and LBH-PS were studied using thermogravimetric (TG) as well as differential thermal analysis (DTA), the results are shown in Figure 4.11. The experiment explored the range of temperatures from room temperature to 140 °C (5 °C/min). For $LiBH_4$, there was a clear endothermic peak around temperature corresponding to the structural transition of $LiBH_4$ from orthorhombic to hexagonal crystal structure. The LBH-PS electrolyte showed a small peak in a similar temperature to the peak of $LiBH_4$, which confirmed the existence of unreacted $LiBH_4$ even if it was not observed during XRD analysis. The small shifting of this peak can be attributed to destabilization of $LiBH_4$ by LPS or $Li_6PS_5(BH_4)$, the $LiBH_4$ was just hand-milled whereas LBH-PS was milled for 5 h. This peak shifting have been also reported for other electrolyte composites [62]. In the case of LBH-LPS, no such peak was observed during this test due to no / low concentration of unreacted $LiBH_4$ after the milling process. It suggests that most of $LiBH_4$ reacted with LPS to form the argyrodite-type $Li_6PS_5(BH_4)$ phase.

4.2.1 Single electrolyte cells

Electrochemical impedance spectroscopy (EIS) was performed to compare the resistance of these electrolytes (Figure 4.12). By employing the equivalent circuit, the resistances associated to the electrolyte layer (R1) were estimated as 178.3 Ω ($4.5x10^{-4}$ S cm^{-1}) for LPS, 54.8 Ω ($2.0x10^{-3}$ S cm^{-1}) for LBH-LPS, and 39.3 Ω ($2.9x10^{-3}$ S cm^{-1}) for LBH-PS. It agrees with the ionic conductivities reported in previous studies, ~10^{-4} for LPS, ~10^{-3} for LBH-LPS and LBH-PS, respectively[35] [60]. According to the results in this study and previous reports, LBH-PS has the highest conductivity, nearly followed by LBH-LPS electrolyte.

Firstly, the cells working with the same electrolyte in the electrolyte layer as well as in the electrode composite were compared. Figure 4.13 shows the cyclic performance of battery cells operated at 30 °C with a C-rate of 0.05. The battery using LBH-PS shown the highest capacity. The coulombic efficiency shows the evaluation of the battery stability, and according to that, LBH-PS reached a higher capacity and efficiency during first cycles. A comparison of the second cycle is shown in Figure 4.14. In this cycle, LPS/LPS developed a capacity of 107.8 $mAhg^{-1}$ (70.5%), whereas LBH-LPS/LBH-LPS and LBH-PS/LBH-PS showed capacities as 537.7 $mAhg^{-1}$ (72.6%) and 892.9 $mAhg^{-1}$ (78%) respectively. The capacity for LBH-PS system represented more than 7 times to that for the LPS system. After 50 cycles, the capacity of LBH-PS/LBH-PS cell was reduced to 195.3 $mAhg^{-1}$, whereas the capacity of LBH-LPS/LBH-LPS system dropped

below this value since 9th cycle (191.8 $mAhg^{-1}$) and reduced down to 83.3 $mAhg^{-1}$ after 50th cycle.

4.2.2 Combination of electrolytes

To investigate on the performance of these electrolytes in the electrode composite, additional cells were fabricated using the same LPS in the electrolyte layer. The results for these cells are shown in Figure 4.15. During cycling, the capacity of three cells decreased drastically compared with cells using the same electrolyte in both layers. Among these cells, LPS/LBH-PS started with an initial capacity of 1587.3 $mAhg^{-1}$, however, the capacity was faded down within few cycles. It was reduced to 763.8 $mAhg^{-1}$ (48.1% of the initial capacity) in the second cycle and 278.1 $mAhg^{-1}$ after 10 cycles (17.5% of the initial capacity). This value was lower than the cell LBH-PS/LBH-PS, where the capacity decreased to 410.4 $mAhg^{-1}$. In the case of LPS/LBH-LPS, the capacity obtained after 10 cycles was 58.6 $mAhg^{-1}$. From EIS analysis, LPS shown the highest resistivity. The low cyclability of these batteries can be partially explained with the use of LPS electrolyte at the electrolyte layer. The performance of cell LPS/LPS (Figure 4.15) shows the low compatibility of this material with MgH_2. On the other hand, LPS/LBH-PS had a higher capacity than other batteries with LPS at the electrolyte layer. One of the reasons for better performance can be the lower resistance of LBH-PS. This resistance was similar to LBH-LPS, but even so, the capacity of LPS/LBH-LPS cell dropped to 62.7 $mAhg^{-1}$, <25% of LPS/LBH-PS.

The cells with a cross combination of electrolytes i.e. LBH-LPS/LBH-PS and LBH-PS/LBH-LPS were also prepared to obtain more information about the behaviour of these electrolytes working at electrode composite. A variation in the initial performance of different cells with the same cell configuration was observed in some cases. The variation in the results could be attributed to the manually assembling process of the cell. This variation in measurements became negligible after first cycle, the representative cases are reported in Figure 4.16. Because of this, second cycle of all cells was used to compare.

Figure 4.17 shows the cycling of both batteries and the galvanostatic discharge/charge curves in 2^{nd} cycle. In second cycle, LBH-LPS/LBH-PS delivered a discharge capacity of 768.8 $mAhg^{-1}$, whereas LBH-PS/LBH-LPS delivered 516.8 $mAhg^{-1}$. In cycle 10^{th}, these capacities faded down to 246.4 $mAhg^{-1}$ and 203.6 $mAhg^{-1}$, respectively, which were lower than the capacity of LBH-PS/LBH-PS cell. The capacity of the electrode using LBH-PS is limited by LBH-LPS working at electrolyte layer. According to these results and previous results (fabricated with LPS electrolyte layer), the performance of LBH-LPS at the working electrode is worse than LBH-PS. This difference could be attributed to the relatively higher concentration of $LiBH_4$ in LBH-PS electrolyte. It suggests that the $LiBH_4$ presence in LBH-PS is enough to contribute with the conversion reaction of MgH_2.

To extend this comparison of electrolytes at the electrolyte layer, the cells using an electrode with $LiBH_4$ were tested. Galvanostatic test results are included in Figure 4.17. For these combinations, LBH-PS/LBH achieved a higher discharge capacity during the first cycle. On comparing the discharge capacities of LBH-LPS/LBH and LBH-PS/LBH in second and 10^{th} cycle, these were 983.7/528.8 $mAhg^{-1}$ and 1114.1/607.6 $mAhg^{-1}$, respectively. It confirms that LBH-PS worked better at electrolyte layer providing a higher conductivity of Li^+. The cells using LiBH4 as electrolyte in the composite electrode works better than the other electrolytes. Even if $LiBH_4$ has a lower ionic conductivity at room temperatures, the performance of electrodes with this electrolyte reached higher capacities, Figure 4.17b. As reported by Sveinbjörnsson *et al.*[59], ionic conductivity of $LiBH_4$ can be improved by ball milling process which change the crystallinity level of $LiBH_4$. The increase of conductivity due to this effect enables the operation of $LiBH_4$ as ionic conductor, even though this conductivity is limited, it helps to enhance the mobility of hydrogen due to the hydrogen exchange effect. The hydrogen exchange effect was observed in MgH_2-$LiBH_4$ system and reported by Zeng *et al.*[58]. Also, it was found that the exchange of hydrogen was enhanced using Nb_2O_5. Based on this, it was assumed that $LiBH_4$ enhanced the mobility of hydrogen for the conversion reaction. In this case, LPS can provide the pathways for Li^+ transportation but it does not promote the hydrogen mobility, required for the conversion reaction, as good as $LiBH_4$

based electrolytes. For this reason, LPS electrode worked but it showed poor reversibility compared to $LiBH_4$ even at high temperatures [56][63].

It is to be noted here that all the cells shown a continuous decrease in capacity with a number of cycles irrespective to the use of different electrolytes/electrode combination. This behavior is quite similar to the previous studies such as using $Li(BH_4)_{0.75}I_{0.25}$-$0.8Li_2S{\cdot}0.2P_2S_5$ and was believed related to the segregation of MgH_2 in electrode layer[36]. It was shown using morphological investigation that after cycling there is a segregation of Mg that led to poor contact between phases. This segregation of Mg could not be eliminated here but could be reduced by the use of a solid electrolyte matrix in the composite and enhanced the stability of the electrode compared to liquid electrolytes. The remarkable point here is the possibility of using an electrolyte with high Li^+ conductivity (which only focus and helped in Li transportation), and using other electrolyte having better compatibility with metal hydrides in electrode composite layer (which helped enhancing conversion reaction).

The batteries are compared in terms of energy and power in Figure 4.18, discarding the combinations with LPS at the electrolyte layer but keeping LPS/LPS as reference. Several batteries exhibited a low initial capacity and then it increased in the second cycle. This effect was observed for batteries with LBH-LPS electrolyte. It can be attributed to the activation of the electrode during the first discharge. In order to have the right comparison, the second cycle was compared for all cases. After the first cycle, he

performance of the battery followed a pattern that can be understood as a regular operation. Since the same specific current was applied in all the cases (0.05C), the electrode polarization can be directly related to the specific power. The lowest polarization was also observed in the case of LBH-PS/LBH. The cell LBH-PS/LBH reached to the higher specific energy (501.7 $Whkg^{-1}$) and power (45.85 Wkg^{-1}). The potential application of MgH_2 as a Li-metal battery is limited by the low operating voltage ~0.45 V of a single cell, but it could be a suitable anode for Li-ion batteries.

During operation of cells LBH-LPS/LBH-LPS at 120°C, a second reaction was observed during charging. The only material available for the reaction was LiH. The theoretical reaction voltage for the possible decomposition of LiH matched with the reaction potential observed during charging (~0.7 V). An additional composite was prepared including 20 wt% of LiH as an active material. Then, during charging, the reaction was pronounced for this new composite. Figure 4.19 shows the comparison between the original LBH-LPS composite and the other one with LiH. However, in the preparation of the original composite electrode, LiH was not used directly as a pristine material.

An additional experiment with metal hydrides was carried out to verify if this second reaction occurs for metal hydrides or is related to the possible decomposition of the electrolyte. MgH_2 composites were prepared in a charged state and can be used after fabrication of the cell. In the case of $FeTiH_2$, the initial composite electrode was prepared

using FeTi + LiH (discharged state). For this experiment, an increase in the initial content of LiH also increased the capacity observed during charging with a potential of 0.7 V (Figure 4.20), clearly similar to previous observations (Figure 4.19). A similar but smaller reaction was observed for composites with MgH_2 and $LiBH_4$ and $3LiBH_4$•LiI operating at 120 °C (Figure 4.5). This reaction occurs only at high temperature and it seems to be specifically related to LiH. To have a better understanding of this reaction, LiH needs to be deeply studied.

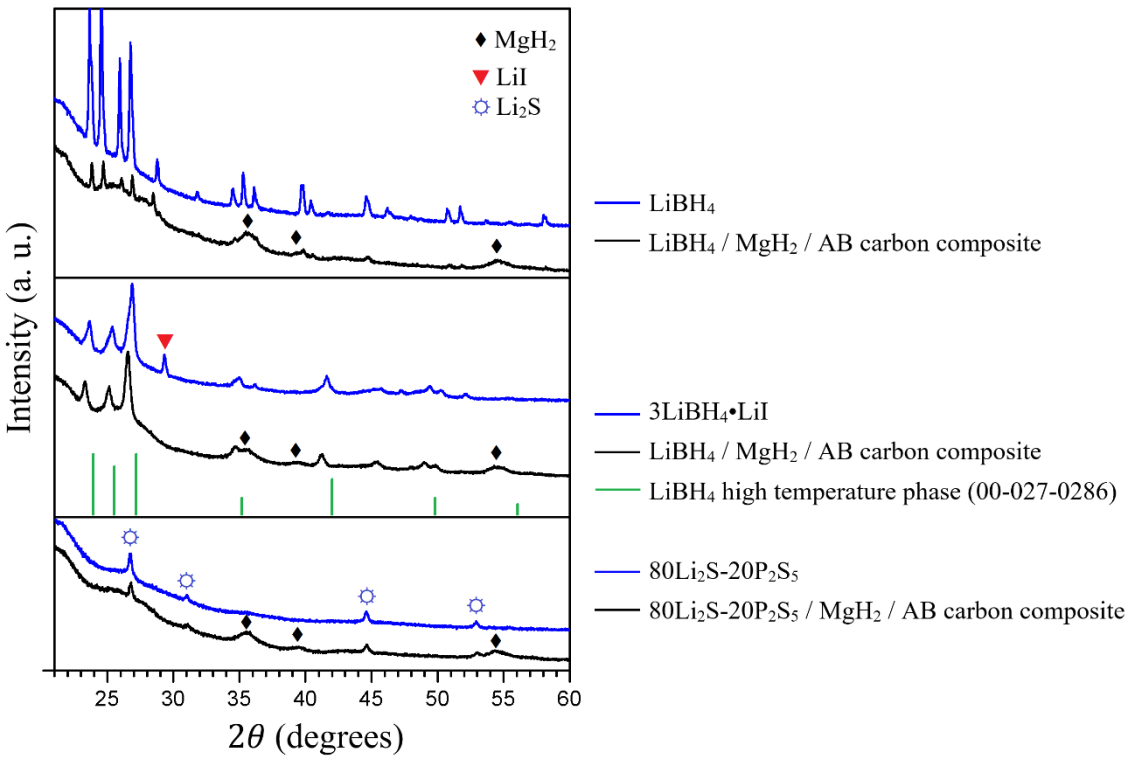

Figure 4.1. XRD pattern for solid electrolytes and their combinations with MgH_2 and Acetylene Black carbon at room temperature

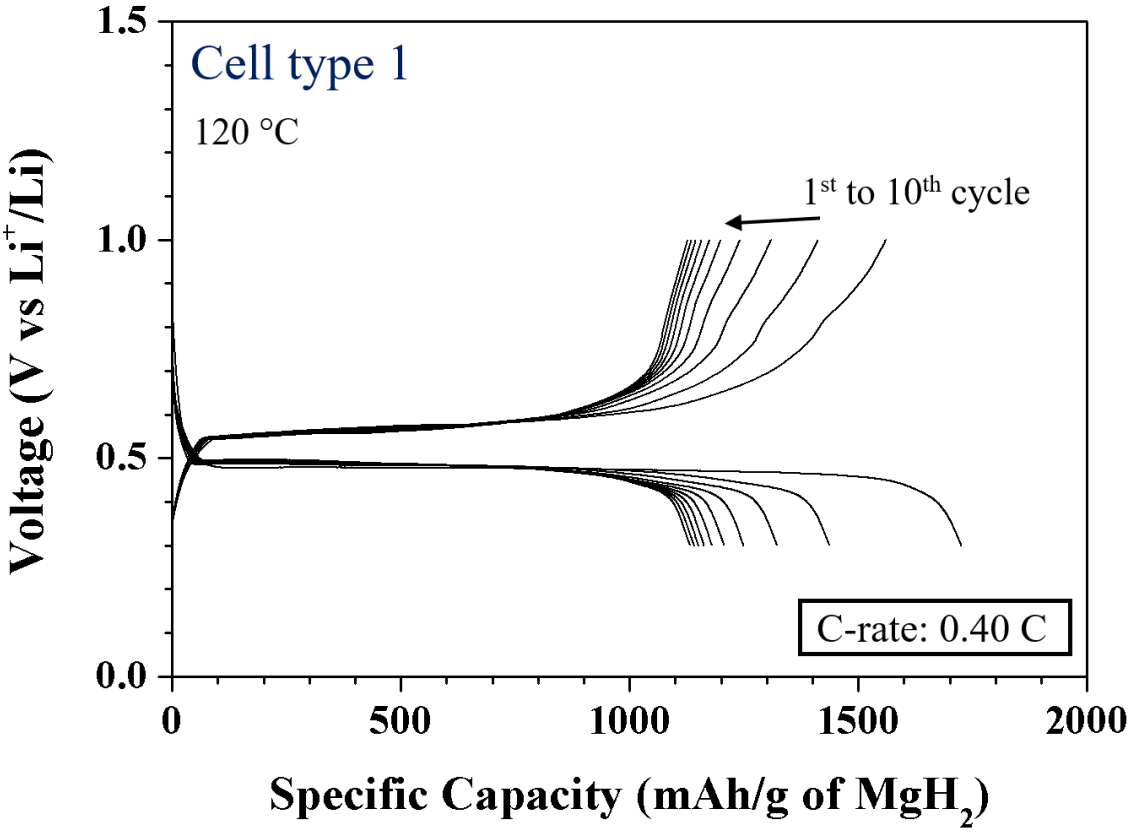

Figure 4.2. Galvanostatic discharge/charge curves for cell type 1.

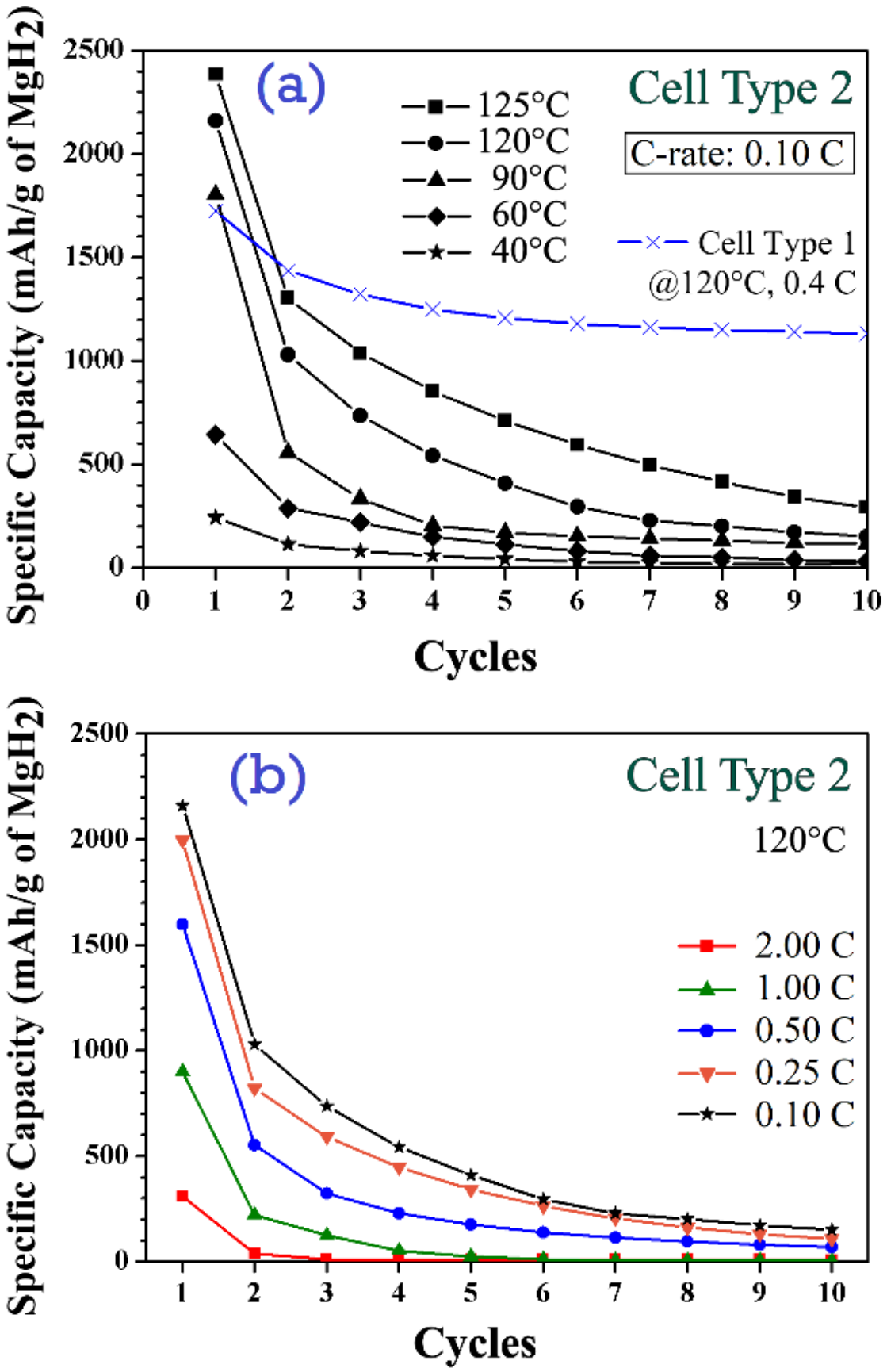

Figure 4.3. Discharge capacity of cell type 2 during cycling: (a) different temperatures, (b) different C-rates.

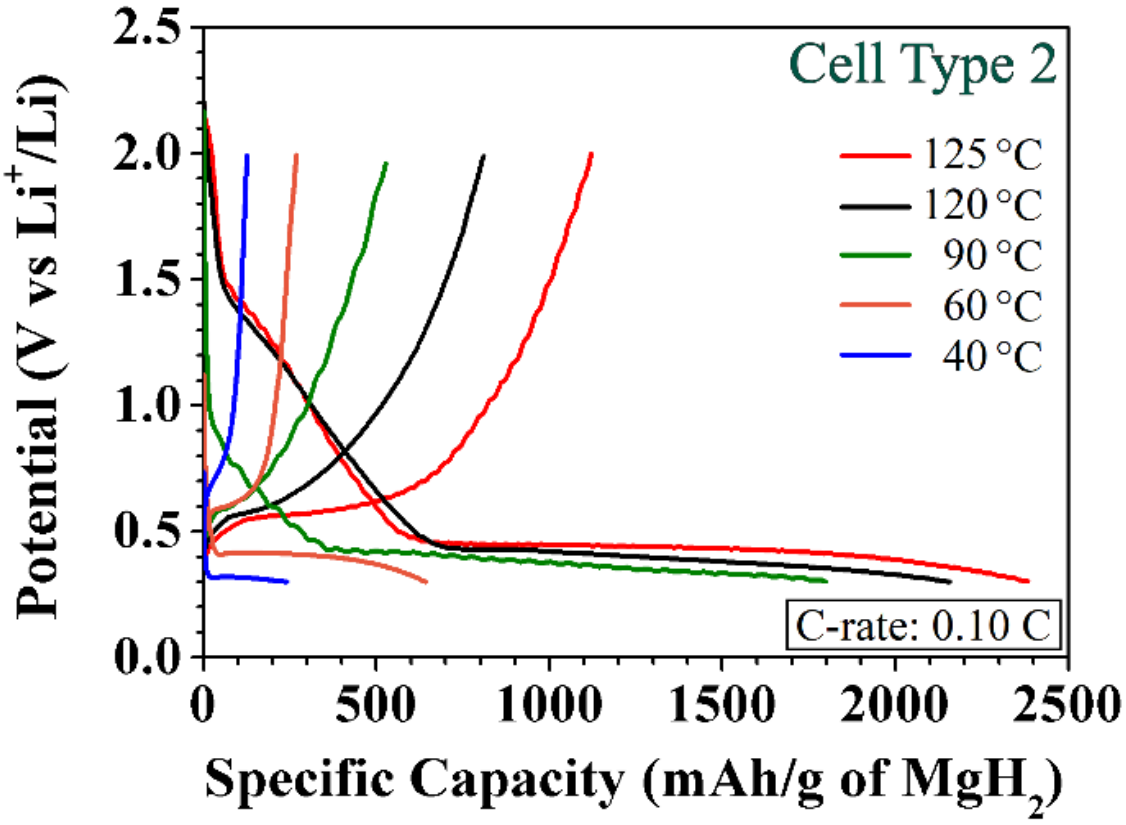

Figure 4.4. The first cycle of cell type 2 at different temperatures.

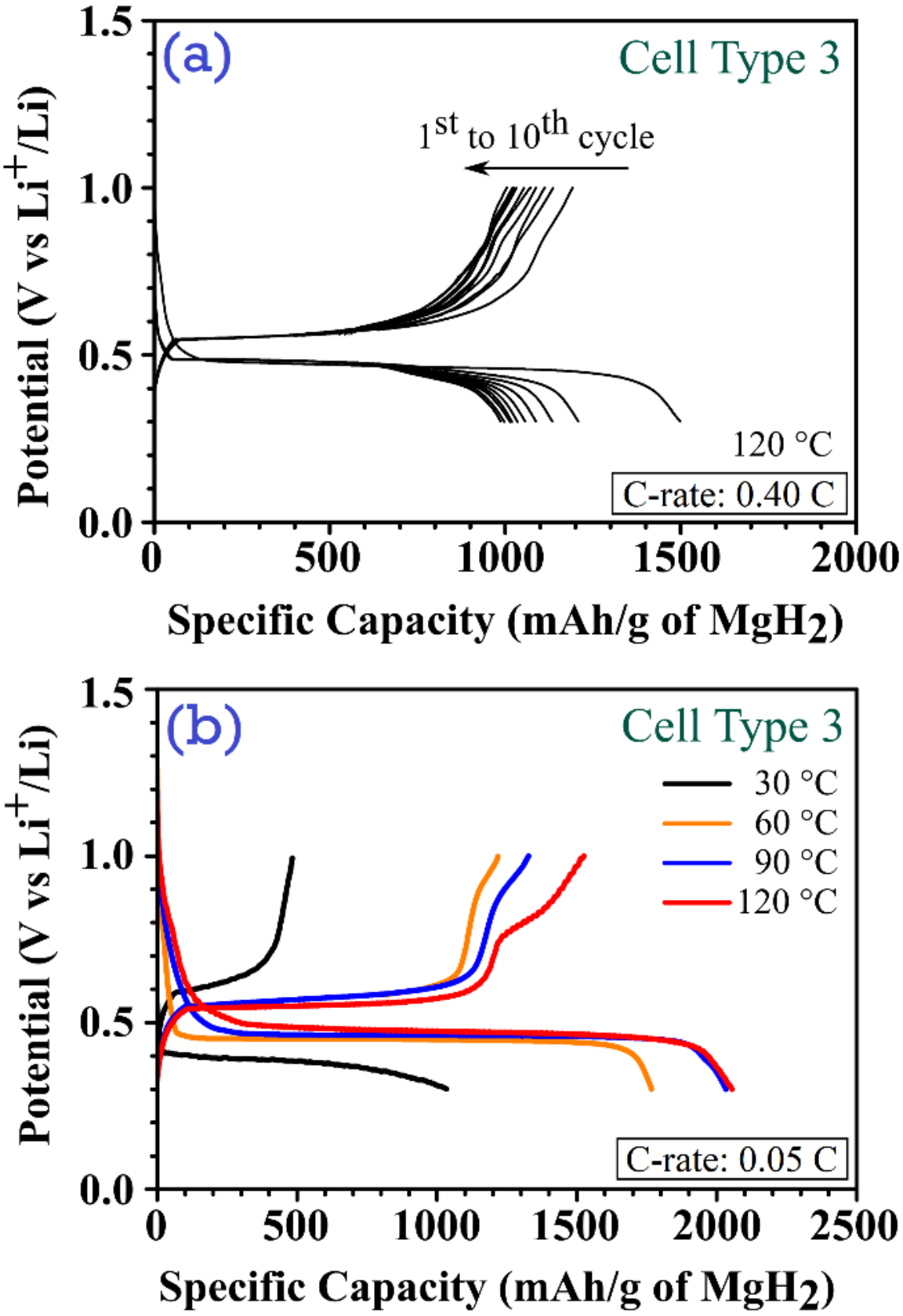

Fig 4.5. Galvanostatic discharge/charge curves for cell type 3 tested at: (a) 120 °C, (b) different temperatures.

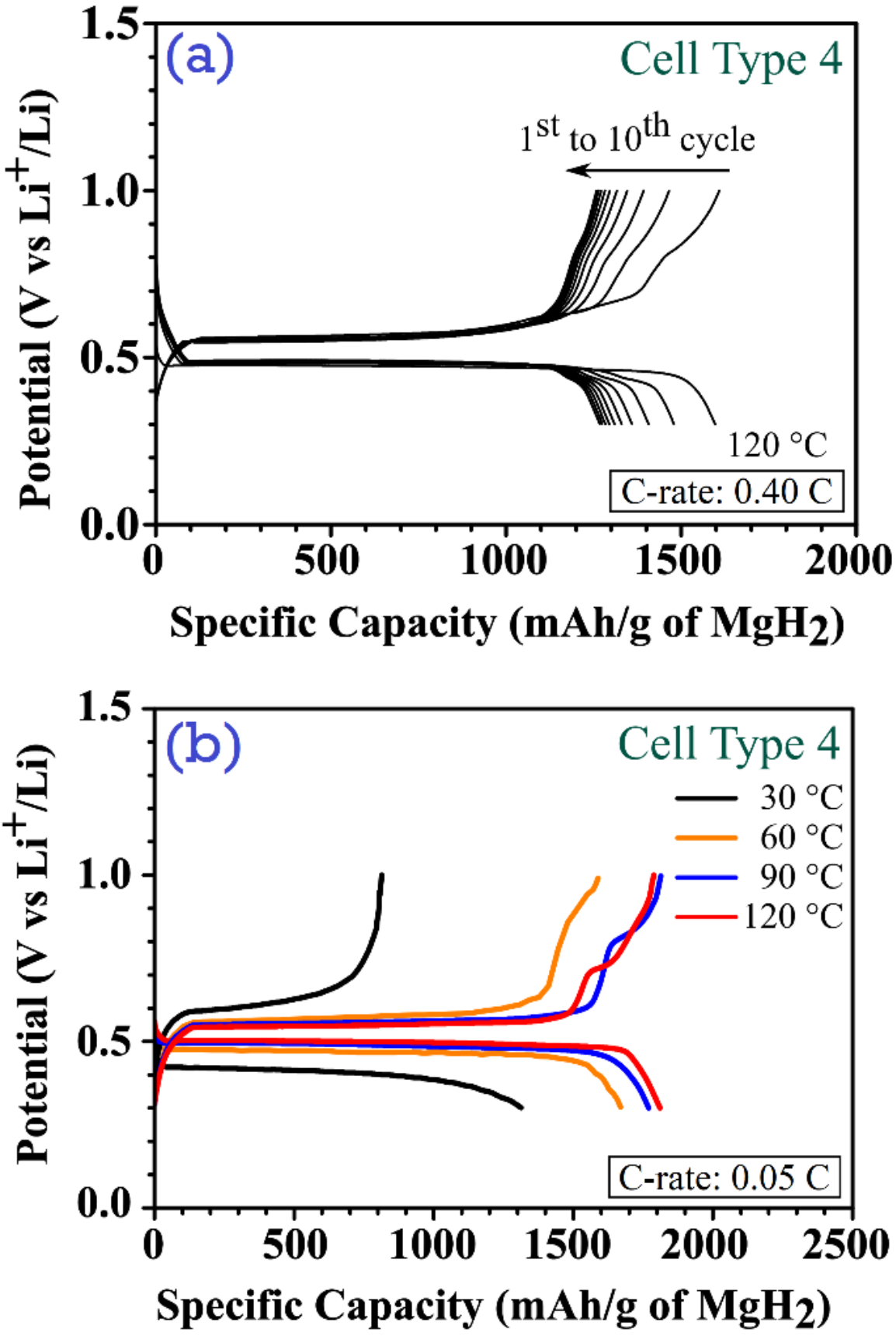

Figure 4.6 Galvanostatic discharge/charge curves for cell type 4 tested at: (a) 120 °C, (b) different temperatures.

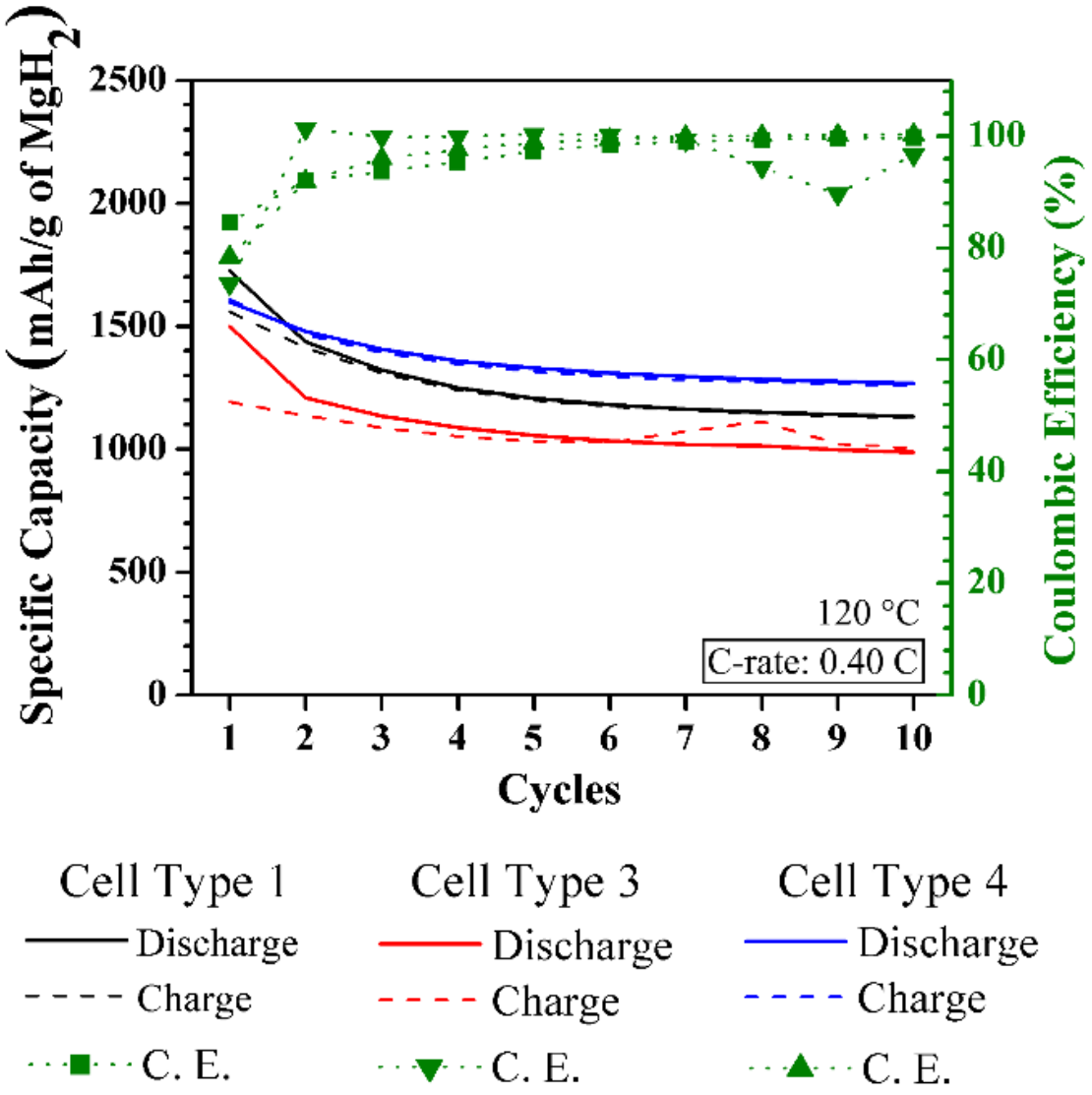

Figure 4.7. Performance of cell type 1, 3 and 4, cycling at high temperature.

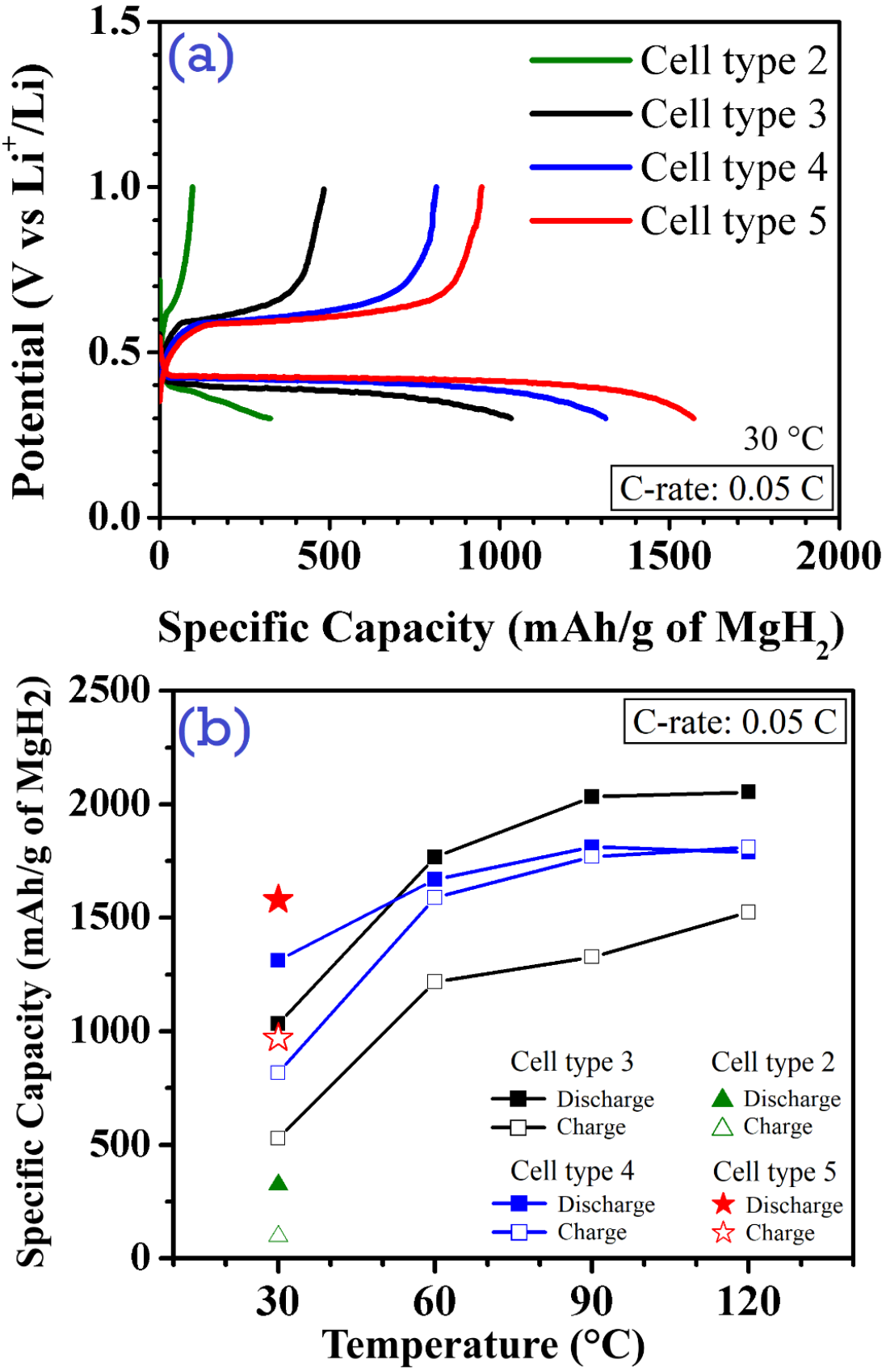

Figure 4.8. The initial capacity of cell type 3,4,5: (a) Galvanostatic discharge-charge curves at 30 °C, (b) specific capacity vs. Temperature.

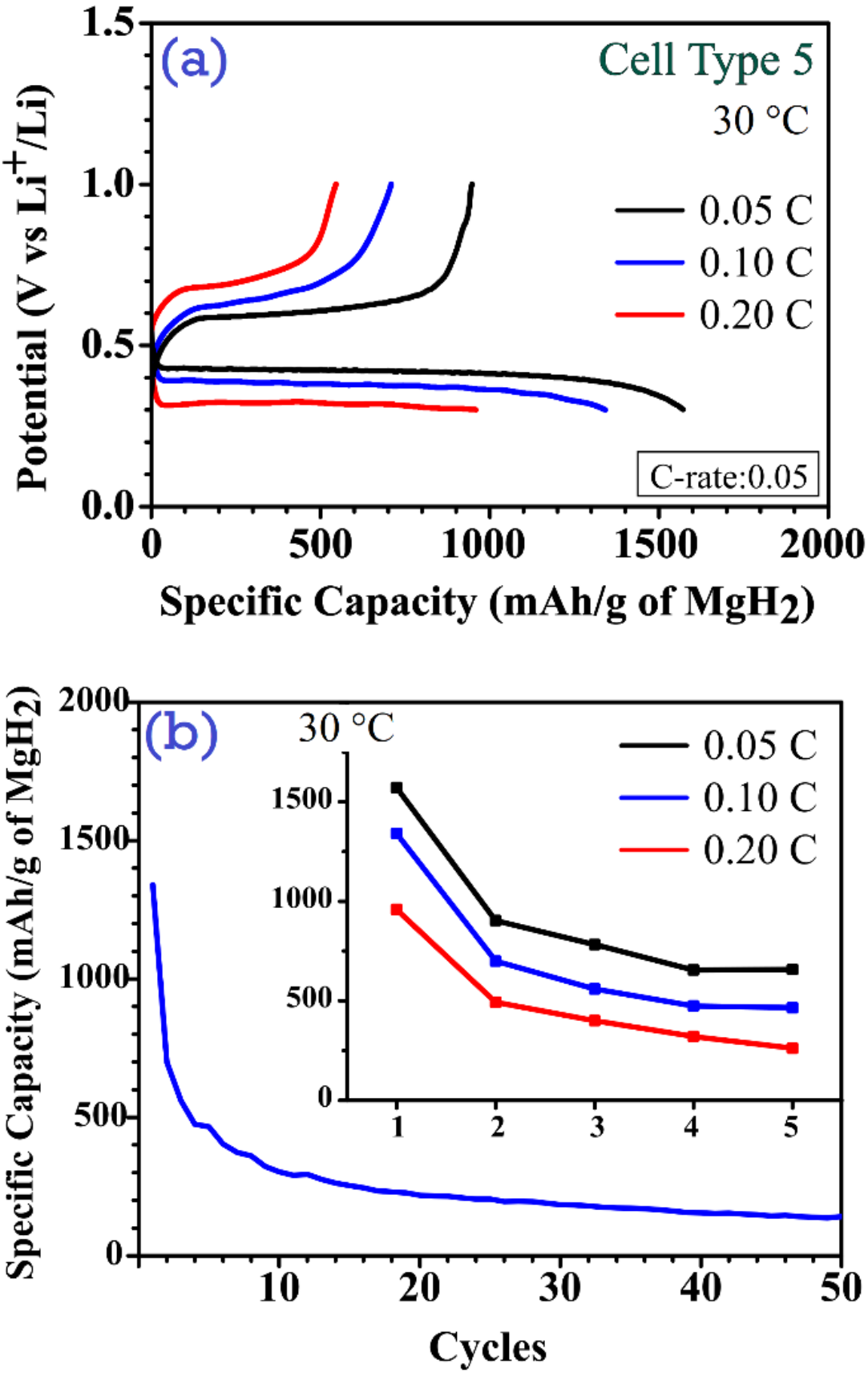

Figure 4.9. Discharge capacity of cell type 5 at different C-rates: (a) 1st cycle, (b) cycling.

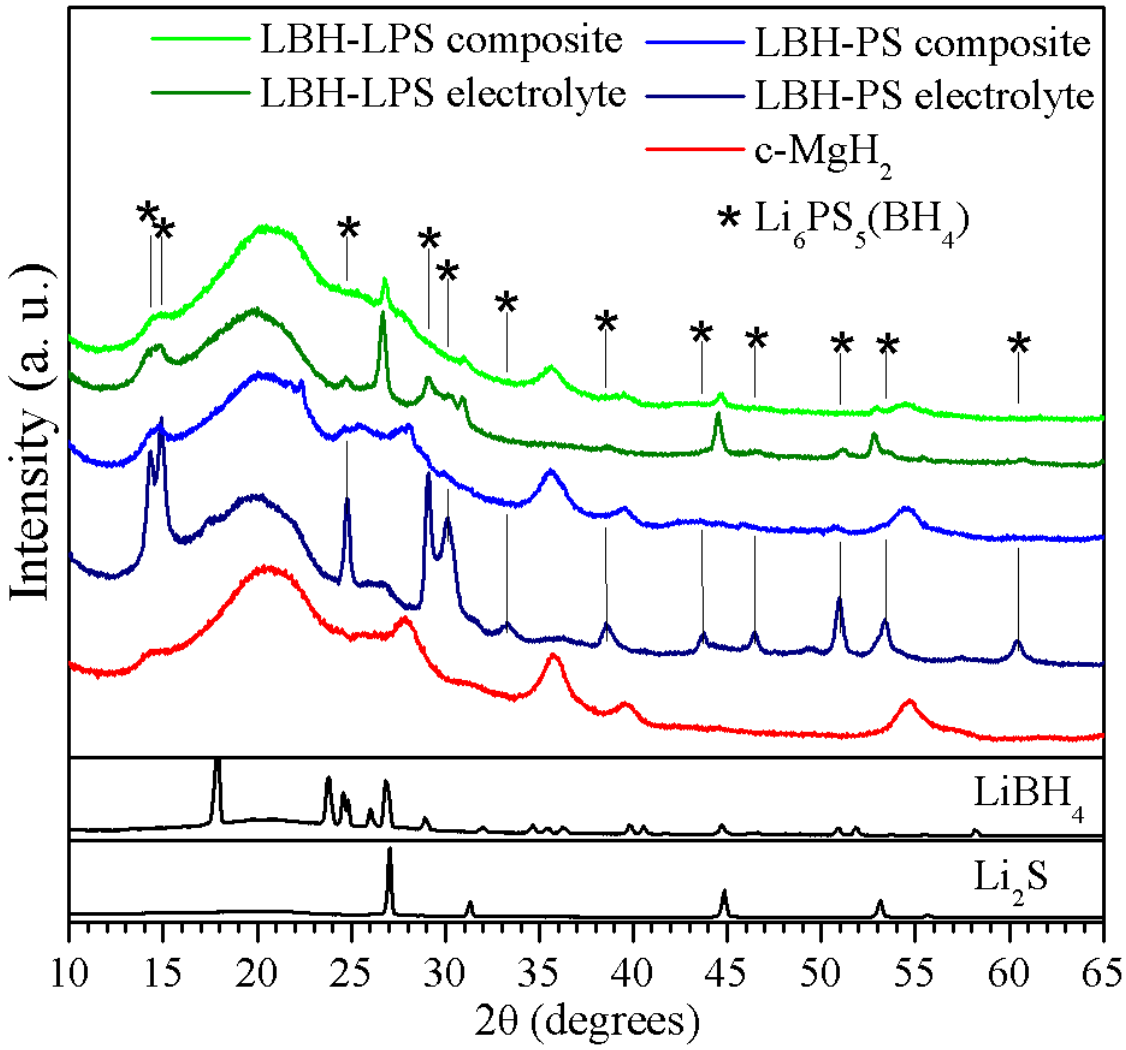

Figure 4.10. XRD pattern of electrolytes and composite electrodes. Peak positions corresponding to $Li_6PS_5(BH_4)$ phase are taken from ref. [34].

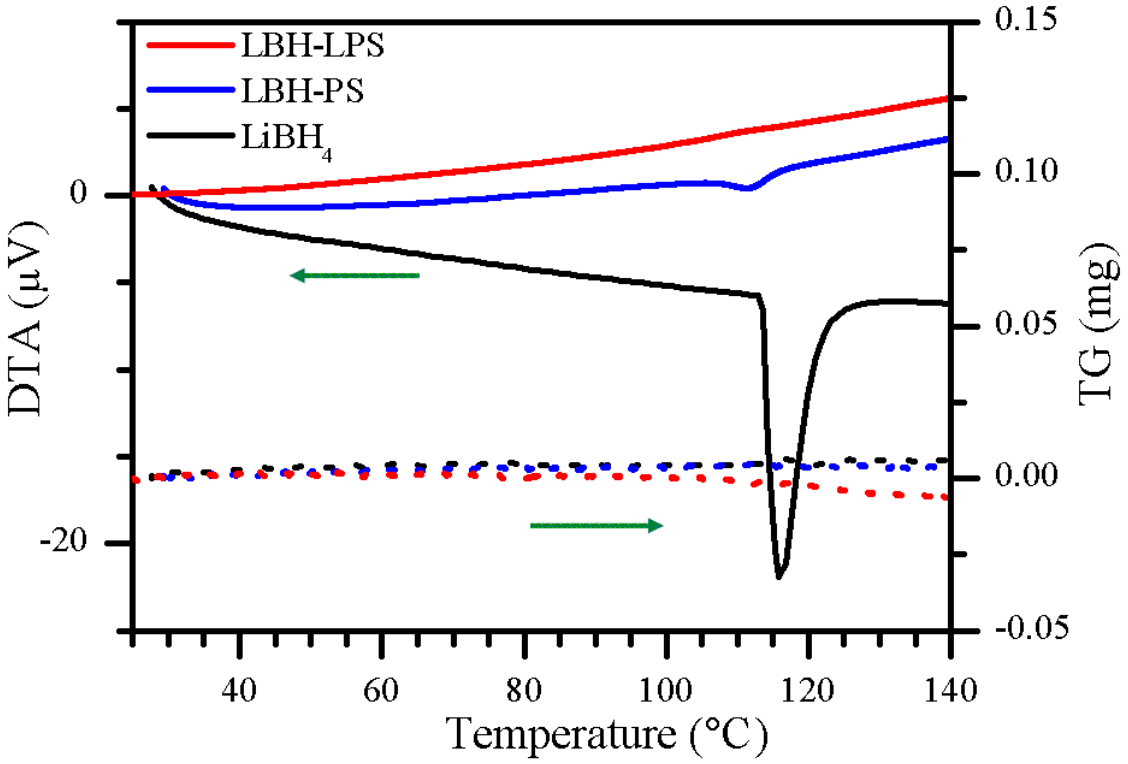

Figure 4.11. TG-DTA profiles of electrolytes.

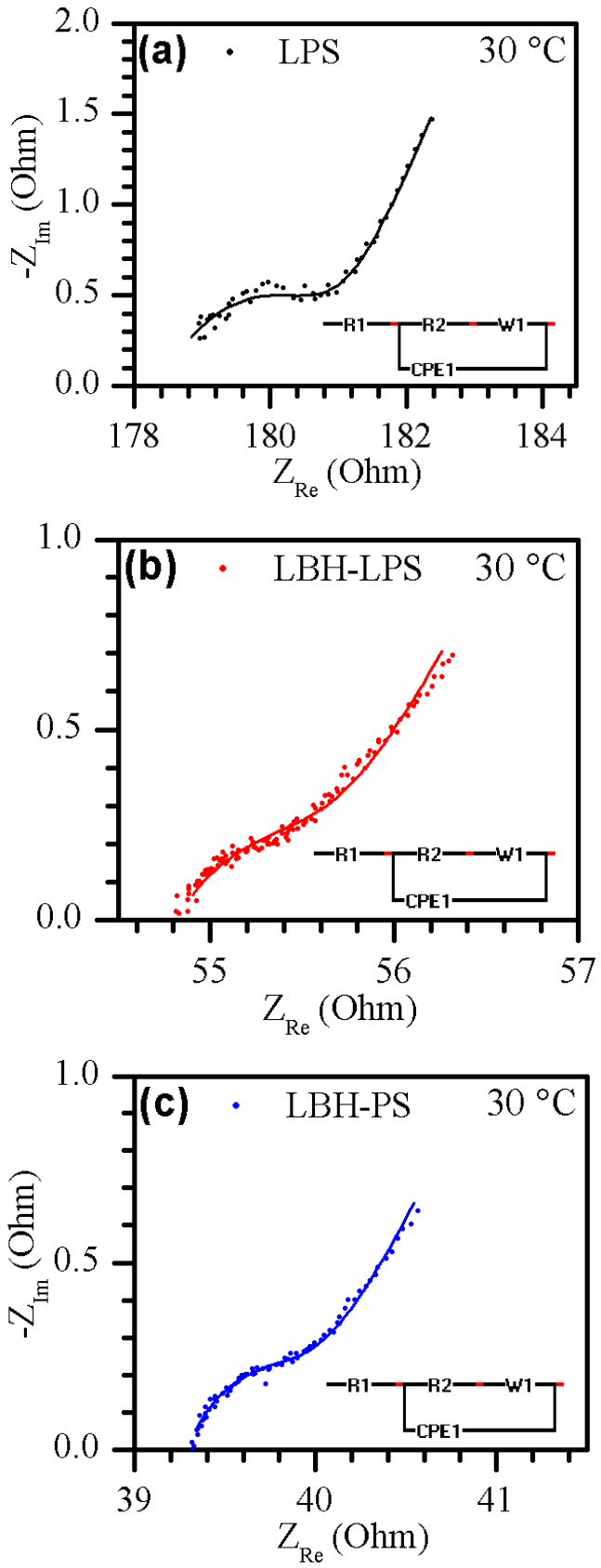

Figure 4.12. Nyquist plot for electrolytes at 30°C: a) LPS, b) LBH-LPS, c) LBH-PS.

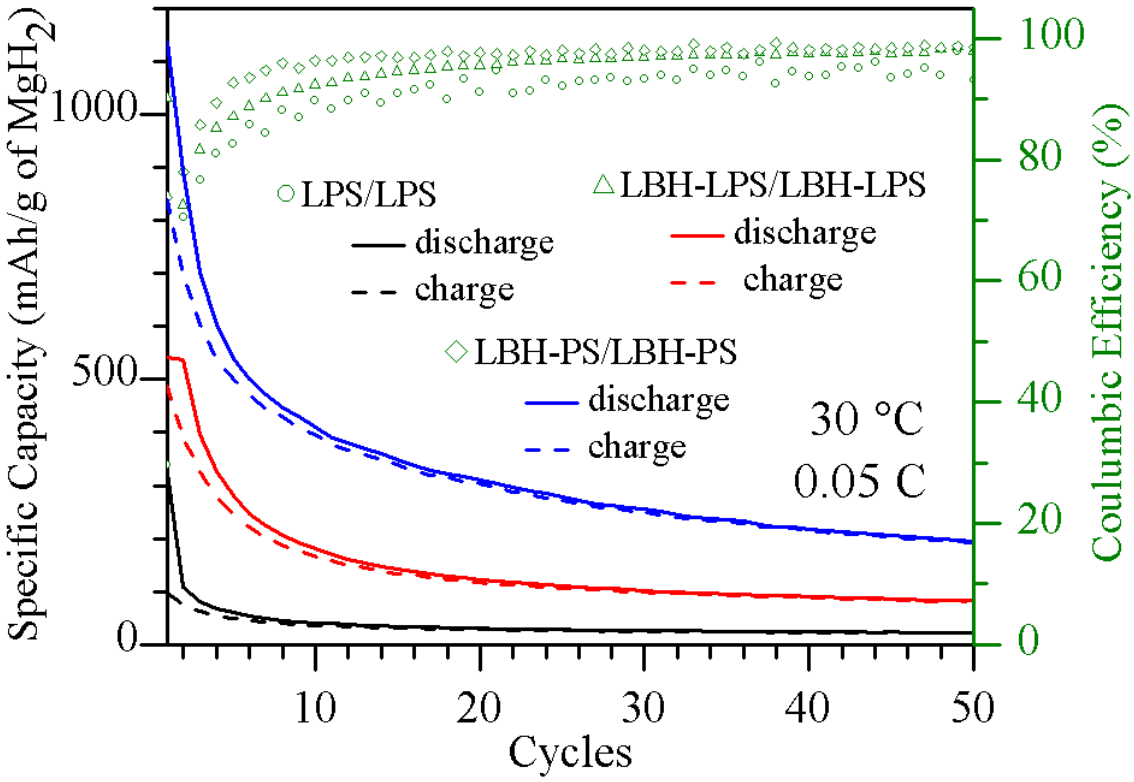

Figure 4.13. Performance of batteries with the same electrolyte in both layers.

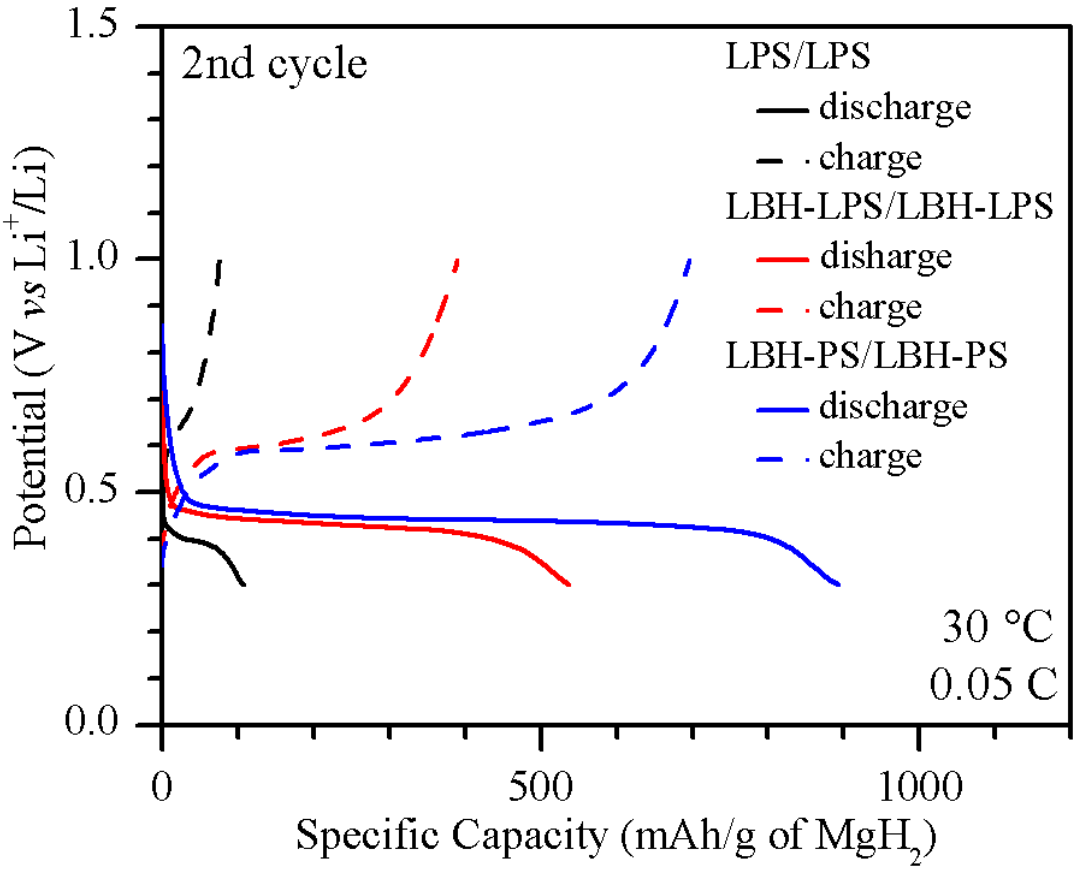

Figure 4.14. Galvanostatic curves for batteries using the same electrolyte in both layers.

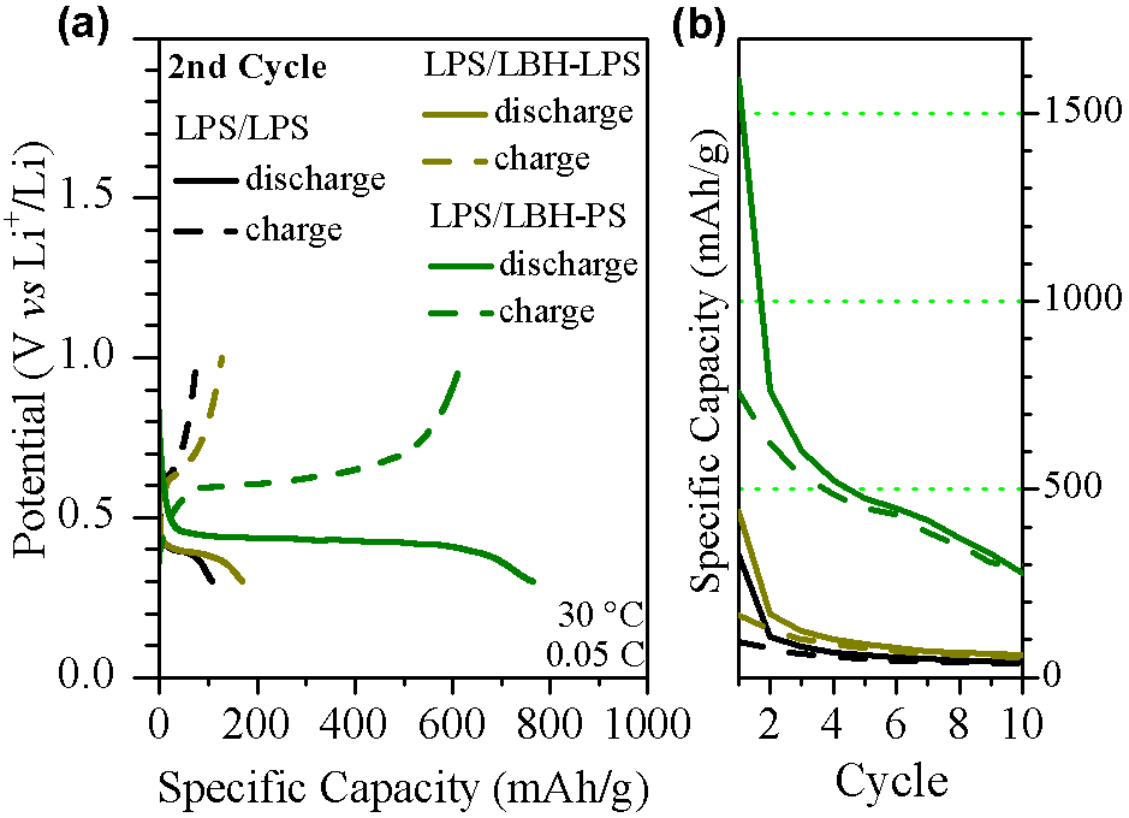

Figure 4.15. Batteries using LPS in the electrolyte layer: a) galvanostatic curves, b) cycling.

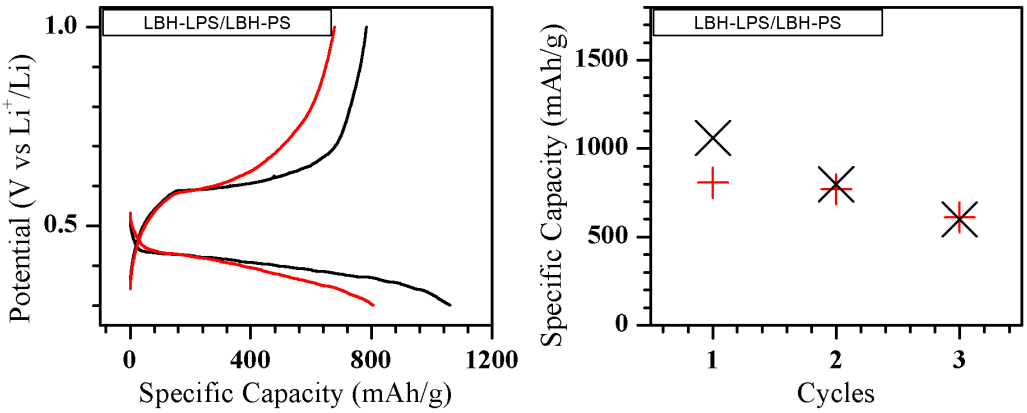

Battery LBH-LPS/LBH-LPS. Battery sample 1 (red), battery sample 2 (black).

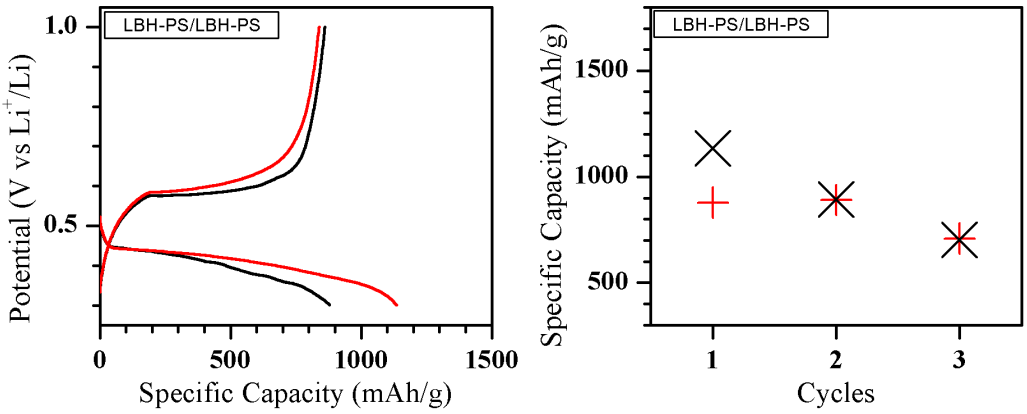

Battery LBH-PS/LBH-PS. Battery sample 1 (red), battery sample 2 (black).

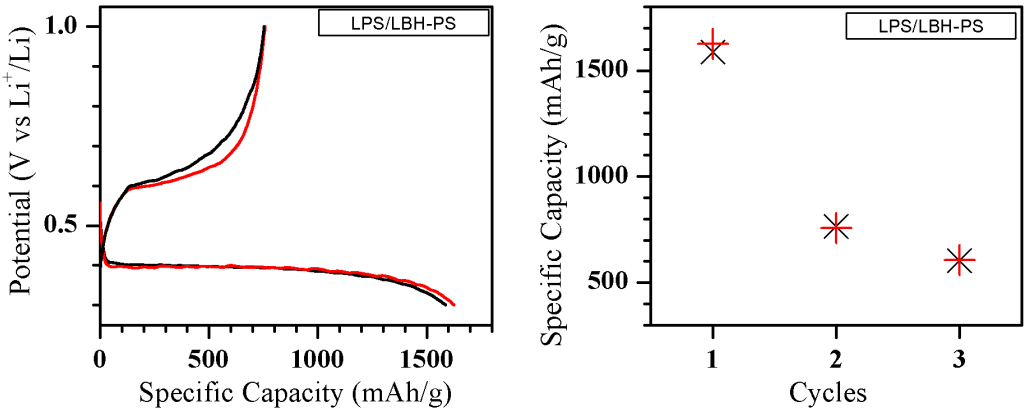

Battery LPS/LBH-PS. Battery sample 1 (red), battery sample 2 (black).

Figure 4.16 Galvanostatic discharge/charge first cycles (left).

Specific capacities for cycles 1-3 (right). 30 °C, 0.05 C.

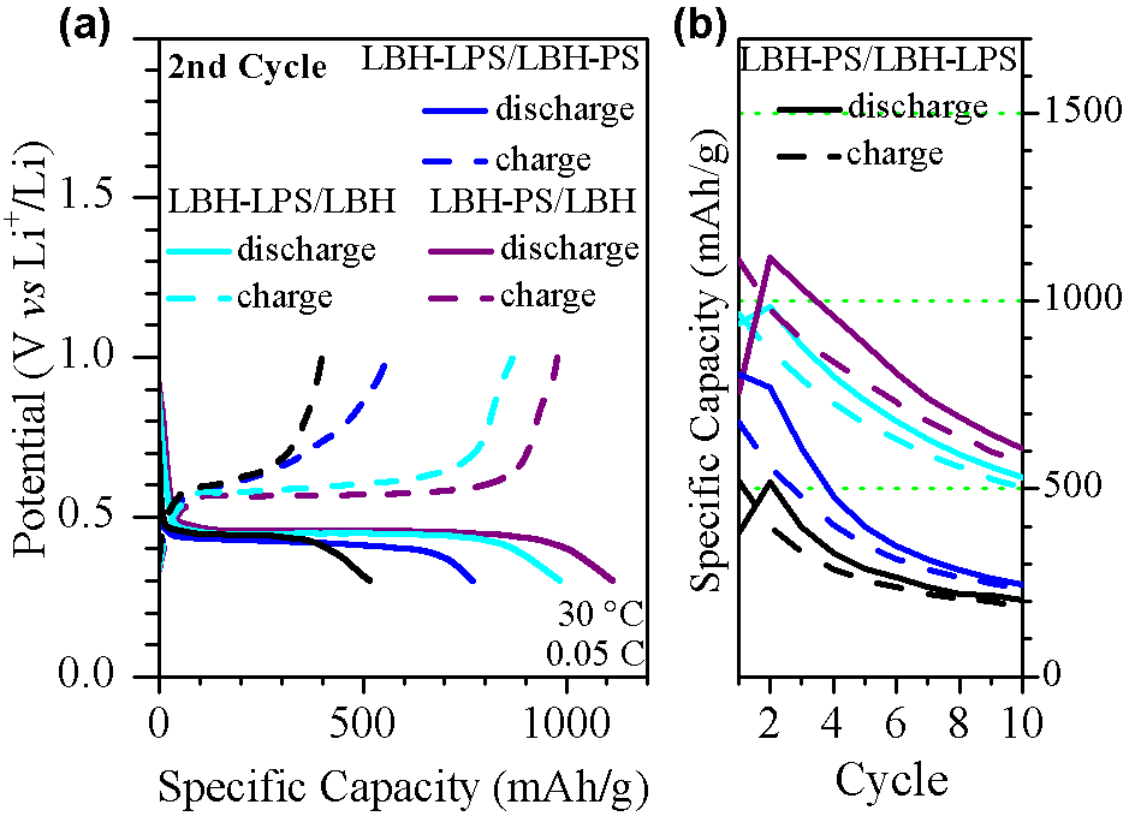

Figure 4.17. Batteries using LBH-LPS and LBH/PS in electrolyte layer: a) galvanostatic curves, b) cycling.

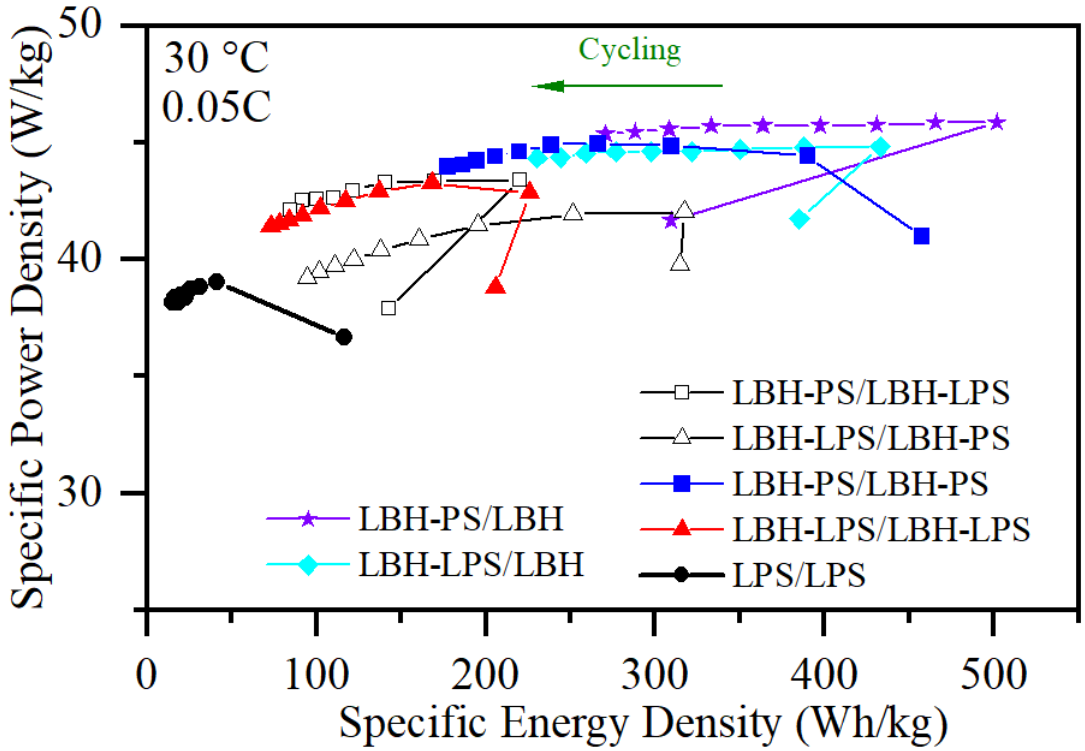

Figure 4.18. Specific Power and Energy during cycling.

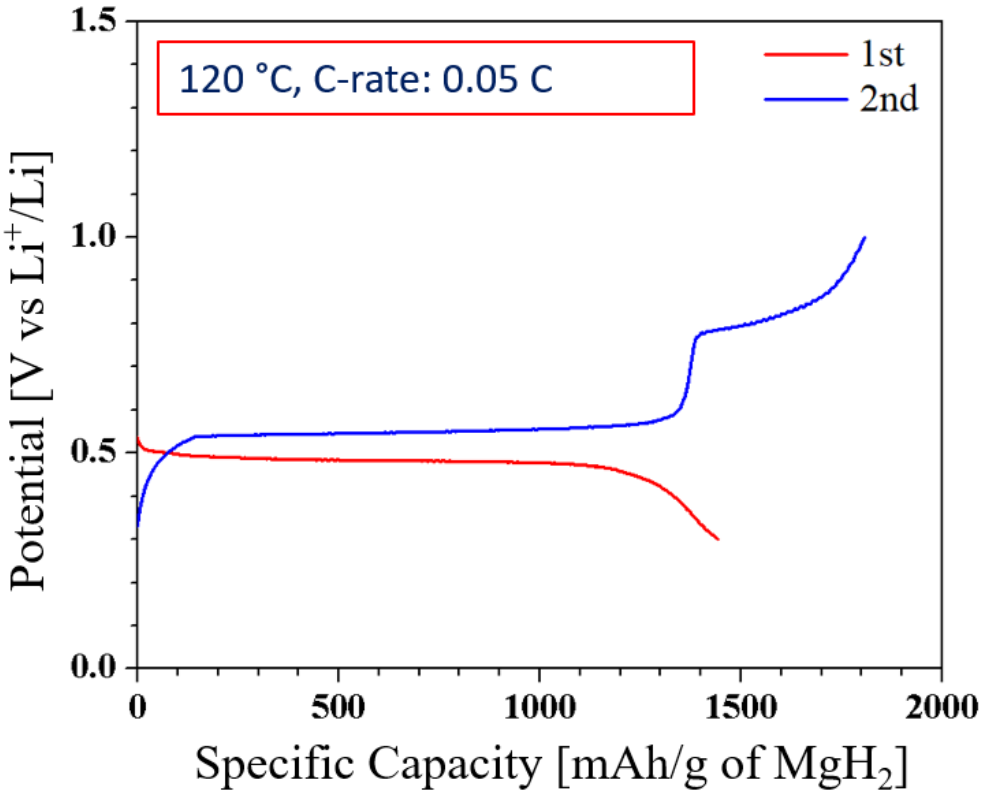

(a)

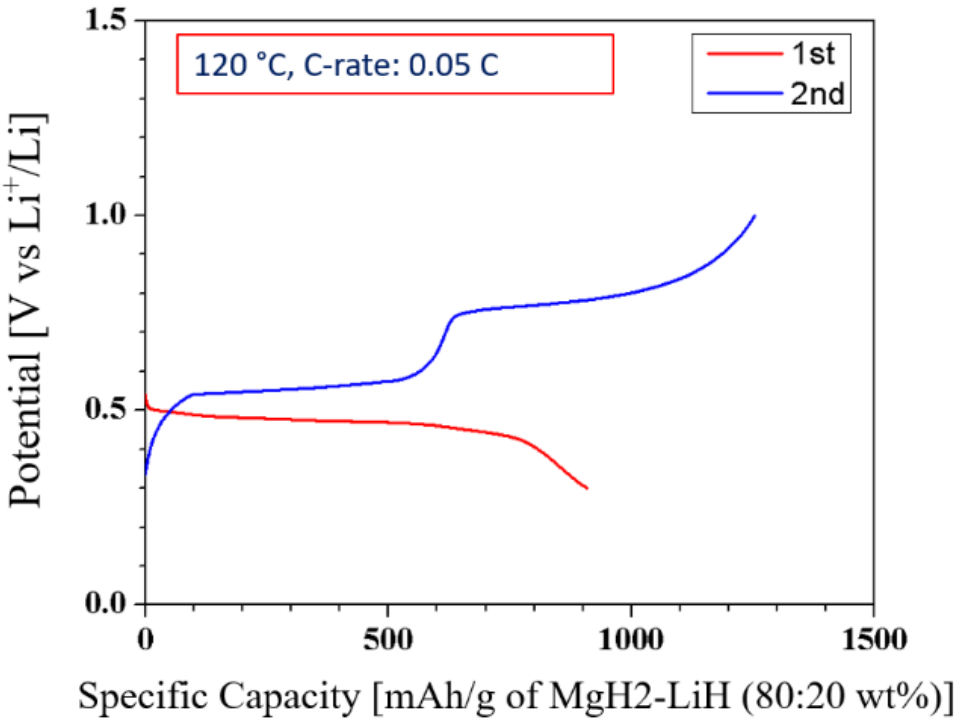

(b)

Figure 4.19. Side reaction for the battery LBH-LPS/LBH-LPS operating at high temperature. (a) original composite, (b) composite with LiH.

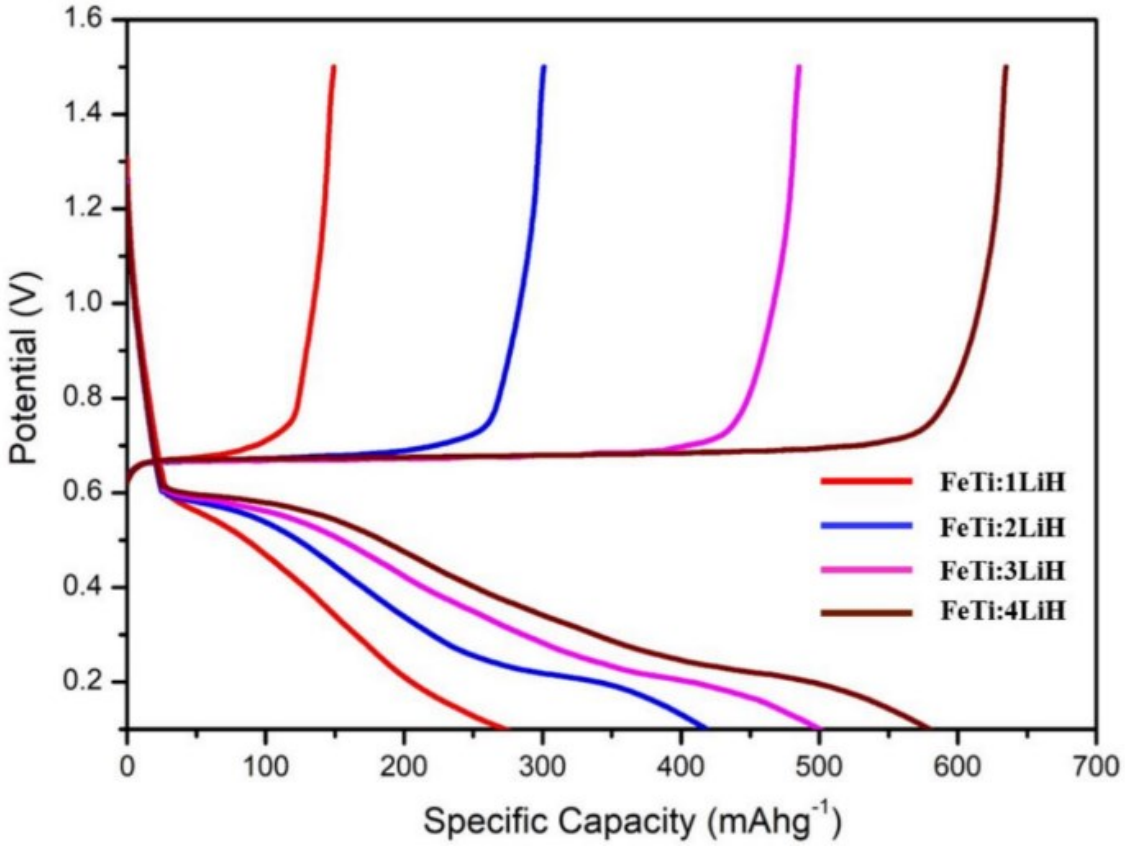

Figure 4.20. Galvanostatic charge/discharge of FeTi+XLiH. X=1, 2, 3, 4. 120 °C, 0.1 C.

5 Conclusions

MgH_2 as an active material for conversion reaction electrode with different electrolyte combination has been investigated in this work. The electrolytes compared in this study had similar conductivities, but they affected the performance of the composite electrode differently.

At room temperature, the battery prepared with $80Li_2S$-$20P_2S_5$/$3LiBH_4$•LiI (cell type 5) shown a better performance than $3LiBH_4$•LiI/$3LiBH_4$•LiI and $80Li_2S$-$20P_2S_5$/$3LiBH_4$ (cell 4 and 3). In this battery, $80Li_2S$-$20P_2S_5$ in the electrolyte layer provided the best ionic conductivity to transport the lithium ions from anode to cathode. The $3LiBH_4$•LiI in the working electrode seems to provide better mobility to lithium ions and hydrogen for the conversion reaction of MgH_2. The initial capacity was recovered during charging of this cell at a C-rate of 0.1 C and 30 °C and was found as 34.6 % (465.5 mAh/g), 22.6 % (303.6 mAh/g) and 10.5 % (140.9 mAh/g) after 5, 10, and 50 cycles, respectively.

The battery using only single electrolyte, $90LiBH_4$+$10P_2S_5$ in both layers (electrolyte and electrode) was found as the best. The discharge capacity delivered by this battery was 410 $mAhg^{-1}$ in 10^{th} cycle and 195.3 $mAhg^{-1}$ during the 50^{th} cycle, whereas for the battery using $33LiBH_4$+$67(80Li_2S+20P_2S_5)$, the capacity was 180.1 and 83.3 $mAhg^{-1}$ in 10^{th} and 50^{th} cycle, respectively.

According to the results, the battery with composite electrode using $LiBH_4$ had best performance among all the combinations. The potential of $LiBH_4$ at electrode composite was enhanced by the electrolyte layer of $90LiBH_4+10P_2S_5$ (LBH-PS), keeping a specific capacity of 645.7 $mAhg^{-1}$ after 10 cycles. It remarks on the importance of hydrogen mobility for the conversion reaction reversibility. Also, $Li_6PS_5(BH_4)$ synthesized by $90LiBH_4+10P_2S_5$ shown better compatibility with MgH_2 electrode.

The $80Li_2S+20P_2S_5$ and the $33LiBH_4+67(80Li_2S+20P_2S_5)$ are interesting electrolytes for all-solid-state batteries, these electrolytes can work with good compatibility in battery systems, such as Li-S batteries or TiS_2. However, for batteries using metal hydrides as an electrode material, the performance of battery seems not to be benefited using these electrolytes in the electrode.

6 References

[1] A. R. Dehghani-Sanij, E. Tharumalingam, M. B. Dusseault, and R. Fraser, "Study of energy storage systems and environmental challenges of batteries," *Renew. Sustain. Energy Rev.*, vol. 104, no. November 2018, pp. 192–208, 2019, doi: 10.1016/j.rser.2019.01.023.

[2] M. Li, M. Feng, D. Luo, and Z. Chen, "Fast Charging Li-Ion Batteries for a New Era of Electric Vehicles," *Cell Reports Phys. Sci.*, vol. 1, no. 10, p. 100212, 2020, doi: 10.1016/j.xcrp.2020.100212.

[3] A. Mahmoudzadeh Andwari, A. Pesiridis, S. Rajoo, R. Martinez-Botas, and V. Esfahanian, "A review of Battery Electric Vehicle technology and readiness levels," *Renew. Sustain. Energy Rev.*, vol. 78, no. October 2015, pp. 414–430, 2017, doi: 10.1016/j.rser.2017.03.138.

[4] Y. Liang *et al.*, "A review of rechargeable batteries for portable electronic devices," *InfoMat*, vol. 1, no. 1, pp. 6–32, 2019, doi: 10.1002/inf2.12000.

[5] C. Zhang, Y. L. Wei, P. F. Cao, and M. C. Lin, "Energy storage system: Current studies on batteries and power condition system," *Renew. Sustain. Energy Rev.*, vol. 82, no. December 2016, pp. 3091–3106, 2018, doi: 10.1016/j.rser.2017.10.030.

[6] C. Pillot, "The Rechargeable Battery Market and Main Trends 2018-2030," *AVICENNE ENERGY*, 2019.

[7] D. Allart, M. Montaru, and H. Gualous, "Model of Lithium Intercalation into Graphite by Potentiometric Analysis with Equilibrium and Entropy Change Curves of Graphite Electrode," *J. Electrochem. Soc.*, vol. 165, no. 2, pp. A380–A387, 2018, doi: 10.1149/2.1251802jes.

[8] V. A. Sethuraman, L. J. Hardwick, V. Srinivasan, and R. Kostecki, "Surface structural disordering in graphite upon lithium intercalation/deintercalation," *J. Power Sources*, 2010, doi: 10.1016/j.jpowsour.2009.12.034.

[9] R. C. Massé, C. Liu, Y. Li, L. Mai, and G. Cao, "Energy storage through intercalation reactions: Electrodes for rechargeable batteries," *Natl. Sci. Rev.*, vol. 4, no. 1, pp. 26–53, 2017, doi: 10.1093/nsr/nww093.

[10] K. Mizushima, P. C. Jones, P. J. Wiseman, and J. B. Goodenough, "LixCoO2 (0," *Solid State Ionics*, 1981.

[11] M. M. Thackeray, W. I. F. David, P. G. Bruce, and J. B. Goodenough, "Lithium insertion into manganese spinels," *Mater. Res. Bull.*, 1983, doi: 10.1016/0025-5408(83)90138-1.

[12] A. K. Padhi, K. S. Nanjundaswamy, and J. B. Goodenough, "Phospho-olivines as Positive-Electrode Materials for Rechargeable Lithium Batteries," *J. Electrochem. Soc.*, 1997, doi: 10.1149/1.1837571.

[13] T. Ohzuku and Y. Makimura, "Layered Lithium Insertion Material of $LiCo_{1/3}Ni_{1/3}Mn_{1/3}O$ for Lithium-ion Batteries," *Chem. Lett.*, 2001.

[14] S. Albrecht *et al.*, “Electrochemical and thermal behavior of aluminum- and magnesium-doped spherical lithium nickel cobalt mixed oxides Li1-x(Ni1-y-zCoyMz)O2 (M = Al, Mg),” 2003, doi: 10.1016/S0378-7753(03)00175-7.

[15] R. Yazami and P. Touzain, “A reversible graphite-lithium negative electrode for electrochemical generators,” *J. Power Sources*, 1983, doi: 10.1016/0378-7753(83)87040-2.

[16] E. Ferg, R. J. Gummow, A. de Kock, and M. M. Thackeray, “Spinel Anodes for Lithium-Ion Batteries,” *J. Electrochem. Soc.*, 1994, doi: 10.1149/1.2059324.

[17] C. K. Chan *et al.*, “High-performance lithium battery anodes using silicon nanowires,” *Nat. Nanotechnol.*, 2008, doi: 10.1038/nnano.2007.411.

[18] B. M. Bang, H. Kim, H. K. Song, J. Cho, and S. Park, “Scalable approach to multi-dimensional bulk Si anodes via metal-assisted chemical etching,” *Energy Environ. Sci.*, 2011, doi: 10.1039/c1ee02310a.

[19] V. Etacheri *et al.*, “Effect of fluoroethylene carbonate (FEC) on the performance and surface chemistry of Si-nanowire li-ion battery anodes,” *Langmuir*, 2012, doi: 10.1021/la203712s.

[20] E. Markevich *et al.*, “Amorphous Columnar Silicon Anodes for Advanced High Voltage Lithium Ion Full Cells: Dominant Factors Governing Cycling Performance,” *J. Electrochem. Soc.*, 2013, doi: 10.1149/2.085310jes.

[21] W. J. Zhang, “A review of the electrochemical performance of alloy anodes for lithium-ion batteries,” *J. Power Sources*, vol. 196, no. 1, pp. 13–24, 2011, doi: 10.1016/j.jpowsour.2010.07.020.

[22] P. Poizot, S. Laruelle, S. Grugeon, L. Dupont, and J. Tarascon, “Nano-sizedtransition-metaloxidesas negative-electrode materials for lithium-ion batteries,” vol. 407, no. September, 2000.

[23] S. H. Yu, X. Feng, N. Zhang, J. Seok, and H. D. Abruña, “Understanding Conversion-Type Electrodes for Lithium Rechargeable Batteries,” *Acc. Chem. Res.*, vol. 51, no. 2, pp. 273–281, 2018, doi: 10.1021/acs.accounts.7b00487.

[24] Y. Oumellal, A. Rougier, G. A. Nazri, J. M. Tarascon, and L. Aymard, “Metal hydrides for lithium-ion batteries,” *Nat. Mater.*, vol. 7, no. 11, pp. 916–921, 2008, doi: 10.1038/nmat2288.

[25] Q. Cheng, D. Sun, and X. Yu, “Metal hydrides for lithium-ion battery application: A review,” *J. Alloys Compd.*, vol. 769, pp. 167–185, 2018, doi: 10.1016/j.jallcom.2018.07.320.

[26] P. Huen and D. B. Ravnsbæk, “All-solid-state lithium batteries – The Mg2FeH6-electrode LiBH4-electrolyte system,” *Electrochem. commun.*, vol. 87, no. January, pp. 81–85, 2018, doi: 10.1016/j.elecom.2018.01.001.

[27] M. N. Guzik, R. Mohtadi, and S. Sartori, “Lightweight complex metal hydrides for Li-, Na-, and Mg-based batteries,” *J. Mater. Res.*, vol. 34, no. 6, pp. 877–904, 2019, doi: 10.1557/jmr.2019.82.

[28] Q. Wang, L. Jiang, Y. Yu, and J. Sun, “Progress of enhancing the safety of lithium ion battery from the electrolyte aspect,” *Nano Energy*, vol. 55, no. August

2018, pp. 93–114, 2019, doi: 10.1016/j.nanoen.2018.10.035.

[29] S. Wang *et al.*, “Interfacial challenges for all-solid-state batteries based on sulfide solid electrolytes,” *J. Mater.*, vol. 7, no. 2, pp. 209–218, 2021, doi: 10.1016/j.jmat.2020.09.003.

[30] C. Sun, J. Liu, Y. Gong, D. P. Wilkinson, and J. Zhang, “Recent advances in all-solid-state rechargeable lithium batteries,” *Nano Energy*, vol. 33, no. December 2016, pp. 363–386, 2017, doi: 10.1016/j.nanoen.2017.01.028.

[31] M. Matsuo and S. I. Orimo, “Lithium fast-ionic conduction in complex hydrides: Review and prospects,” *Adv. Energy Mater.*, vol. 1, no. 2, pp. 161–172, 2011, doi: 10.1002/aenm.201000012.

[32] S. Ikeda, T. Ichikawa, K. Kawahito, K. Hirabayashi, H. Miyaok, and Y. Kojima, “Anode properties of magnesium hydride catalyzed with niobium oxide for an all solid-state lithium-ion battery,” *Chem. Commun.*, vol. 49, no. 64, pp. 7174–7176, 2013, doi: 10.1039/c3cc43987a.

[33] B. R. Shin, Y. J. Nam, D. Y. Oh, D. H. Kim, J. W. Kim, and Y. S. Jung, “Comparative study of TiS2/Li-In all-solid-state lithium batteries using glass-ceramic Li3PS4and Li10GeP2S12 solid electrolytes,” *Electrochim. Acta*, vol. 146, pp. 395–402, 2014, doi: 10.1016/j.electacta.2014.08.139.

[34] A. Yamauchi, A. Sakuda, A. Hayashi, and M. Tatsumisago, “Preparation and ionic conductivities of (100 - X)(0.75Li 2S·0.25P2S5)· xLiBH4 glass electrolytes,” *J. Power Sources*, vol. 244, pp. 707–710, 2013, doi: 10.1016/j.jpowsour.2012.12.001.

[35] A. Unemoto, H. Wu, T. J. Udovic, M. Matsuo, T. Ikeshoji, and S. I. Orimo, “Fast lithium-ionic conduction in a new complex hydride-sulphide crystalline phase,” *Chem. Commun.*, vol. 52, no. 3, pp. 564–566, 2016, doi: 10.1039/c5cc07793a.

[36] A. El kharbachi *et al.*, “Reversibility of metal-hydride anodes in all-solid-state lithium secondary battery operating at room temperature,” *Solid State Ionics*, vol. 317, no. September 2017, pp. 263–267, 2018, doi: 10.1016/j.ssi.2018.01.037.

[37] T. LEI, Z. YANG, Z. LIN, and X. ZHANG, “State of art on energy management strategy for hybrid-powered unmanned aerial vehicle,” *Chinese J. Aeronaut.*, vol. 32, no. 6, pp. 1488–1503, 2019, doi: 10.1016/j.cja.2019.03.013.

[38] K. Kubota, M. Dahbi, T. Hosaka, S. Kumakura, and S. Komaba, “Towards K-Ion and Na-Ion Batteries as ‘Beyond Li-Ion,’” *Chem. Rec.*, vol. 18, no. 4, pp. 459–479, 2018, doi: 10.1002/tcr.201700057.

[39] M. Winter and R. J. Brodd, “What are batteries, fuel cells, and supercapacitors?,” *Chem. Rev.*, vol. 104, no. 10, pp. 4245–4269, 2004, doi: 10.1021/cr020730k.

[40] H. D. Yoo, E. Markevich, G. Salitra, D. Sharon, and D. Aurbach, “On the challenge of developing advanced technologies for electrochemical energy storage and conversion,” *Mater. Today*, vol. 17, no. 3, pp. 110–121, 2014, doi: 10.1016/j.mattod.2014.02.014.

[41] C. X. Zu and H. Li, “Thermodynamic analysis on energy densities of batteries,” *Energy Environ. Sci.*, vol. 4, no. 8, pp. 2614–2624, 2011, doi: 10.1039/c0ee00777c.

[42] L. Aymard, Y. Oumellal, and J. P. Bonnet, “Metal hydrides: An innovative and challenging conversion reaction anode for lithium-ion batteries,” *Beilstein J. Nanotechnol.*, vol. 6, no. 1, pp. 1821–1839, 2015, doi: 10.3762/bjnano.6.186.

[43] S. Brutti, D. Meggiolaro, A. Paolone, and P. Reale, “Magnesium hydride as negative electrode active material in lithium cells: A review,” *Mater. Today Energy*, vol. 3, pp. 53–59, 2017, doi: 10.1016/j.mtener.2016.12.003.

[44] R. Mohtadi and S. I. Orimo, “The renaissance of hydrides as energy materials,” *Nat. Rev. Mater.*, vol. 2, no. 3, pp. 1–16, 2016, doi: 10.1038/natrevmats.2016.91.

[45] H. Maekawa, M. Matsuo, H. Takamura, M. Ando, and Y. Noda, “Halide-Stabilized LiBH 4 , a Room-Temperature Lithium Fast-Ion Conductor,” pp. 894–895, 2009.

[46] C. Dietrich *et al.*, “Lithium ion conductivity in Li2S-P2S5 glasses-building units and local structure evolution during the crystallization of superionic conductors Li3PS4, Li7P3S11 and Li4P2S7,” *J. Mater. Chem. A*, vol. 5, no. 34, pp. 18111–18119, 2017, doi: 10.1039/c7ta06067j.

[47] M. Matsuo, Y. Nakamori, S. I. Orimo, H. Maekawa, and H. Takamura, “Lithium superionic conduction in lithium borohydride accompanied by structural transition,” *Appl. Phys. Lett.*, vol. 91, no. 22, pp. 2–5, 2007, doi: 10.1063/1.2817934.

[48] N. Kamaya *et al.*, “A lithium superionic conductor,” *Nat. Mater.*, 2011, doi: 10.1038/nmat3066.

[49] F. Mizuno, A. Hayashi, K. Tadanaga, and M. Tatsumisago, “New, highly ion-conductive crystals precipitated from Li 2S-P2S5 glasses,” *Adv. Mater.*, vol. 17, no. 7, pp. 918–921, 2005, doi: 10.1002/adma.200401286.

[50] R. Kanno and M. Murayama, “Lithium Ionic Conductor Thio-LISICON: The Li[sub 2]S-GeS[sub 2]-P[sub 2]S[sub 5] System,” *J. Electrochem. Soc.*, vol. 148, no. 7, p. A742, 2001, doi: 10.1149/1.1379028.

[51] M. Itoh, Y. Inaguma, W.-H. Jung, L. Chen, and T. Nakamura, “High lithium ion conductivity in the perovskite-type compounds,” *Solid State Ionics*, vol. 70–71, no. 0, pp. 196–202, 1994, [Online]. Available: http://linkinghub.elsevier.com/retrieve/pii/0167273894903107.

[52] R. Murugan, V. Thangadurai, and W. Weppner, “Fast lithium ion conduction in garnet-type Li7La 3Zr2O12,” *Angew. Chemie - Int. Ed.*, vol. 46, no. 41, pp. 7778–7781, 2007, doi: 10.1002/anie.200701144.

[53] M. Latroche *et al.*, “Full-cell hydride-based solid-state Li batteries for energy storage,” *Int. J. Hydrogen Energy*, vol. 44, no. 15, pp. 7875–7887, 2019, doi: 10.1016/j.ijhydene.2018.12.200.

[54] L. Zeng, T. Ichikawa, K. Kawahito, H. Miyaoka, and Y. Kojima, “Bulk-Type all-solid-state lithium-ion batteries: Remarkable performances of a carbon nanofiber-supported MgH2composite electrode,” *ACS Appl. Mater. Interfaces*, vol. 9, no. 3, pp. 2261–2266, 2017, doi: 10.1021/acsami.6b11314.

[55] R. Miyazaki *et al.*, “Room temperature lithium fast-ion conduction and phase relationship of LiI stabilized LiBH4,” *Solid State Ionics*, vol. 192, no. 1, pp. 143–

147, 2011, doi: 10.1016/j.ssi.2010.05.017.

[56] L. Zeng, K. Kawahito, S. Ikeda, T. Ichikawa, H. Miyaoka, and Y. Kojima, "Metal hydride-based materials towards high performance negative electrodes for all-solid-state lithium-ion batteries," *Chem. Commun.*, vol. 51, no. 48, pp. 9773–9776, 2015, doi: 10.1039/c5cc02614h.

[57] B. A. Mei, O. Munteshari, J. Lau, B. Dunn, and L. Pilon, "Physical Interpretations of Nyquist Plots for EDLC Electrodes and Devices," *J. Phys. Chem. C*, vol. 122, no. 1, pp. 194–206, 2018, doi: 10.1021/acs.jpcc.7b10582.

[58] L. Zeng, H. Miyaoka, T. Ichikawa, and Y. Kojima, "Superior hydrogen exchange effect in the MgH2-LiBH4 system," *J. Phys. Chem. C*, vol. 114, no. 30, pp. 13132–13135, 2010, doi: 10.1021/jp1042443.

[59] D. Sveinbjörnsson *et al.*, "Effect of heat treatment on the lithium ion conduction of the LiBH 4-Lii solid solution," *J. Phys. Chem. C*, vol. 117, no. 7, pp. 3249–3257, 2013, doi: 10.1021/jp310050g.

[60] A. Unemoto, G. Nogami, M. Tazawa, M. Taniguchi, and S. I. Orimo, "Development of 4V-Class bulk-type all-solid-state lithium rechargeable batteries by a combined use of complex hydride and sulfide electrolytes for room temperature operation," *Mater. Trans.*, vol. 58, no. 7, pp. 1063–1068, 2017, doi: 10.2320/matertrans.M2017022.

[61] A. Sakuda *et al.*, "Mechanochemically Prepared Li2S-P2S5-LiBH4 Solid Electrolytes with an Argyrodite Structure," *ACS Omega*, vol. 3, no. 5, pp. 5453–5458, 2018, doi: 10.1021/acsomega.8b00377.

[62] M. Xiang, Y. Zhang, Y. Zhu, X. Guo, J. Chen, and L. Li, "Ternary LiBH4-NaBH4-MgH2 composite as fast ionic conductor," *Solid State Ionics*, vol. 324, no. May, pp. 109–113, 2018, doi: 10.1016/j.ssi.2018.06.015.

[63] A. Hayashi, A. Sakuda, and M. Tatsumisago, "Development of sulfide solid electrolytes and interface formation processes for bulk-type all-solid-state Li and Na batteries," *Front. Energy Res.*, vol. 4, no. JUL, pp. 1–13, 2016, doi: 10.3389/fenrg.2016.00025.

Acknowledgements

Firstly, I would like to thank CONACYT for the scholarship provided during my doctor degree studies. I am aware that the money comes from all Mexican people pockets. All students, who are supported by this kind of programs, have a duty to do our best.

I would like to express my deepest gratitude to my patient and supportive supervisor, **Professor Dr. Takayuki Ichikawa**, who has supported me throughout this research project. I am extremely grateful to work under his guidance. I know how busy you are, so I really appreciated the time you spent with me. Your insightful feedback pushed me to sharpen my thinking and brought my work to a higher level.

A special acknowledgement is dedicated to **Professor Dr. Ankur Jain**. Thank you for supporting me with my experiments. During this stage, I learned a lot about experimentation. The meetings and conversations were vital in inspiring me to think outside the box. Thank you for your advice and support.

Further, I would like to thank **Professor Dr. Abel Hernandez** who has always believed in me, even when I did not believe in myself. Thank you for your advice and support. As always, I am grateful to hear your viewpoint.

I would also like to extend my gratitude to **Professor Dr. Hiroki Miyaoka** and **Professor Dr. Rini Singh** for the thoughtful comments and recommendations on this dissertation and for helping me to clear my mind when I had doubts about my research.

With many thanks to all the laboratory members. Professors, classmates, lab-mates and friends, thank you for this great time at university. Professors, I have acquired a lot of knowledge in your lectures and improved my skills at different areas due to your assignments and advices. I thank to Junya Hashimoto, Hiroyuki Gi, Dr. Keita Shinzato, Masakuni Yamaguchi, Fangqin Guo and other friends for being there for me when I need someone to have a discussion about some issues or someone to just listen. I am also thankful to the Graduate School of Engineering and all its member's staff for all the considerate guidance.

Finally, I thank to my family, you were always there for me in good and bad times. Thank you for supporting me in many ways, I love you. Father and mother, thank you for believing in me and encouraging me when I needed it most, I love you.

Fernando Cano-Banda

Research articles

"Enhanced performance of MgH_2 composite electrode using glass-ceramic electrolytes for all-solid-state Li-ion batteries"

Fernando Cano-Banda, Rini Singh, Abel Hernandez-Guerrero, Ankur Jain, Takayuki Ichikawa

Journal of Alloys and Compounds,

Volume 863, 2021, Page 158729, ISSN 0925-8388,

https://doi.org/10.1016/j.jallcom.2021.158729.

"High capacity MgH_2 composite electrodes for all-solid-state Li-ion battery operating at ambient temperature"

Fernando Cano-Banda, Ana Gallardo-Gutierrez, Luis Luviano-Ortiz, Abel Hernandez-Guerrero, Ankur Jain, Takayuki Ichikawa,

International Journal of Hydrogen Energy,

Volume 46, Issue 1, 2021, Pages 1030-1037, ISSN 0360-3199,

https://doi.org/10.1016/j.ijhydene.2020.09.202.

Coauthored article

"Conversion reaction of TiFe Hydride as anode material for all-solid-state Lithium-ion batteries"

Rini Singh, **Cano Banda Fernando**, Takayuki Ichikawa, and Ankur Jain

Materials Letters: X,

Volume 10, 2021, Pages 100067-100070, ISSN: 2590-1508,

https://doi.org/10.1016/j.mlblux.2021.100067